Selwyn Region Cu-Au-Mo Deposits

Figure 4.1: Aerial view looking ENE of historic Mount Elliott mine area with slag dumps (and historic smelter just front and right of central slag dump) and more recent decline boxcut accessing Corbould ore. Dark area in centre of image is breakthrough from underground Corbould workings. Image from Doug Kirwin presentation, 2008.

PREAMBLE

A number of deposits and resources, with historic production, brownfields extensions and new discoveries within the Selwyn Region have been grouped in this Chapter. These deposits and resources are: Merlin Mo -Re, Mount Dore Cu-Au, Mount Elliott-SWAN Cu-Au, and the Starra Line of Cu-Au deposits.

LOCATION

Geological Domain

Marimo-Staveley Domain (Starra Au-Cu deposits) and on or very close to the contact of Marimo-Staveley and Kuridala-Selwyn Domains (Mount Elliott-SWAN Cu-Au, Merlin Mo -Re & Mount Dore Cu-Au).

Co-ordinates

Mount Elliott:
Lat: 21° 32’ 25” S, Long: 140° 30’ 6” E
MGA Zone 54: 448,386 E, 7,617,967 N

SWAN:
Lat: 21° 32’ 30” S, Long: 140° 29’ 38” E
MGA Zone 54: 447,595 E, 7,617,808 N

Merlin:
Lat: 21° 39’ 16” S, Long: 140° 29’ 34” E
MGA Zone 54: 447,529 E, 7,605,333 N

Mount Dore:
Lat: 21° 39’ 43” S, Long: 140° 29’ 33” E
MGA Zone 54: 447,492 E, 7,604,504 N

Starra 276:
Lat: 21° 39’ 43” S, Long: 140° 28’ 37” E
MGA Zone 54: 445,876 E, 7,604,510 N

Starra 222:
Lat: 21° 42’ 37” S, Long: 140° 28’ 0” E
MGA Zone 54: 444,831 E, 7,599,142 N

NATURE OF MINES

Mined Commodities

Cu, Au and some Co have been mined intermittently in the Selwyn region since the early 1890’s up until 2014 (when the last UG mining was undertaken at Starra 276). Table 4.1 presents the historic production from the Selwyn region’s mines compiled by Chinova (2017).

Mining Methods & Depths of Mining

Historic mining has been from relatively shallow open pits and underground sub-level stoping. Details of mining methods for individual deposits and groups of deposits are presented in Table 4.1. The maximum depth of underground mining was at 460m below surface at Starra 222. Starra 276 has been mined to around 400m below surface and Mount Elliott to around 340m.

PRODUCTION AND RESOURCES

Historic production from the Selwyn Region mines is presented in Table 4.1. More detailed production histories can be found in the references cited for each of the following individual deposits. Resource and reserve

Table 4.1: Historic Production, discovery date and mining methods of Cu-Au-Co deposits in the Selwyn Region

	Starra Line			Starra Line			Mount Dore	Mount Elliott		Corbould			Lady Ella			Mount Cobalt	Victoria/Stuart		
Discovery	1980			1980			1908	1898		1995			1995			1900	1971		
Mining Method	Open Pit & Sub Level Open Stoping			Open Pit & Sub Level Open Stoping			Small Open Pits & Adits	Open Pit & Sub Level Stoping		Sub Level Open Stoping			Open Pit			Shaft & Adits	Open Pit		
	Tonnage	Cu	Au	Tonnage	Cu	Au	Cu	Cu	Au	Tonnage	Cu	Au	Tonnage	Cu	Au	Co	Tonnage	Cu	Au
	(mT)	(%)	(g/t)	(mT)	(%)	(g/t)	(T)	(T)	(oz)	(mT)	(%)	(g/t)	(mT)	(%)	(g/t)	(T)	(mT)	(%)	(g/t)
Production	6.84	2.1	4.6	11.4	2.1	3.2	15.7	24,800	34,000	5.1	2.9	1.5	0.5	1.6	1.3	779	0.2	2.5	0.3
Dates	1980-1999			1890 -2014				1909-1919								1919-1934			
Source	Porter (2016)			Chinova Resources (2017)			Chinova Resources (2017)	Chinova Resources (2017)		Chinova Resources (2017)			Chinova Resources (2017)			Chinova Resources (2017)	Chinova Resources (2017)		

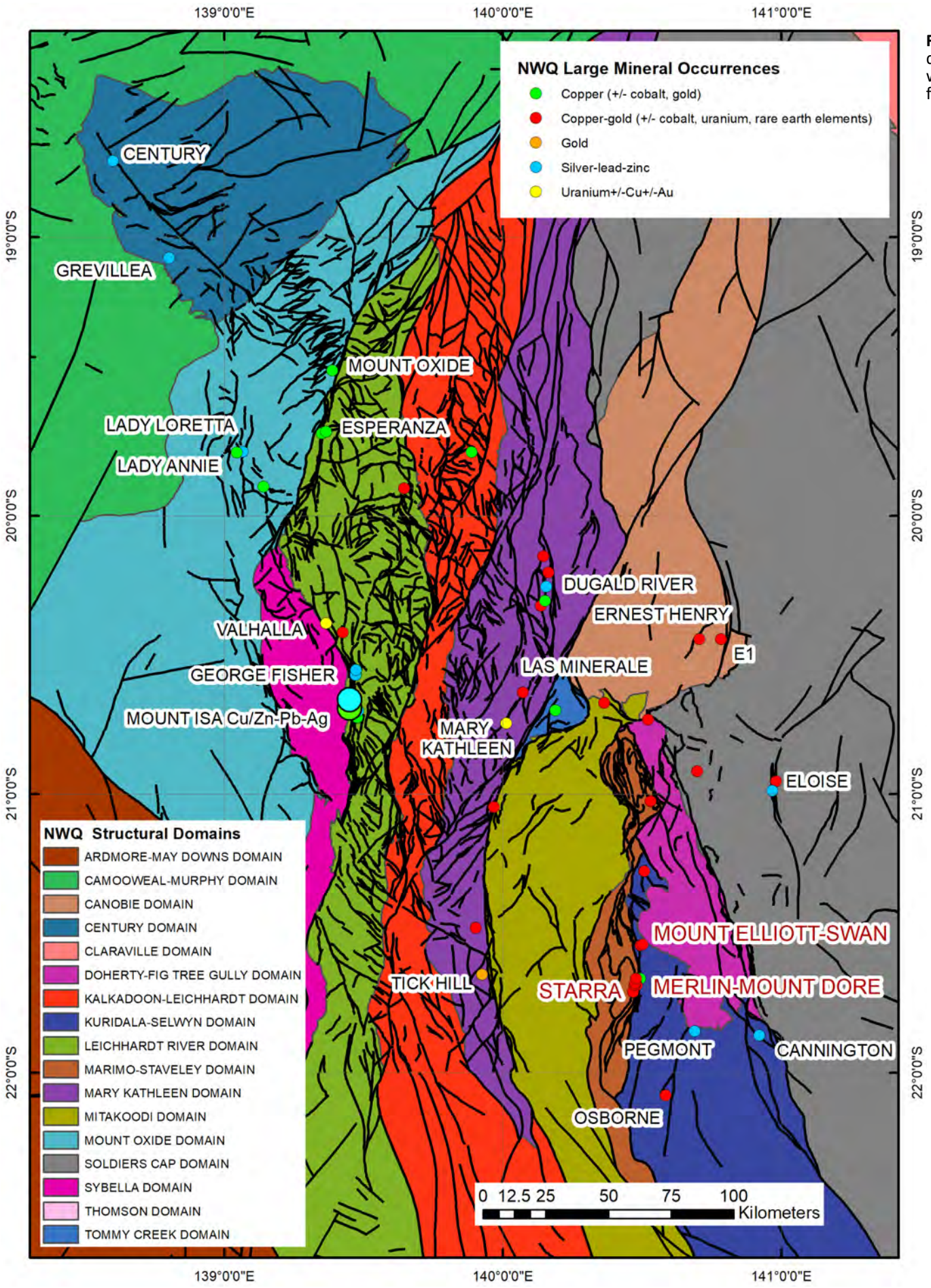

Figure 4.2: Regional location of the Selwyn Region deposits and resources covered in this chapter shown with respect to the Mount Isa Strcutural Domain Map from the 2010 NWQMEP GIS.

dimensions are individually presented in the following sections. Current measured, indicated and inferred mineral resource estimates for Starra 276, Starra 222, Merlin, Mount Dore, Mount Elliott, Corbould West, SWAN and Victoria-Stuart reported by Chinova (2017, 2014) are presented in Table 4.2.

HOST ROCKS

Regional Geology

The Selwyn Region deposits lie within the Eastern Fold Belt of the Mount Isa Inlier on or close to the contact of the Marimo-Staveley and Kuridala-Selwyn Domains as defined by the 2010 NWQMEP project (Figure 4.2).

The Eastern Fold Belt successions accumulated between 1790Ma and 1610Ma in two major packages of sedimentary and volcanic rocks traditionally called Cover Sequence 2 (CS2; 1790-1740Ma) and Cover Sequence 3 (CS3; 1720-1610Ma).

The earlier CS2 packages comprise felsic volcanics and clastics of the Argylla Formation, Boomarra Metamorphics, Bulonga Volcanics, Marraba Volcanics, Ballara Quartzite and Mitakoodi Quartzite and are overlain by laterally more extensive platformal carbonates of the Corella Formation. These successions are well developed and preserved within the Mitakoodi Domain (Figure 4.2) west of a major structure, the Overhang Fault, that is believed to separate them from an allochthonous CS3 block to the east and south (Murphy et al., 2017) that host the Selwyn region deposits as well as the Cannington, Pegmont, Osborne, Kulthor and Eloise deposits.

The 1740-1780Ma Double Crossing Metamorphics (Figure 4.4) are higher grade metamorphic equivalents of the CS2 Mitakoodi Quartzite and Marraba Volcanics that occur as a inlier in structural juxtaposition with CS3 rocks in the Marimo-Staveley Domain that contains some of the Selwyn region deposits (Figure 4.2).

The CS2 rocks are deformed during the 1740Ma Wonga Extensional Event (Holcombe et al., 1991) with a mid-crustal extensional detachment exhumed and exposed along the Wonga Belt in the Mary Kathleen Domain. These packages are extensively, syn-deformationally intruded by 1750-1730Ma Wonga-Burstall aged felsic-mafic intrusives.

In the Selwyn region, the Double Crossing Metamorphics are deformed during the Wonga event and syn-deformationally intruded by the 1743Ma Gin Creek Granite (Figure 4.4).

The extrusive, Wonga-coeval, Mount Fort Constantine Volcanics are interbedded with Corella Formation carbonates north of the northeastern extension of the Overhang Fault in the Canobie Domain (see Chapter 3 Ernest Henry solid geology interpretation; Figure 4.2). No Corella Formation or Mount Fort Constantine Volcanic-aged rocks are know east and south of the Overhang Fault.

The bulk of Cover Sequence 3 rocks in the Eastern Fold Belt lie to the east and south of the Overhang Fault that marks the allothchonous terrain boundary between the Marimo-Staveley, Kuridala-Selwyn, Doherty-Fig Tree Gully and Soldiers Cap Domains in the south and east and the Mitakoodi and Quamby Domains to their west and north (Murphy et al., 2017). The Eastern Fold Belt CS3 packages are thought to comprise a continuous depositional sequence, now significantly dismembered, ramped, imbricated and reverse faulted during subsequent 1590-1500Ma Isan Orogeny.

Table 4.2: Measured, indicated and inferred mineral resource estimates of Cu-Au & Mo-Re deposits in the Selwyn Region

	Starra 276 (using 0.5%Cu cut-off)			Starra 222 (using 0.5%Cu cut-off)			Merlin (using 0.3%Mo cut-off)				Mount Dore (using 0.25%Cu cut-off)			Mount Elliott (using 0.5eq%Cu cut-off*)			Corbould West (using 0.5eq%Cu cut-off*)			SWAN (using 0.5eq%Cu cut-off*)			Victoria/Stuart (using 0.6%Cu cut-off*)		
	Tonnage (mT)	Cu (%)	Au (g/t)	Tonnage (mT)	Cu (%)	Au (g/t)	Tonnage (mT)	Mo (%)	Re (ppm)	Cu (%)	Tonnage (mT)	Cu (%)	Au (g/t)	Tonnage (mT)	Cu (%)	Au (g/t)	Tonnage (mT)	Cu (%)	Au (g/t)	Tonnage (mT)	Cu (%)	Au (g/t)	Tonnage (mT)	Cu (%)	Au (g/t)
Measured							0.84	2.3	34	0.33	1.1	0.69	0.12												
Indicated	1.69	1.22	0.71	2.29	0.87	1.20	4.2	1.5	26	0.23	66.9	0.58	0.08	18.5	1.04	0.55	1.1	0.86	0.49	154.5	0.60	0.37	1.87	1.21	0.18
Inferred	4.42	1.11	0.39	4.67	0.86	1.18	1.4	1.1	24	0.48	42.4	0.49	0.13	6.3	0.66	0.34	10.1	0.85	0.48	163.2	0.52	0.30	3.21	1.07	0.17
Total Resource	6.11	1.14	0.48	6.96	0.86	1.19	6.4	1.5	26	0.30	110.8	0.55	0.10	24.8	0.94	0.50	11.3	0.86	0.49	317.7	0.56	0.34	5.08	1.12	0.18
Date	December-2017			December-2017			June-2014				December-2017			December-2017			December-2017			December-2017			December-2017		
Source	Chinova Resources			Chinova Resources			Chinova Resources				Chinova Resources			Chinova Resources			Chinova Resources			Chinova Resources			Chinova Resources		

* eq%Cu calculated as Cu(%) + 0.8Au(g/t)

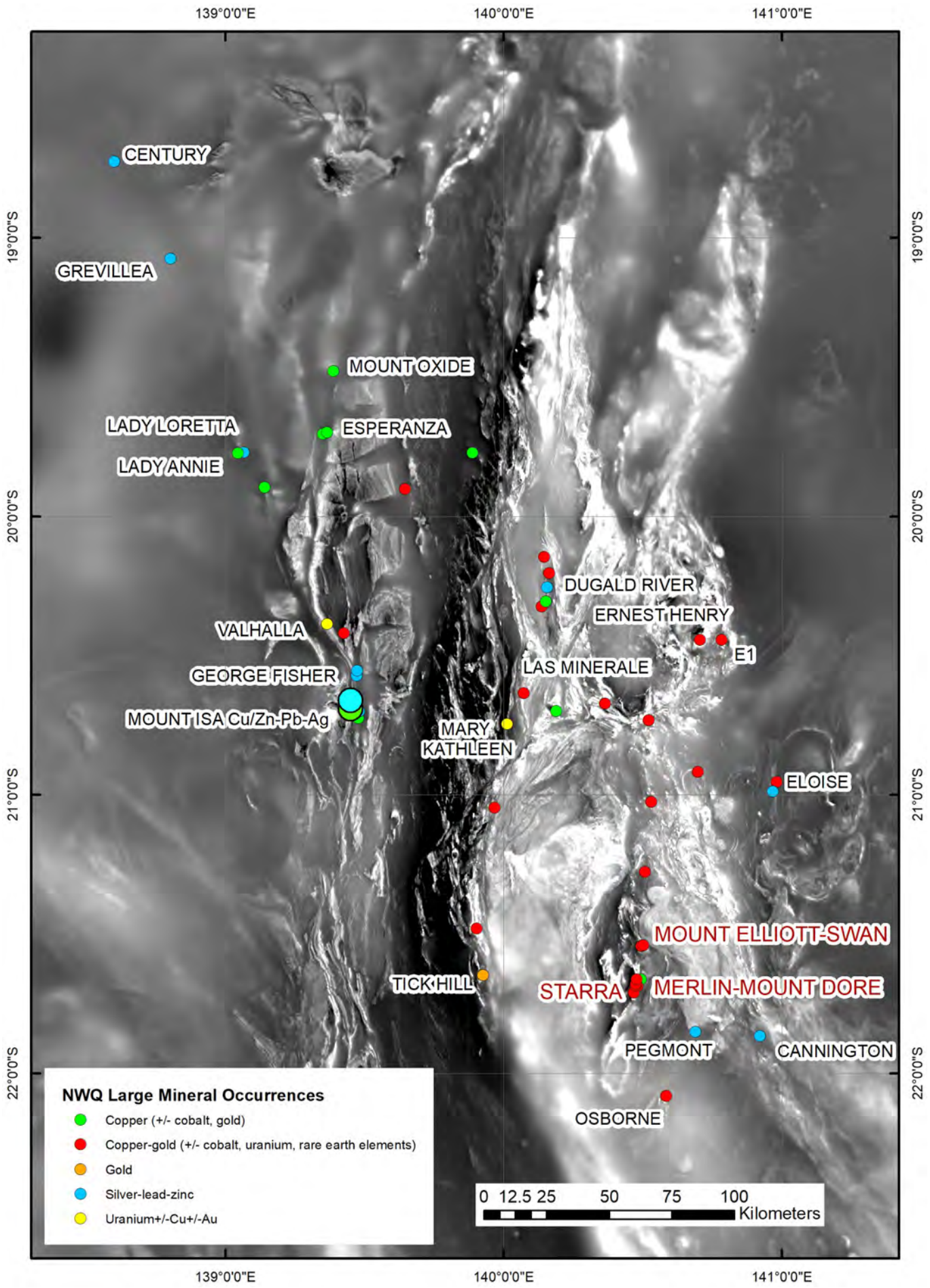

Figure 4.3: Regional location of the Selwyn Region deposits and resources covered in this chapter overlain on an image of total magnetic intensity from the GADDS data of the region.

The oldest Eastern Fold Belt CS3 package comprises the variably calcareous, sandstone -siltstone-dominated and iron formation-bearing, ca1725-1710Ma Staveley Formation. No confirmed base of Staveley Formation has been identified with the western and southern contacts with Corella Formation, Mitakoodi Formation and the Double Crossing Metamorphics currently interpreted to be structural (Figures 4.4 & 4.6) and reflecting Isan D1 thin -skinned thrusting from the south to south southeast (O'Dea et al., 2006; Murphy et al., 2017).

In the Selwyn region, the western-most (and assumed lower-most stratigraphically) Staveley Formation is in fault contact over a complex D1, D2-D3-D4 reactivated, fault zone, the Starra Shear, with Double Crossing Metamorphics and further west across a major D2 Fault with Answer Slate (Figure 4.4).

Towards the top of the Staveley Formation, a relatively clean clastic unit, the 1710Ma Roxmere Quartzite marks a significant basin reactivation and heralds the initiation of basin deepening. The Roxmere Quartzite is relatively thin in the Selwyn region (Figure 4.4; and much thicker to the north in the Marimo Synform region) but is an important marker of a following, significant, regionally-extensive, redox transition from relatively oxidized platformal Staveley Formation carbonates into finer grained and carbonaceous sediments of the Kuridala Formation.

This stratigraphic redox transition (and its associated structural juxtapositionings) is very significant in the location of many Selwyn region deposits and resources (Figure 4.4; and see following Mount Elliott-SWAN and Merlin Mount Dore sections) and in regional IOCG prospectivity (Murphy et al., 2017).

The overlying ca1710-1680Ma Kuridala Formation comprises phyllites, phyllitic siltstones, carbonaceous metasiltstones, psammo-pelitic schists and metagreywacke deposited as relatively fine-grained sediment dominated turbidites. The Starcross and Llewellyn Creek Formations are potential time equivalents (Murphy et al., 2017). Higher metamorphic grade schistose variants elsewhere in the Eastern Fold Belt are garnet, staurolite and andalusite-bearing.

The Kuridala Formation is overlain by coarser grained turbidites of the New Hope Sandstone package that comprise quartzo-feldspathic meta sandstones, siltstones, mudstones and minor schists (Figure 4.4). The ca1680-1665Ma New Hope Sandstone and its potential time-equivalent further east, the Mount Norna Quartzite, reflect a basin (rift) re -activation, coarsening event accompanied by significant mafic silling.

This mafic silling is strongly developed in the Mount Norna Quartzite and overlying Toole Creek Volcanics east of the Cloncurry Fault in the Soldiers Cap Domain where the thermal input into a rift-re-activating basin has been suggested to drive BHT-style Ag-Pb-Zn mineralization (Murphy et al., 2017; Hinman, 2018). The Cannington deposit is thought to be hosted in the upper portions of the Mount Norna Quartzite package.

The period of coarsened New Hope Sandstone and Mount Norna Quartzite turbiditic deposition is terminated by a major episode of significant basin deepening. The ca1665-1650Ma Answer Slate and Toole Creek Volcanics comprise graphitic slates, phyllites, metasiltstones, mica schists, slates, carbonaceous mudstones, metabasalts, metadolerites, amphibolites and chert.

While the Toole Creek Volcanics and Answer Slate are locally in smooth stratigraphic transition with the underlying Mount Norna Quartzite and New Hope Sandstone in the Soldiers Cap and Kuridala-Selwyn Domains, the Answer Slate further west in the Marimo-Staveley Domain (and in the Selwyn deposits region, Figure 4.4) is commonly in D1, D2 or D4 fault juxtaposition with Staveley Formation, Corella Formation and Mitakoodi Formation (Murphy et al., 2017).

The package of rocks hosting the Mount Elliott deposit (Figures 4.4 & 4.20) comprise carbonaceous metasiltstones, phyllites metabasalts and metadolerites. They have in the past been assigned to the Kuridala Formation but recent interpretation (Murphy et al., 2017) has suggested they might be Answer Slate-Toole Creek Volcanic equivalents D1-structurally juxtaposed with Staveley and Kuridala Formations to their west.

Eastern Fold Belt deposition east and south of the Overhang Fault terminates around 1650Ma. Ongoing deposition of carbonates and fine clastics to ca1610Ma is preserved in the structural enclave of the Tommy Creek Block which also preserves an episode of fel-

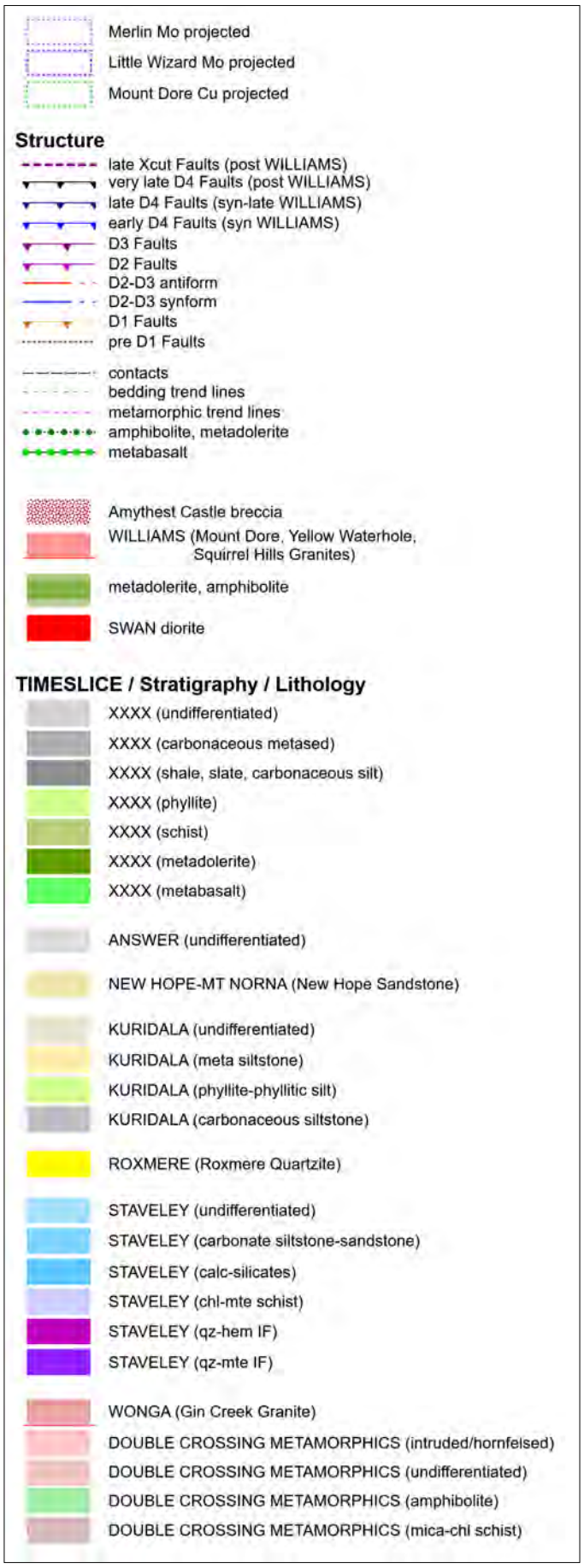

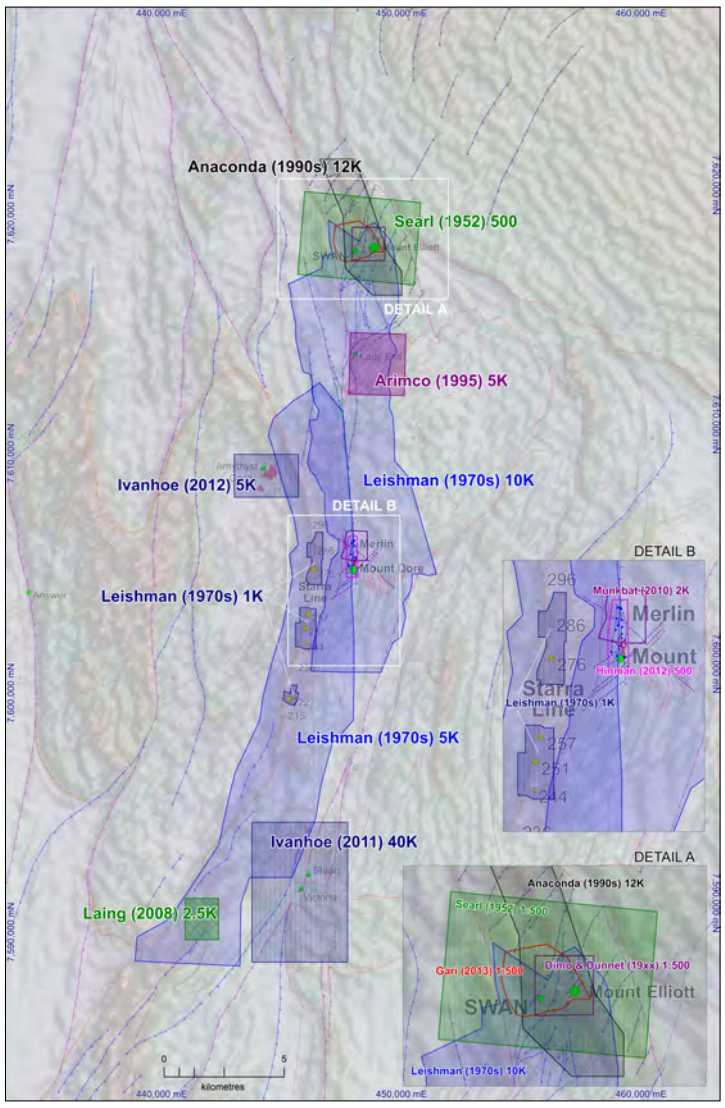

Figure 4.4: Regional solid geology compilation-interpretation of the Selwyn Region deposits and resources in the Eastern Fold Belt of the Mount Isa block from Deep Mining Queensland (Murphy et al. 2017). Map Projection GDA94 (MGA54)

sic magmatism around 1655-1650Ma. This Eastern Fold Belt felsic magmatism is regionally expressed as the Ernest Henry Diorite, the Tommy Creek Microgranite and potentially the SWAN diorite at Mount Elliott-SWAN (Figure 4.4).

Regional Deformation

Deposition in the overall Isa Inlier was terminated by the onset of Isan Orogeny around 1590Ma. Isan D1 deformation between ca1590-1570Ma has been interpreted to have been thin-skinned, north to north north-west-directed (O'Dea et al., 2006; Betts et al., 2006) and associated with the allochthonous thrust emplacement and internal ramping of the Eastern Fold Belt Staveley to Toole Creek packages into their current geometric relationships (Murphy et al., 2017). Originally east-west D1 folding is well preserved (and currently identified) in the immediate footwall and hanging wall domains of major D1 thrusts: in the Snake Creek Anticline area (Rubenach et al., 2008); at the northern end of the Marimo Synform; in the footwall of the Overhang Shear in the Mitakoodi Culmination (O'Dea et al., 2006); and in the hanging wall of the folded Cloncurry Overthrust around Cannington (Hinman, 2018). Many thrusts,

Figure 4.5: Data sources for the Selwyn Region Deep Mining Queensland (Murphy et al. 2017) Map compilation-interpretation. Map area identical to Figure 4.4

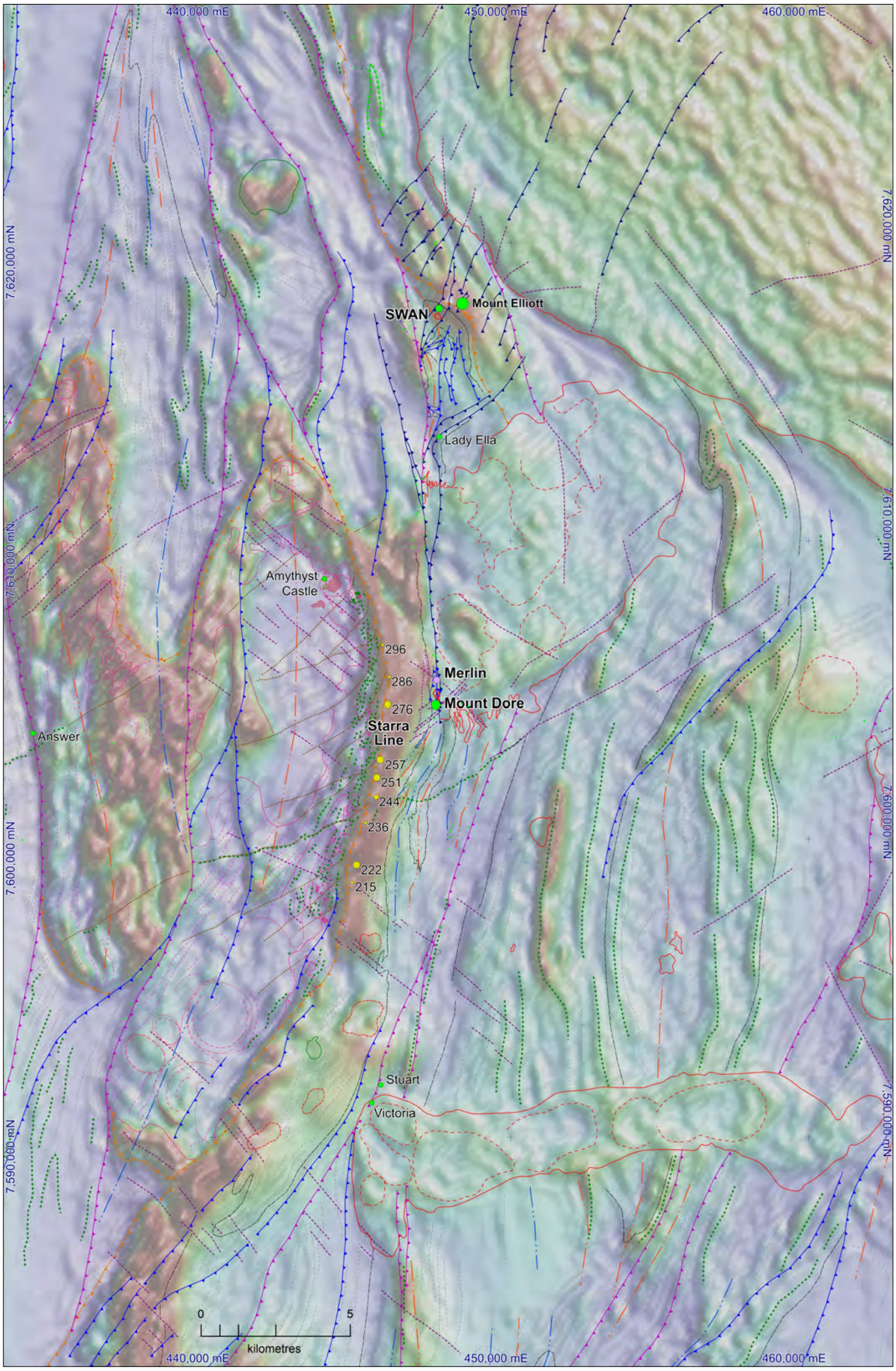

Figure 4.6: Regional Mount Isa 200m line-spaced magnetics. Colour tmi-rtp over greyscale tmi-rtp-2vd image with structural skeleton. Image area identical to Figure 4.4. Map Projection GDA94 (MGA54)

folds and linked ramp structures likely remain unidentified especially within the highly deformed and metasomatised (and recessive) Staveley Formation calc-silicate packages (Marshall, 2003).

In the Selwyn region (Figure 4.4), the Starra Shear is interpreted to have initiated as a D1 structure, thrusting Staveley Formation over exhumed Double Crossing Metamorphics and Gin Creek Granite and being folded during D2. At Mount Elliott-SWAN, potential Toole Creek Volcanic-Answer Slate equivalents are interpreted to be in D1 thrust juxtapositioning with Staveley and Kuridala Formations (Murphy et al., 2017).

Around 1555-1535Ma thick-skinned, Isan D2 orogeny is associated with east-west shortening and the development initially of large scale north-south meridional folds of both stratigraphy and earlier D1 folds and thrusts (eg. folded Starra Shear, Figure 4.4). Subsequently, when shortening could no longer be accommodated by folding, regional scale D2 reverse faulting with very significant strike extents and major throws juxtapose packages of contrasting ages, compositions and metamorphic grades (Figure 4.4).

Progressive high temperature-high pressure metamorphism and the hypothesized emplacement of voluminous mafic magma into the lower crust (Mark et al., 2004; Rubenach et al., 2008) during ongoing D3-D4 deformation yields the 1550-1500Ma Williams-Naraku Suites of A-type batholithic intrusions that are emplaced at mid crustal levels.

North-northwest to north-northeast trending D3 folding and faulting (ca1525-1520Ma) is locally and heterogenously developed in a significantly thickened crust (Bell & Hickey, 1998; Murphy, 2004; Austin & Blenkinsop, 2008) under ongoing east-west'ish shortening.

Between 1515Ma and 1500Ma voluminous Williams-Naraku intrusion into the middle and upper crust is accompanied by rotated D4 northwest-southeast shortening. The shallower crustal levels promote brittle deformation where specific post-peak metamorphic lithologies are amenable to brittle deformation and not prone to pre-existing fabric 'ductile' re-activation (Murphy et al., 2017).

In addition, strain partitioning around crystallising granites results in fracturing and brecciation of brittle lithologies. Significant boudinage of metadolerite sills around Mount Elliott focus iron oxide alteration and suggest strong strain partitioning adjacent to the Williams-aged Squirrell Hills Granite (Figure 4.4 and 4.20).

In contrast with D2 and D3 structures, brittle D4 structures are generally small-scale with relatively small displacements but commonly accompanied by significant damage zones.

Circulating IOCG fluids focus into D4 brittle fracture and breccia networks to form the IOCG Cu-Au-Mo deposits of the Eastern Fold Belt in this latter phase of Isan Orogeny.

In the Selwyn region (and in the wider Eastern Fold Belt) significant subsurface Williams-aged intrusions have been modelled (Murphy et al., 2017) and are evidenced at Selwyn by multiple small intrusive apophasis mapped and interpreted south of the Mount Dore Granite (Figure 4.4). Subsurface Williams-Naraku Granite morphology is hypothesized to play a significant role in hydrothermal fluid flow and therefore IOCG Cu-Au-Mo prospectivity (Murphy et al., 2017)

Figure 4.7 Solid geology compilation-interpretation of the Selwyn Region deposits and resources in the Eastern Fold Belt of the Mount Isa block from Deep Mining Queensland (Murphy et al. 2017). Legend as for Figure 4.4. Map Projection GDA94 (MGA54)

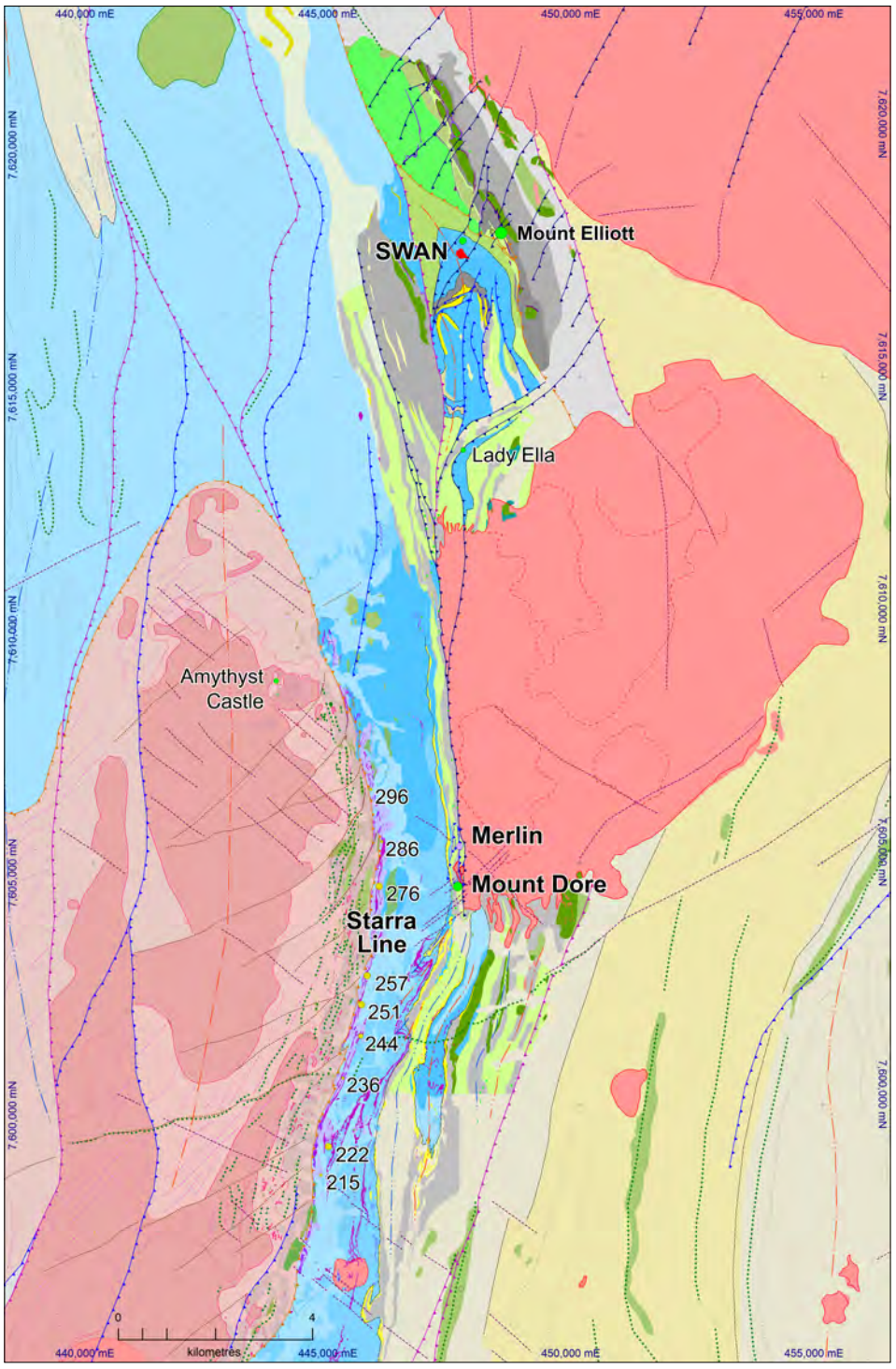

REGIONAL GEOPHYSICAL EXPRESSION

One hundred meter line-spaced, detailed aero-magnetics and radiometrics (2018 '1370' Cloncurry Survey) combined with Chinova Resources 2012 ground gravity and 2011 Heli-TEM data (Figures 4.8-4.16) have highlighted a number of regional to prospect scale features that characterise the geophysical settings and expressions of Selwyn Cu-Au-Mo deposits and resources. Figures 4.7 to 4.17 present the detailed geology, aero-magnetic, ground gravity, Heli-TEM and aero-radiometric data over the Selwyn region.

Magnetic, Gravity & TEM

The magnetic, gravity and TEM data (Figures 4.8-4.11) highlight the following when compared with the compiled geology (Figure 4.7):

- Portions of the Wong-deformed Double Crossing Metamorphics which are hornfelsed and intruded by the Wonga-aged Gin Creek Granite are strongly magnetic.
- The Double Crossing Metamorphics and Gin Creek Granite have low EM response (conductivity) apart from an area around Amythest Castle (of unknown origin).
- The Gin Creek Granite has low magnetic susceptibility compared with the Williams-aged Mount Dore and Squirrel Hills Granites.
- The interbedded, variably calcareous, siltstone-sandstone Staveley Formation has a well bedded, moderate to low magnetic susceptibility expression (eg. west of Lady Ella) and moderate conductivity (eg. east of Starra 286 to 222) **except** where it has been strongly calc-silicate altered (eg. between the Mount Dore Granite and the Double Crossing Metamorphics north of Merlin, and at SWAN) where it exhibits strong, incoherent magnetic signatures and low conductivity (destruction of more conductive silt layers).
- The phyllitic and carbonaceous metasiltstone Kuridala Formation (eg. south & immediately west of the Mount Dore Granite) has subdued magnetic susceptibility and low residual gravity signatures (apart from its metadoleritic sills). Its carbonaceous metasiltstone components are strongly conductive. Some cultural features are present in the EM response.
- The poorly-constrained package north of Mount Elliott (Figures 4.4 & 4.8), previously mapped as Kuridala Formation but potentially Toole Creek Volcanic equivalent (see Regional Geology above; Murphy et al., 2017) has strong magnetic and gravity signatures due to its significant metabasalt and metadolerite components in very stark contrast with the relatively quiet Kuridala Formation signatures south of the Mount Dore Granite.
- The New Hope Sandstone has a strongly banded, low to moderate magnetic signature and low conductivity EM response.
- The chlorite-magnetite schists and magnetite iron formations along the Starra Line have a very strong magnetic response, a strong residual gravity response and low EM conductivity response. Individual deposits along the Starra Line do not show particular magnetic, gravity or EM responses despite the whole zone exhibiting significantly anomalous alteration signatures compared to the adjacent Staveley Formation.
- The SWAN and Mount Elliott deposits are associated with a broad and strong magnetic anomaly suggesting significant magnetite addition over significant volumes at depth (see following Mount Elliot -SWAN Section).
- Metadolerites in all packages and the metabasalt north of Mount Elliott have strong magnetic and gravity expression.
- The Merlin and Mount Dore deposits do not have direct magnetic or gravity expression but, not unlike the overall Starra Line, appears to be associated with some loss of EM conductivity response. At Merlin-Mount Dore the loss is within/from the Kuridala Formation carbonaceous meta siltstones, while at Starra the loss appears to be focused along the Starra Shear and is likely the product of alteration of the more conductive siltstones within the western portions of the Staveley Formation (see following Merlin-Mount Dore and Starra Sections).
- In this light, the very significant loss of EM conductivity response and de-texturing of the magnetic response associated with calc-silicate alteration of the Staveley Formation north and west of Merlin is of significant interest.

Figure 4.8 (top left opposite) Detailed 100m line-spacing, 2018 '1370' Cloncurry TMI-RTP-1VD Magnetic Image with major deposits & resources and structural skeleton overlain. Same map area as Figure 4.7. Map Projection GDA94 (MGA54)

Figure 4.9 (bot left opposite) Detailed 100m line-spacing, 2018 '1370' Cloncurry TMI-RTP-2VD overlain on coloured TMI-RTP with Gaussian stretch. Magnetic Image with major deposits & resources and structural skeleton overlain. Same map area as Figure 4.7. Map Projection GDA94 (MGA54)

Figure 4.10 (top right opposite) Merged detailed 2012 Residual Bouguer Anomaly ground gravity data with major deposits & resources and structural skeleton overlain. Same map area as Figure 4.7. Map Projection GDA94 (MGA54)

Figure 4.11 (bot right opposite) Detailed 100m line-spacing, 2011 Heli-TEM EM Amplitude Channel 15 with major deposits & resources and structural skeleton overlain. Same map area as Figure 4.7. Map Projection GDA94 (MGA54)

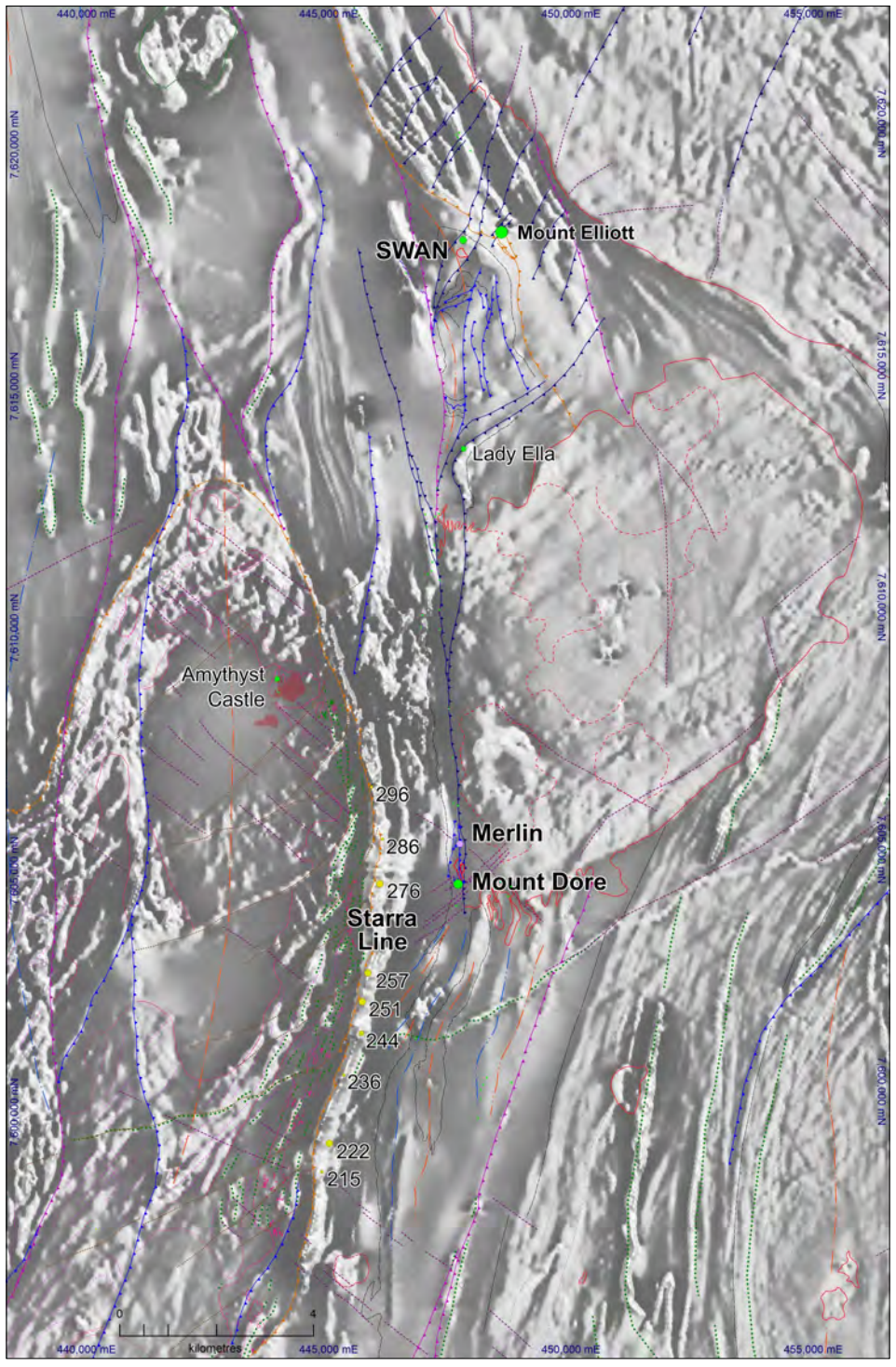
SWAN
Mount Elliott
Lady Ella
Amythyst Castle
296
286
276
Merlin
Mount Dore
Starra Line
257
251
244
236
222
215
440,000 mE
445,000 mE
450,000 mE
455,000 mE
7,620,000 mN
7,615,000 mN
7,610,000 mN
7,605,000 mN
7,600,000 mN
0
4
kilometres

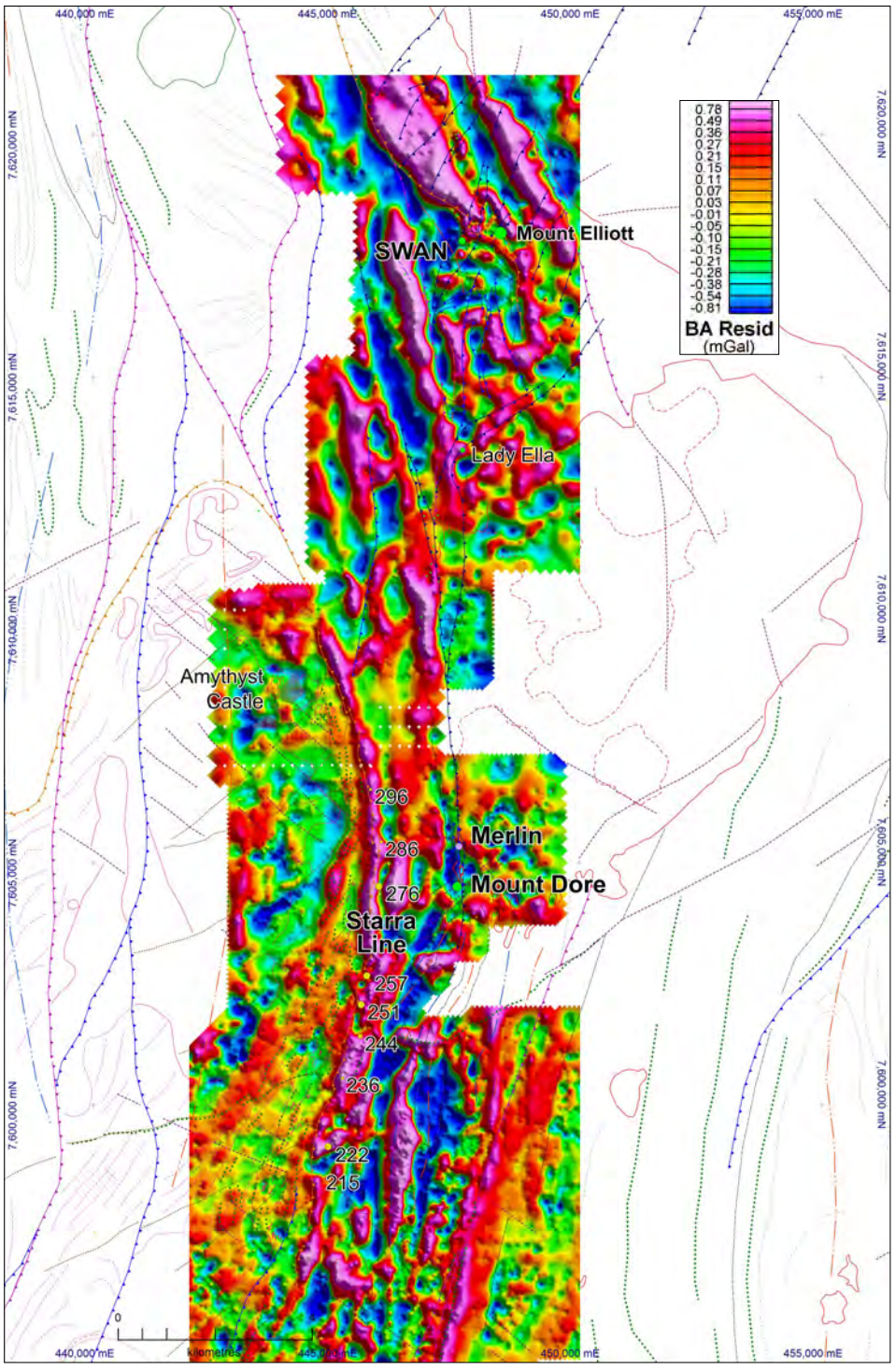
0.78
0.49
0.36
0.27
0.21
0.15
0.11
0.07
0.03
-0.01
-0.05
-0.10
-0.15
-0.21
-0.28
-0.38
-0.54
-0.81
BA Resid
(mGal)
SWAN
Mount Elliott
Lady Ella
Amythyst Castle
296
286
276
Merlin
Mount Dore
Starra Line
257
251
244
236
222
215
440,000 mE
445,000 mE
450,000 mE
455,000 mE
7,620,000 mN
7,615,000 mN
7,610,000 mN
7,605,000 mN
7,600,000 mN
0
kilometres

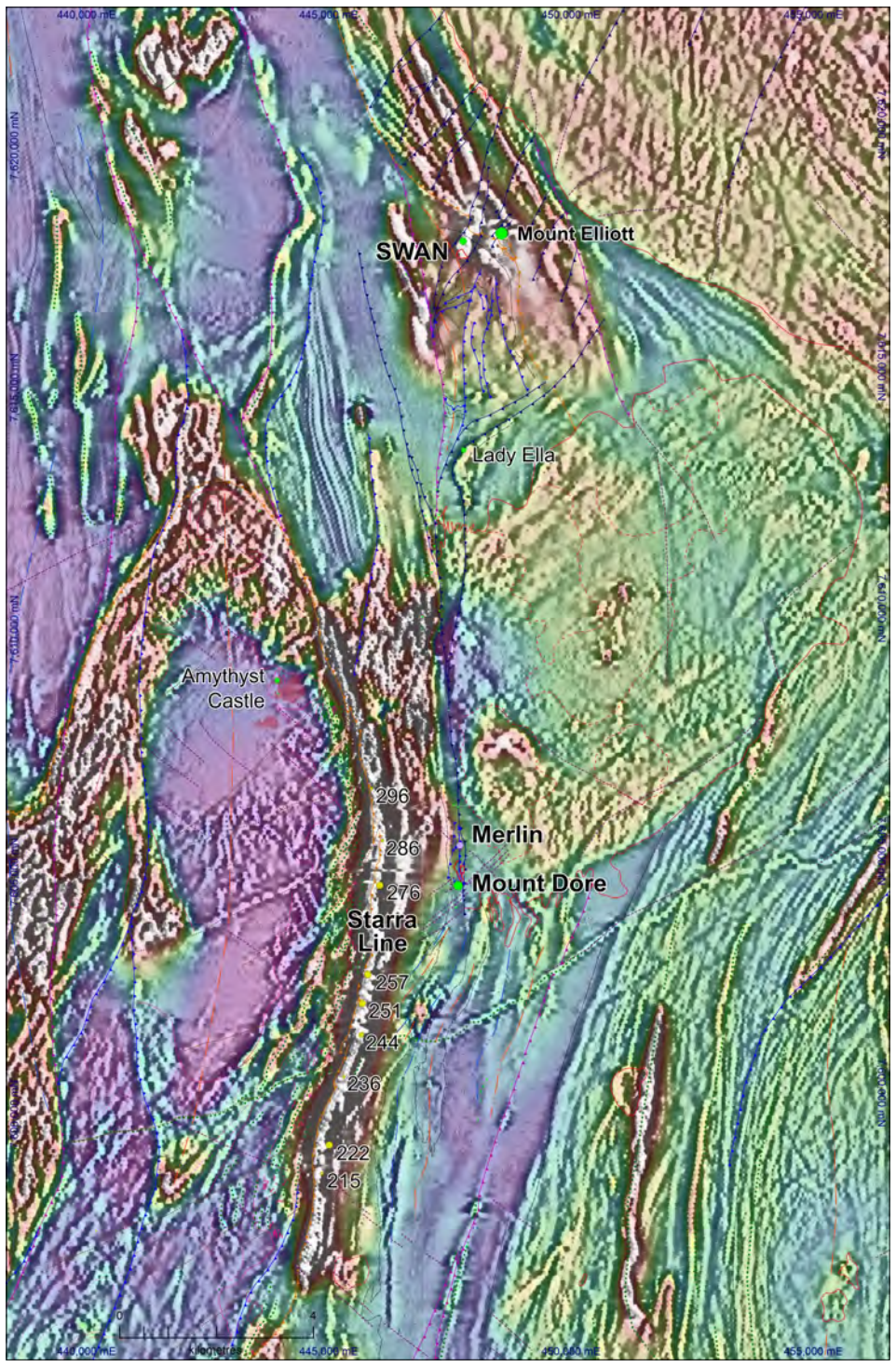
SWAN
Mount Elliott
Lady Ella
Amythyst Castle
296
286
276
Merlin
Mount Dore
Starra Line
257
251
244
236
222
215
440,000 mE
445,000 mE
450,000 mE
455,000 mE
7,620,000 mN
7,615,000 mN
7,610,000 mN
7,605,000 mN
7,600,000 mN
0
4
kilometres

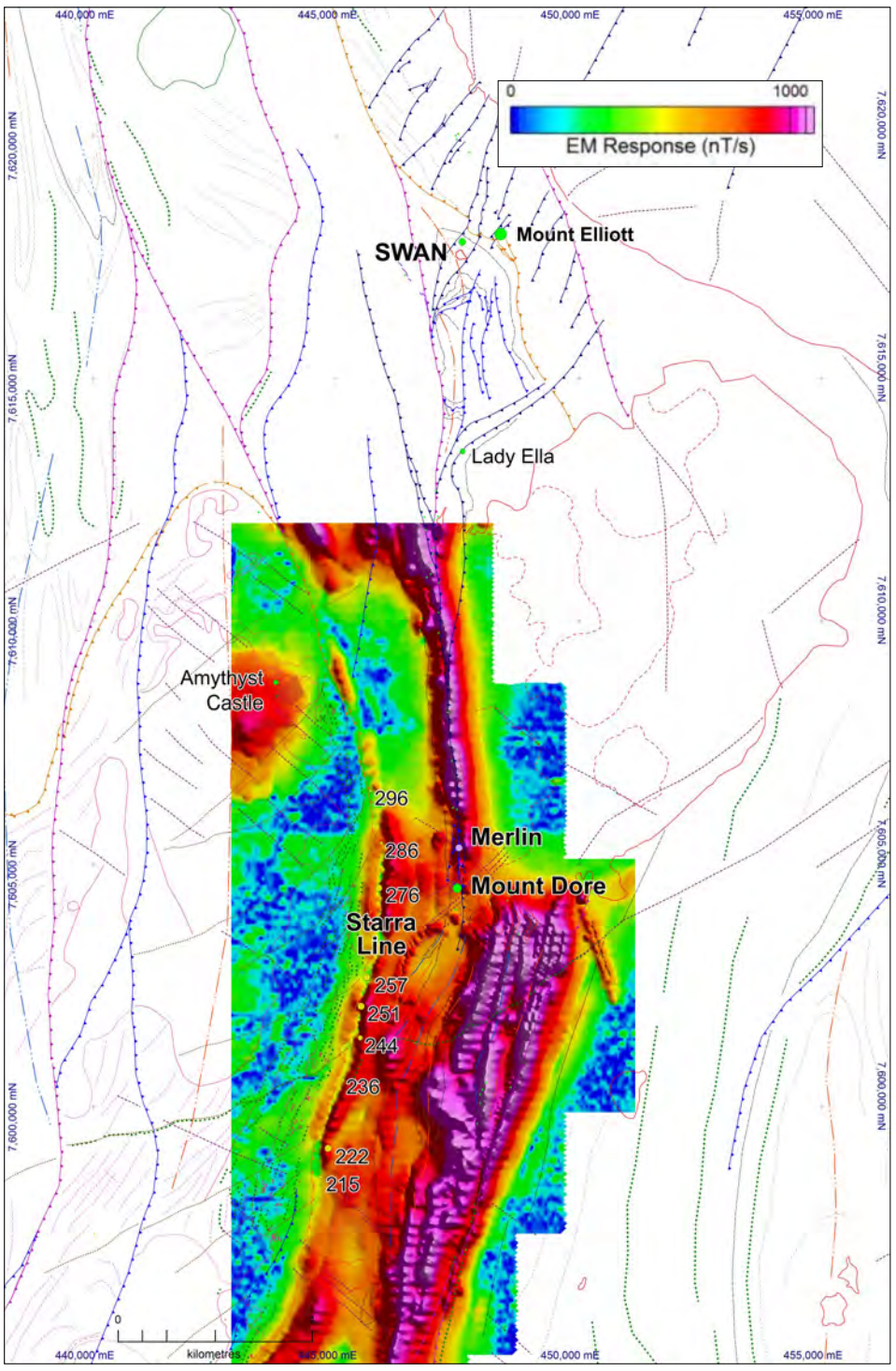
0
1000
EM Response (nT/s)
SWAN
Mount Elliott
Lady Ella
Amythyst Castle
296
286
276
Merlin
Mount Dore
Starra Line
257
251
244
236
222
215
440,000 mE
445,000 mE
450,000 mE
455,000 mE
7,620,000 mN
7,615,000 mN
7,610,000 mN
7,605,000 mN
7,600,000 mN
0
kilometres

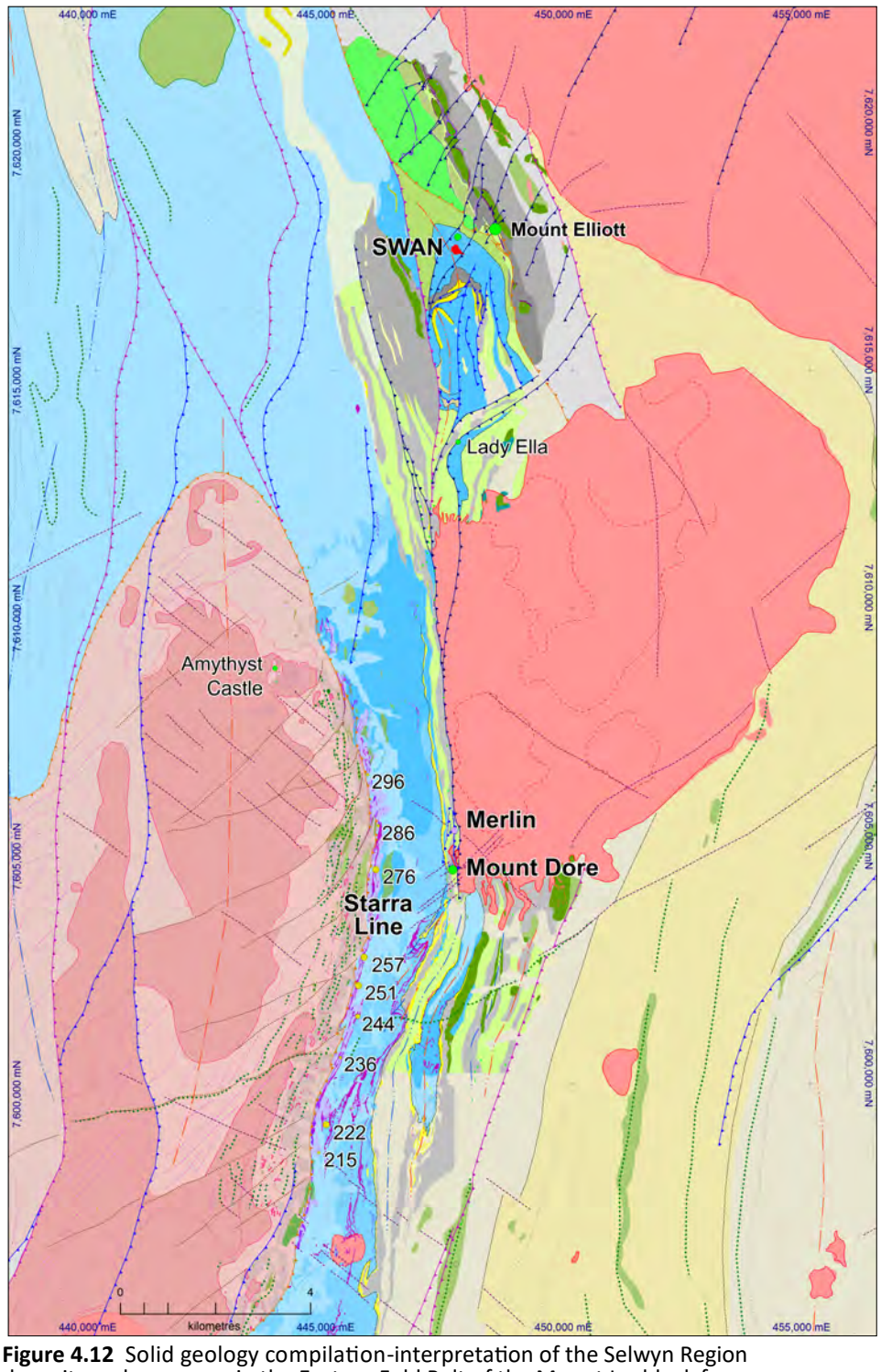

Figure 4.12 Solid geology compilation-interpretation of the Selwyn Region deposits and resources in the Eastern Fold Belt of the Mount Isa block from Deep Mining Queensland (Murphy et al. 2017). Legend as for Figure 4.4. Map Projection GDA94 (MGA54)

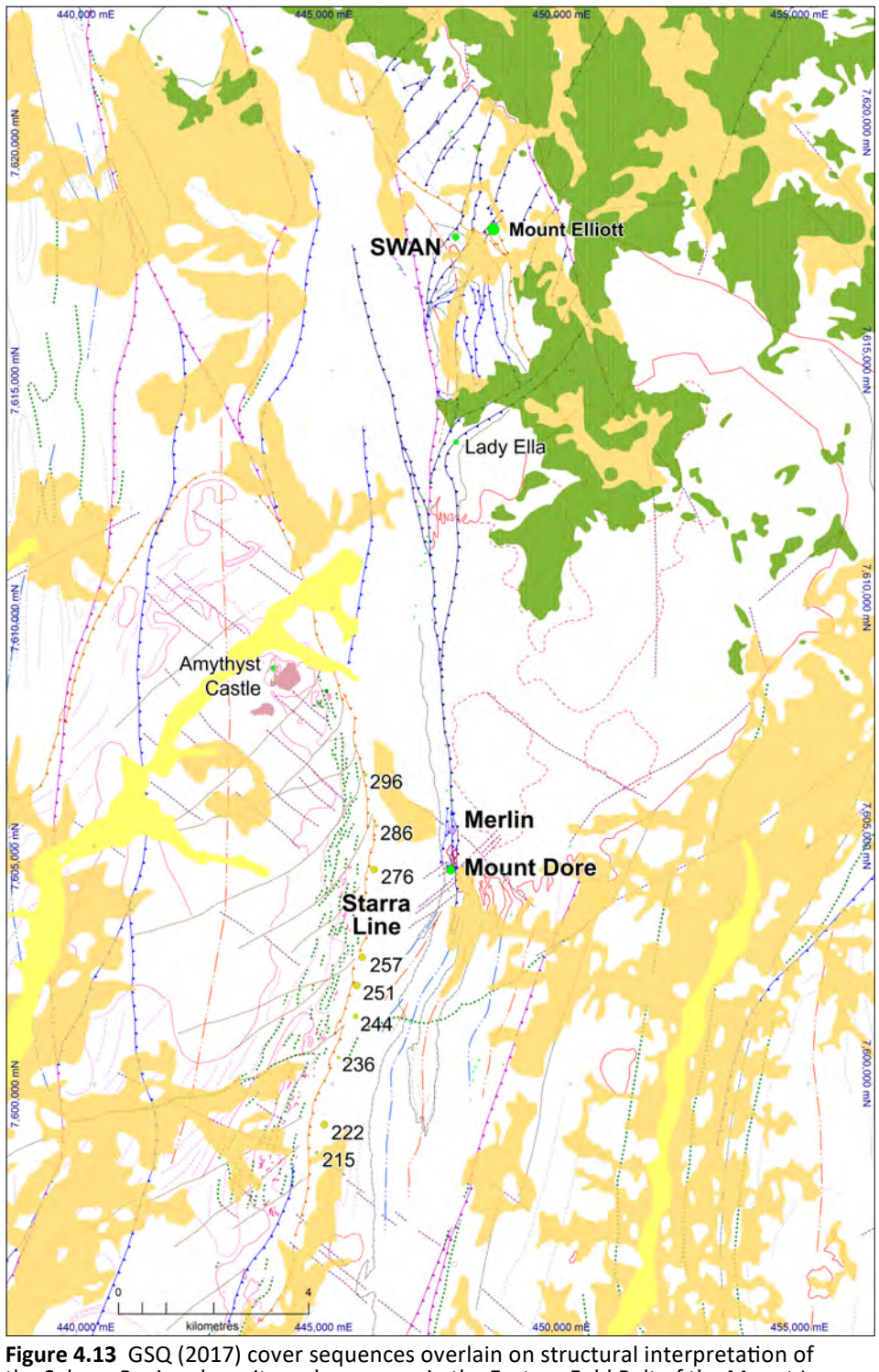

Figure 4.13 GSQ (2017) cover sequences overlain on structural interpretation of the Selwyn Region deposits and resources in the Eastern Fold Belt of the Mount Isa block from Deep Mining Queensland (Murphy et al. 2017). Legend as for Figure 4.4. Map Projection GDA94 (MGA54)

Radiometrics

The 2018, '1370' Cloncurry Survey, detailed radiometric data (Figures 4.14-4.17) highlight the following when compared with the compiled geology (Figure 4.12), the distribution of Mesozoic to Recent cover rocks (Figure 4.13) and the magnetic, gravity and TEM data (Figures 4.8-4.11) on the previous pages:

- The Mount Dore, the (largely covered) Squirrel Hills and the small Mount Cobalt Granites (south of the Mount Dore Granite) all have strong K, Th and U radiometric responses. Some potentially different intrusive phases in the central and southern Mount Dore Granite are suggested in the radiometric K response.
- The Staveley and Kuridala Formations exhibit patchy radiometric K and U anomalism reflecting their fine-grained sediment components **while** the calc-silicate altered portions of the Staveley Formation highlighted in the magnetics (Figures 4.8-4.9) west of the Mount Dore Granite have stronger and more coherent radiometric K and U responses reflecting alteration.
- The Roxmere Quartzite ridge (and its scree slopes) towards the stratigraphic top of the Staveley Formation is devoid of K anomalism but does appear to be U anomalous.
- Mount Elliott, SWAN and Amythyst Castle all shown strong radiometric U responses.
- Merlin and Mount Dore while situated at the southern end of the strongly K and U anomalous Staveley calc-silicate zone are not themselves anomalous.
- The Starra Line and the Starra deposits are not associated with any K or U anomalism. Rather they may be relatively U depleted.
- Patchy U anomalism along the southern margin of the Mount Dore Granite appears to be in Kuridala Formation and New Hope Sandstone but may reflect secondary accumulation in Tertiary sediments shed from the Mount Dore Granite.
- The U^2/Th treatment of the radiometric data highlights U anomalism not associated with Th anomalism in an attempt to focus on alteration U rather than direct intrusive-related U. Mount Elliott, SWAN, Amythyst Castle and the calc-silicate altered Staveley Formation west of the Mount Dore Granite are again strongly highlighted. The strong anomalism northwest of Mount Elliott remains relatively uninvestigated.

Figure 4.14 (top left opposite) Detailed 100m line-spacing, 2018 '1370' Cloncurry Potassium Radiometric Image with major deposits & resources and structural skeleton overlain. Same map area as Figure 4.7. Map Projection GDA94 (MGA54)

Figure 4.15 (top right opposite) Detailed 100m line-spacing, 2018 '1370' Cloncurry Thorium Radiometric Image with major deposits & resources and structural skeleton overlain. Same map area as Figure 4.7. Map Projection GDA94 (MGA54)

Figure 4.16 (bot left opposite) Detailed 100m line-spacing, 2018 '1370' Cloncurry Uranium Radiometric Image with major deposits & resources and structural skeleton overlain. Same map area as Figure 4.7. Map Projection GDA94 (MGA54)

Figure 4.17 (bot right opposite) Detailed 100m line-spacing, 2018 '1370' Cloncurry Radiometric Image displaying ($Uranium^2/Thorium$) with major deposits & resources and structural skeleton overlain. Same map area as Figure 4.7. Map Projection GDA94 (MGA54)

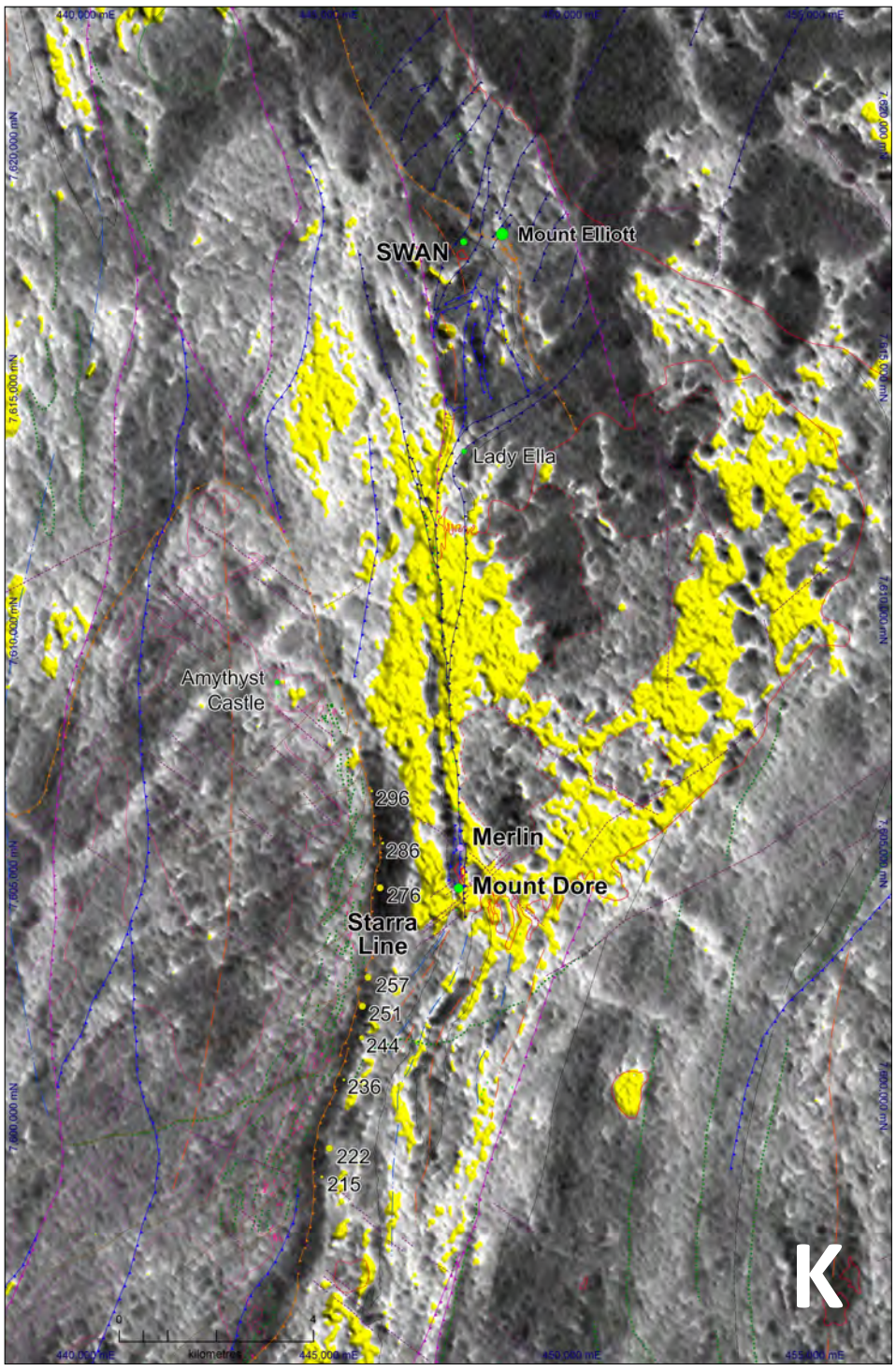
SWAN
Mount Elliott
Lady Ella
Amythyst Castle
296
286
276
Starra Line
257
251
244
236
222
215
Merlin
Mount Dore
K

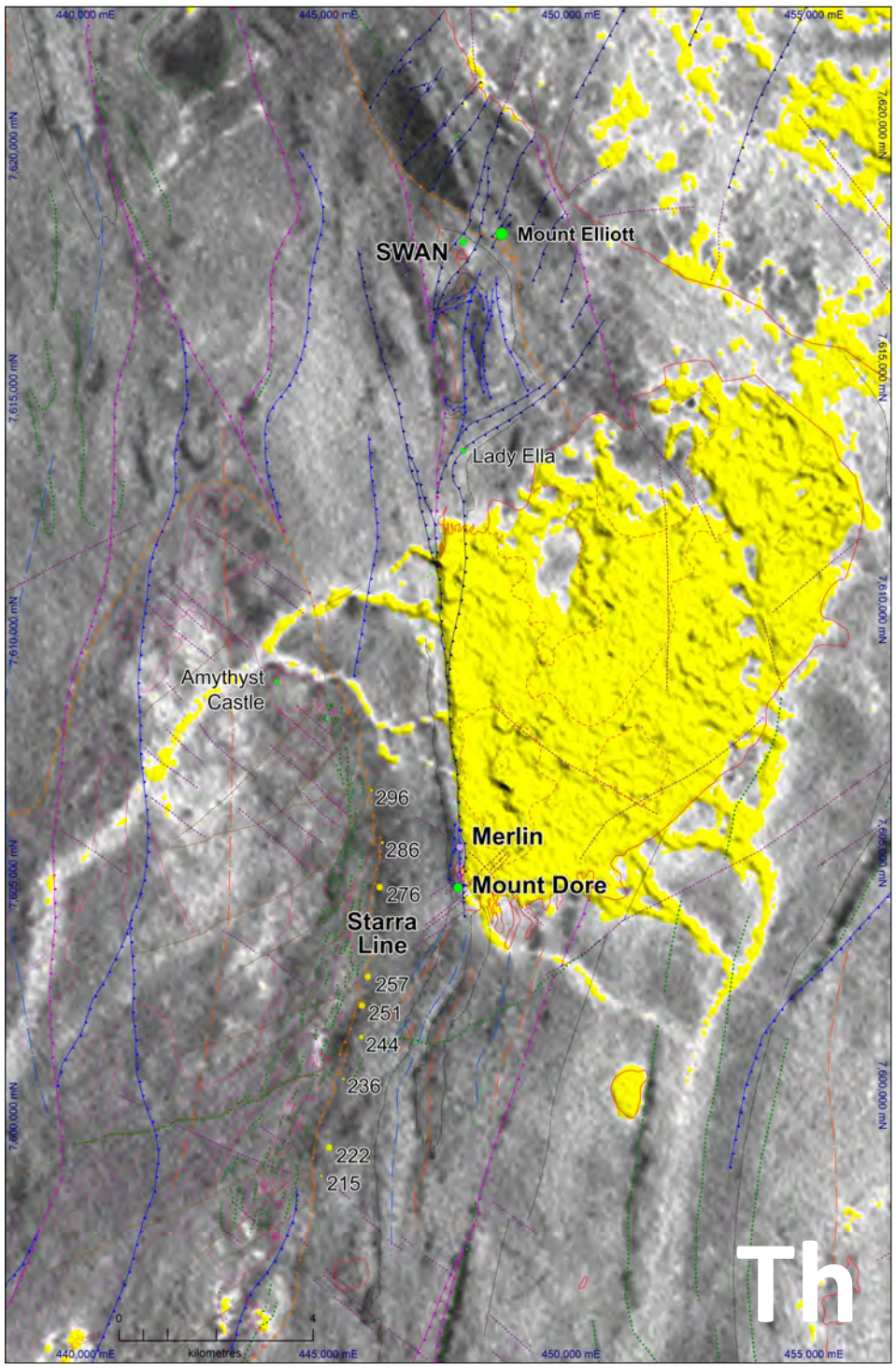
SWAN
Mount Elliott
Lady Ella
Amythyst Castle
296
286
276
Starra Line
257
251
244
236
222
215
Merlin
Mount Dore
Th

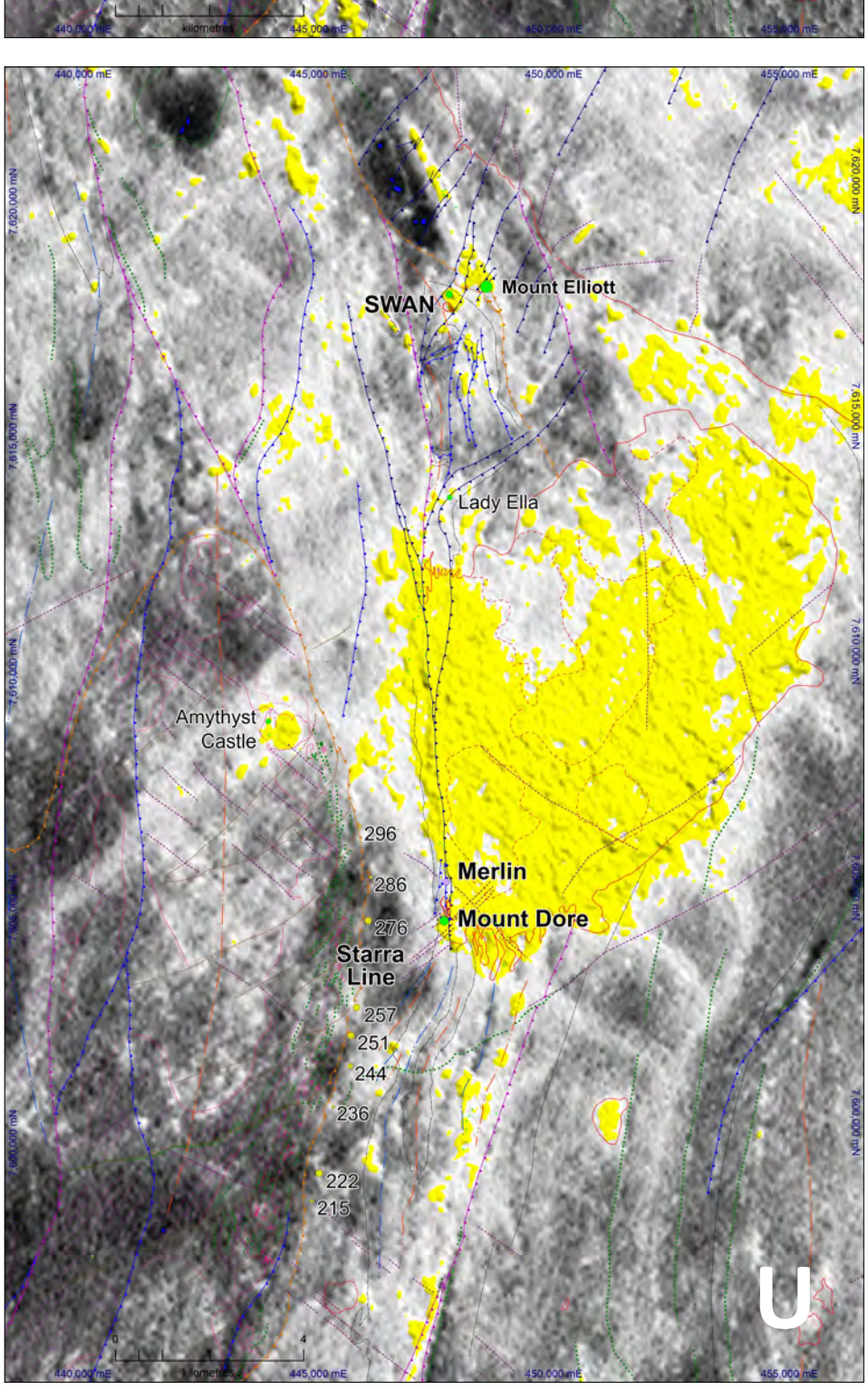
SWAN
Mount Elliott
Lady Ella
Amythyst Castle
296
286
276
Starra Line
257
251
244
236
222
215
Merlin
Mount Dore
U

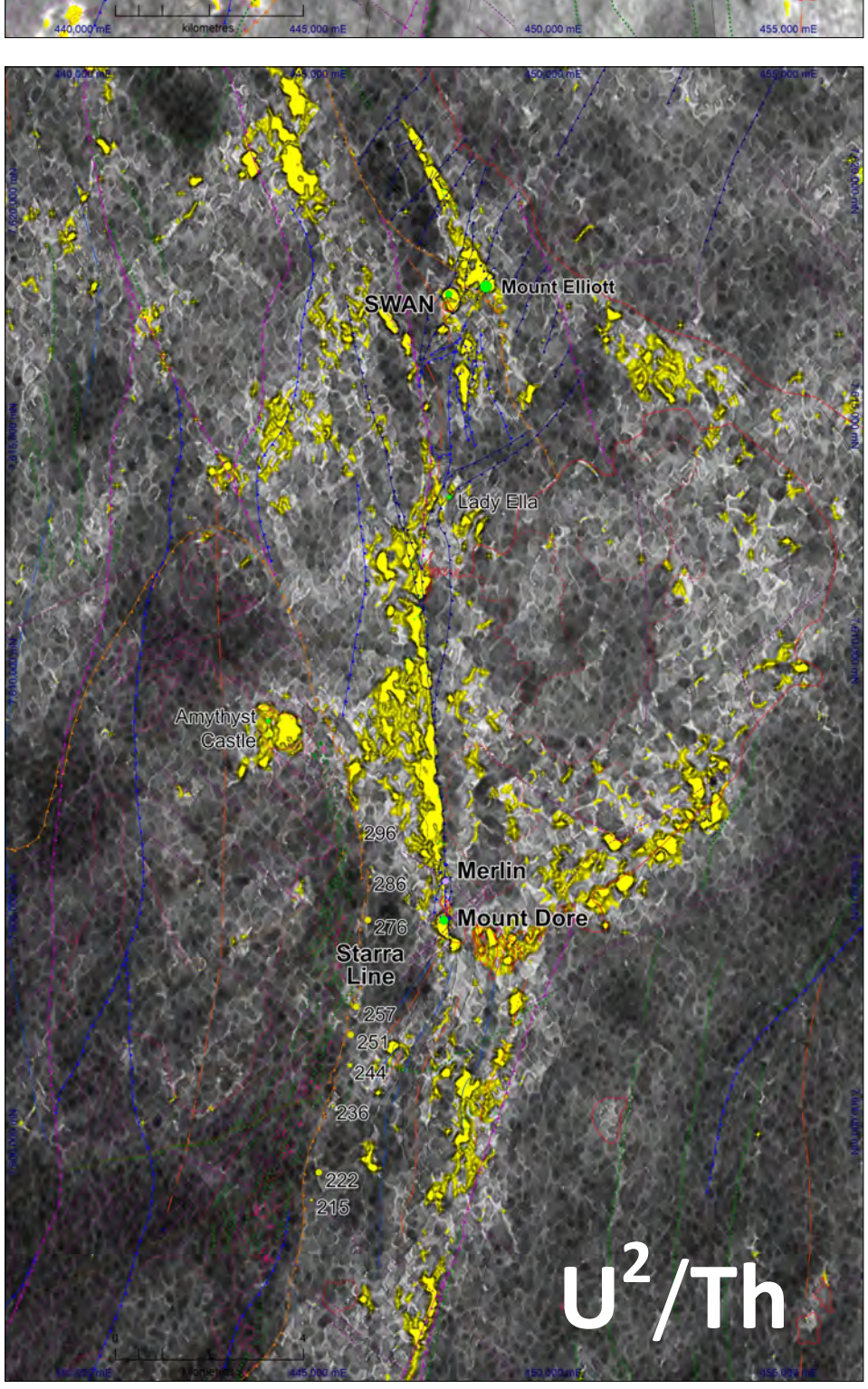
SWAN
Mount Elliott
Lady Ella
Amythyst Castle
296
286
276
Starra Line
257
251
244
236
222
215
Merlin
Mount Dore
U²/Th

Mount Elliott-SWAN Cu-Au Deposits

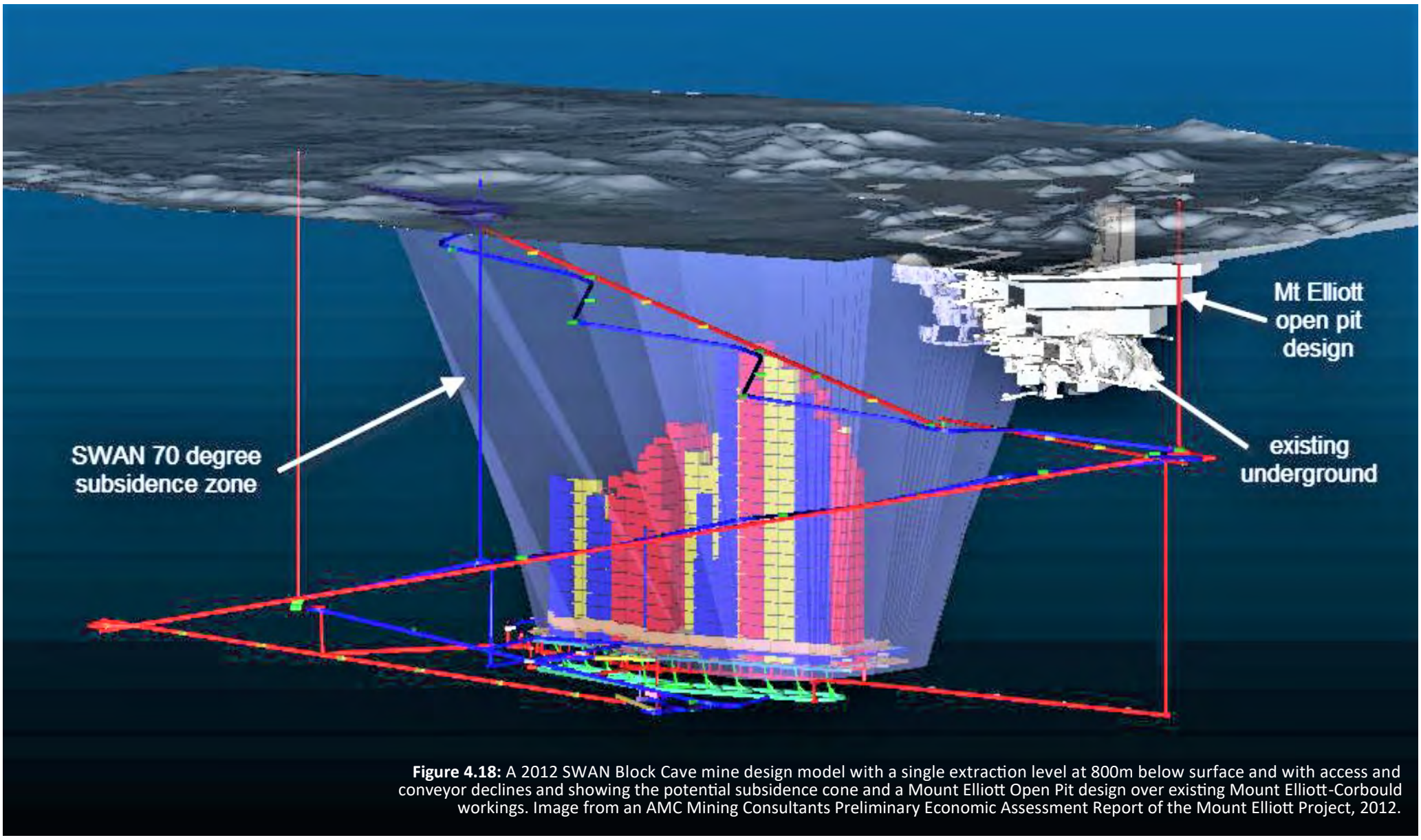

Figure 4.18: A 2012 SWAN Block Cave mine design model with a single extraction level at 800m below surface and with access and conveyor declines and showing the potential subsidence cone and a Mount Elliott Open Pit design over existing Mount Elliott-Corbould workings. Image from an AMC Mining Consultants Preliminary Economic Assessment Report of the Mount Elliott Project, 2012.

PRODUCTION AND DIMENSIONS

Mineralised bodies

Historic Mount Elliott and Corbould production has come from northwest-trending, moderately to steeply northeast-dipping stopes over a volume of 450m strike, 150m width and depths to around 360m below surface (Figures 4.20 & 4.24). The SWAN resource has a crude 70° northward plunge and an overall extent of 1300m strike, 400m width and 1300m depth extent (Figures 4.20 & 4.24). SWAN mineralisation starts just 8 meters below surface (Chinova, 2015).

Historic Production and Resources

The Mount Elliott gossan was discovered by James Elliott, a hermit gold prospector in 1899. Small scale mining commenced in 1901 and the Mount Elliott Company was formed in London and floated on the Melbourne Stock Exchange in 1906 (Brown & Porter, 2010; Chinova, 2015). The smelter (Figure 4.19) was designed by William Henry Corbould and built in 1908. Cyprus (1991) reported two periods of early mine production:

1901-1909: 161kt @ 11.8%Cu, 6.5g/tAu
1909-1919: 102kt @ 5.2%Cu, unknown Au

A depletion of high grade ore, falling copper prices and labour unrest resulted in both mining and smelting ceasing around 1921.

No work was done for several decades until between 1952 and 1957 drilling under the existing Mount Elliott workings by Broken Hill South, Mount Isa Mines and Rio Tinto Southern confirmed lower grade extensions under the existing workings (Fortowski & McCracken, 1998).

Between 1972 and 1975 a joint venture between Union Miniere and Anaconda Australia undertook detailed geological mapping, stream sediment sampling and airborne magnetics and identified a coincident geochemical anomaly and circular magnetic feature known as the Southwest Magnetic Anomaly (later to become SWAN) 500m to the west-southwest of Mount Elliott. Drilling intersected significant thickness of ~1%Cu, 1g/tAu but the JV withdrew in 1975 to concentrate on the more promising Starra string of deposits 15km to the south.

In 1978, the Selwyn Mining Project partners (Amoco Minerals Australia (later Cyprus Minerals), Arimco NL and Elders Resources NL) acquired title to the area and carried out detailed resource definition drilling at Mount Elliott and SWAN. In 1989 they released resource estimates but did not proceed to production.

Mount Elliott: 2.9Mt @ 3.33%Cu, 1.47g/tAu
SWAN: 13.5Mt @ 0.9%Cu, 0.5g/tAu
(Fortowski & McCracken, 1998)

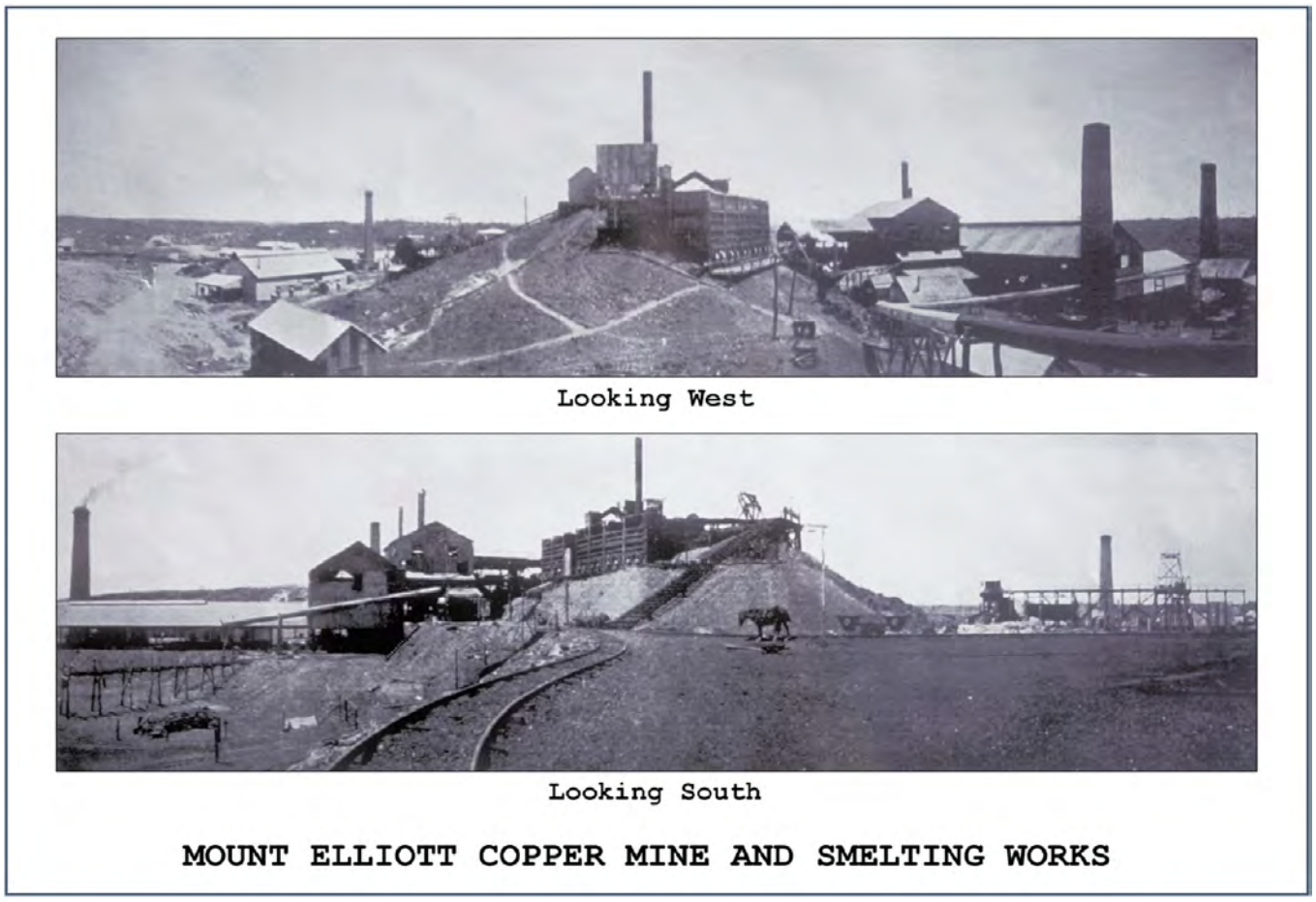

Figure 4.19 Mount Elliott Mine smelting works in the early 1900s

In 1993, Australian Resources Ltd purchased the Mining Lease titles, developed a decline into Mount Elliott and produced ore in 1994. The Corbould zone, west of Mount Elliott was discovered in 1995 and a resource was defined.

Corbould: 0.55Mt @ 3.35%Cu, 1.5g/tAu
(Fortowski & McCracken, 1998)

In 1999, Australian Resources Ltd went into receivership and the Mount Elliott Mine closed until 2000 when Selwyn Mines Ltd purchased the operations. Selwyn Mines carried out further resource drilling, re-evaluated the reserves and resources and re-started mining at Mount Elliott with a revised resource.

Mount Elliott: 11Mt @ 2.9%Cu, 1.2g/tAu
(using 1.5eq%Cu cut-off)
within: 20Mt @ 1.11%Cu, 0.57g/tAu
(Sleigh, 2002a,b)

A re-evaluation of SWAN at the same time produced a resource estimate.

SWAN: 43Mt @ 0.58%Cu, 0.4g/tAu
(using 0.5eq%Cu cut-off)

Low metal prices again forced mine closure in 2003 but between 1993 and 2003 the Mount Elliott-Corbould mine had produced significant ore.

1993-2003: 5.6Mt @ 2.9%Cu, 1.5g/tAu

Ivanhoe Cloncurry Mines Ltd purchased the Mining Leases in late 2003. Between 2003 and 2008 Ivanhoe focused on various possibilities at SWAN including (1) a shallow oxide resource for heap leach that founded due to poor metallurgical recoveries, (2) a down-dip search for higher grade transition zone ore that did not return significant grades, and (3) in 2006, a northern down-plunge search for transition ore based on a then northern-most, mixed chalcocite and chalcopyrite intercept of 147m @ 0.69%Cu, 0.38g/tAu including 13m @ 1.92%Cu, 0.56g/tAu (Brown & Porter, 2010).

Subsequent deep holes (up to 1000m from surface) returned significant intercepts and defined a September, 2008 JORC compliant resource for an overall SWAN-Mount Elliott-Corbould-SWELL system of

475Mt @ 0.5%Cu, 0.3g/tAu
(Brown & Kirwin, 2009)

In 2013 when Ivanhoe sold Oyu Tolgoi to Rio Tinto, Ivanhoe Australia Ltd was forced to restructure and changed its name to Inova Resources Ltd and in December 2013 Inova Resources was brought by Shanxi Coal and Chemical Company, a private Chinese Company, and became Chinova Resources Pty Ltd (pers comm. Mark McGeough)

Further Chinova drilling in the region, refined the definition of shallower resources at Megelli and Domain 81 (see Figures 4.24-4.28). Overall drilling on the Mount Elliott-Corbould-SWAN-SWELL system totals 306,235m in 2,974 holes with 125,988m in 215 holes drilled by Ivanhoe-Inova-Chinova. The current indicated resources published by Chinova (2017) are:

Mount Elliott: 18.5Mt @ 1.04%Cu, 0.55g/tAu Corbould West: 1.1Mt @ 0.86%Cu, 0.86g/tAu SWAN: 154.5Mt @ 0.60%Cu, 0.37g/tAu

Detailed measured, indicated, inferred and total resources for all the Selwyn region including the Mount Elliott, Corbould and SWAN deposits are presented in Table 4.2.

The Mount Elliott surface smelter workings were placed on the Queensland Heritage Register in 2011.

HOST ROCKS

Mine Stratigraphy

Recent geological interpretation in the Selwyn region (Murphy et al., 2017) have suggested the potential complexity of geological relationships at Mount Elliott-SWAN (Figures 4.4 & 4.7). Previous interpretations have the bulk of the SWAN and SWELL mineralization hosted by Staveley Formation and the Mount Elliott and Corbould mineralized zones hosted within Kuridala Formation (Brown et al., 2009).

As outlined above (Regional Geology and Regional Deformation), on the basis of the very significant lithological and geophysical differences between the Mount Elliott-Corbould host packages and the well-exposed Kuridala Formation south of the Mount Dore Granite, the possibility that the Mount Elliott-Corbould host package is of Toole Creek Volcanic prodgeny and is in early (Isan D1) thrust juxtapositioning with folded Staveley-Kuridala Formation to their west, needs further investigation.

Figure 4.20 presents a zoomed view of the geology of the immediate Mount Elliott-SWAN region.

Host Rocks

The following lithological, alteration and mineralogical descriptions come from Fortowski and McCracken (1998), Brown and Porter (2010) and Gunter (2015).

SWAN is very largely hosted within a fracture and breccia system that has formed in banded and massive calc-silicates of the Staveley Formation (Fortowski & McCracken, 1998; Wang & Williams, 2001; Brown et al., 2009) whose precursors are interbedded calcareous sandstone, lesser siltstone and marble. Brown and Porter (2010) interpret a stratigraphy in the upper Staveley Formation at SWAN comprising more massive-dominated calc-silicate overlain by a more regularly banded calc-silicate unit (Figure 4.23C) but both are equally well mineralised.

The massive calc-silicates comprise calcite, tremolite-actinolite, albite, scapolite, muscovite and chlorite.

The banded calc-silicates are made up of cm-scale (0.5-10cm) bands of very fine grained, hematitic and albite-altered siltstone interlayered with coarse grained calc-silicate with the same mineralogy as the massive calc-silicate (Figure 4.23A).

Deformation in the banded calc-silicates is evidenced by boudinage accompanied by variable rotation of the siltstone band fragments in the calc-silicate matrix. Except in extreme cases, gross layering is commonly preserved.

The contact into the schists of the Kuridala Formation to the east (Figure 4.20) is gradational over 10-30m (Wang & Williams, 2001).

The Kuridala Formation schists (informally ‘Town Beds’) comprise quartz-mica schist and are locally strongly garnet-bearing and are only weakly mineralised due to their tight schistose nature.

Mount Elliott, Corbould and Domain 81 are hosted within a package of intensely altered carbonaceous meta-siltstones, phyllites, metabasalts, schists and metadoleritic/amphibolitic sills. The alteration has been described as skarn-like and variably comprises clinopyroxene, diopside-hedenbergite, actinolite, magnetite, biotite, scapolite, calcite and apatite (Wang & Williams, 1996; 2001).

A metabasaltic unit is the lowermost unit and comprises massive to vesicular flows (Figure 4.23D) with possible pillows separated by calcareous sediment. The metabasalt and its internal fabrics are truncated against the Staveley and Kuridala Formations to its west (Figures 2.20 & 2.21) to produce a south-plunging wedge that appears to control the overall location of Mount Elliott and Corbould. Domain 81 mineralisation is hosted in highly altered metabasalt.

The immediate host for Mount Elliott and Corbould (informally ‘Elliott Beds’), where unaltered, comprise fine grained, carbonaceous metasiltstones, phyllites and minor schists which are progressively altered to the ‘skarn’ mineralogy towards ore and to massive ‘skarn’ around lower ore bodies along the footwall contact with the Kuridala Formation schists (’Town Beds’ in Figure 4.31; Fortowski & McCracken, 1998). To the east fine-grained, carbonaceous phyllites and schists are composed predominantly of quartz, muscovite, biotite and graphite with local andalusite and bands of pyrite and pyrrhotite.

METAMORPHISM

Metamorphic Grade

Regional metamorphism in the Mount Elliott-SWAN region reached amphibolite facies (Fortowski & McCracken, 1998) during Isan D1-D2 deformation (Rubenach et al, 2008) prior to Cu-Au mineralisation.

INTRUSIVE ROCKS IN REGION

Granitoids

The Squirrel Hills Granite is a large batholithic granite intrusion of the William-Naraku Suite to the northeast of Mount Elliott-SWAN dated at 1514±4Ma and 1511±9Ma (Pollard & McNaughton, 1997).

Intermediate Intrusives

The relatively small (200-400m diameter; Figure 4.20) SWAN Diorite intrudes the Staveley Formation immediately to the southwest of the near surface SWAN mineralisation and has an intimate spatial relationship with brecciation and SWAN mineralisation at depth (Figures 4.20, 4.24-4.30). Murphy et al. (2017) attribute brecciation controlling SWAN mineralisation to deformation partitioning within the brittle Staveley Formation calc-silicates between the rigid Diorite and the schistose Kuridala Formation.

The SWAN Diorite is not as yet dated but is potentially ca1657Ma, the same age as the Ernest Henery Diorite and the Tommy Creek Microgranite.

Mafic Intrusives

Metadoleritic sills intrude the fine grained metasediments in the belt east of Mount Elliott. They are regarded as being approximately syn-depositional with their hosting sediments, are metamorphosed to hornblende-plagioclase mineralogy (Brown & Porter, 2010) and have been significantly boudinaged during Isan Orogeny.

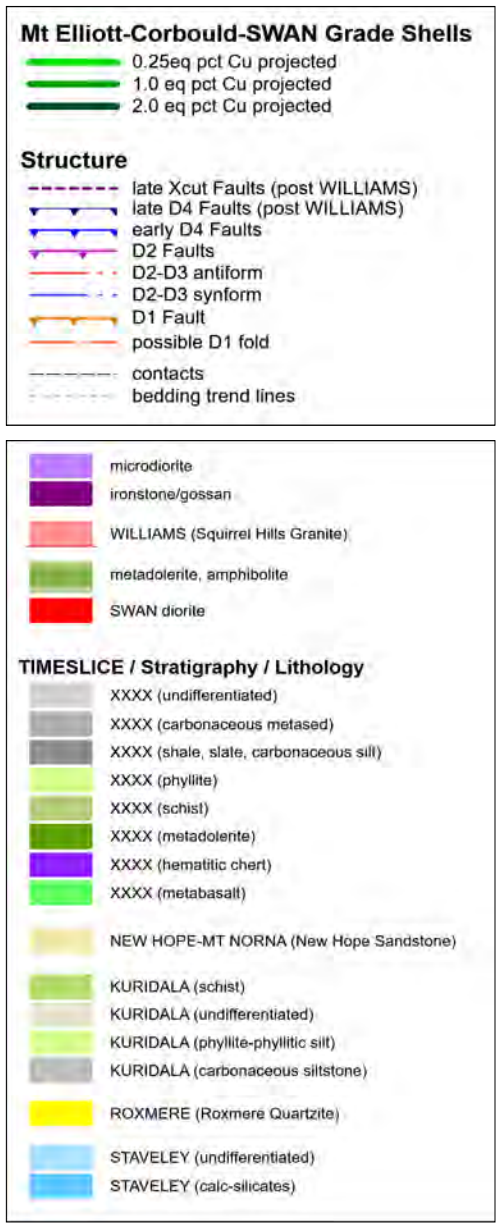

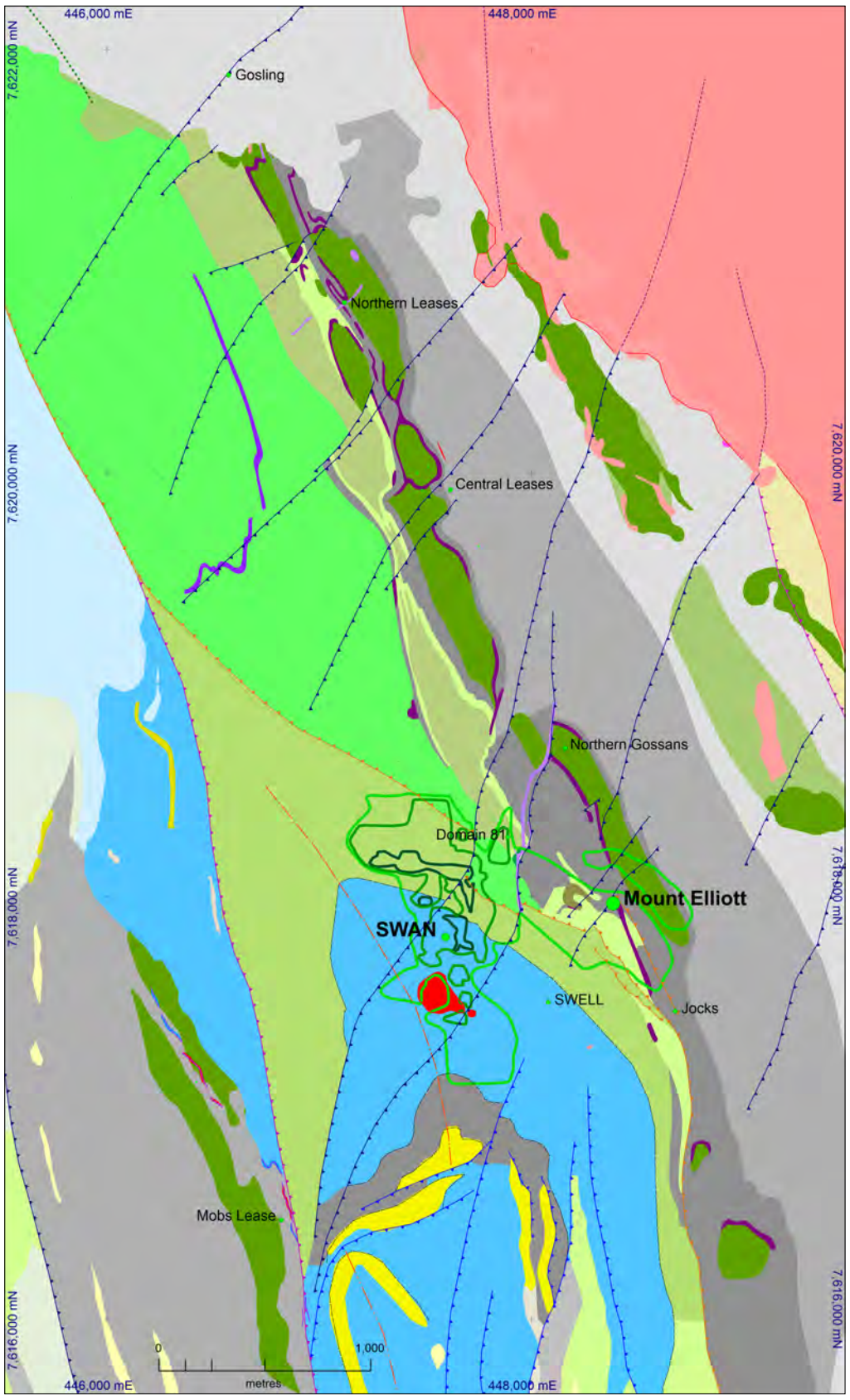

Figure 4.20 Detailed geology of the Mount Elliott-SWAN region compiled from historic and recent company mapping and interpretation with vertically projected grade shells. Mapping and interpretation attribution as in Figure 4.5. Structural interpretation from Deep Mining Queensland (Murphy et al., 2017). Map Projection GDA94 (MGA54)

Other Intrusives

Fine- to medium-grained, unmetamorphosed, post-mineral, microdioritic (Fortowski & McCracken, 1998) dykes of a few to tens of meters thickness exploit late faults and fractures (Figure 4.20), are intercepted in the drilled SWAN volume and been mapped in the Corbould Mine (Little, 1997). Brown & Porter (2010) suggest they have trachyandesite composition and Gunter (2015) report that they were the trachyandesites dated by Duncan et al. (2011) with ages of 1116±12Ma.

STRUCTURAL CHARACTERISTICS

Structural Setting

The Mount Elliott-Corbould orebodies occur as (mega)breccias developed within 'skarn' altered carbonaceous metasiltstones and meta-pelites in a volume eastward of the D1-fault wedge termination of the metabasaltic unit (Figures 4.24 to 4.30).

Based on the work of Dredge (1992), Garrett (1992) and McLean and Benjamin (1993), Fortowski and McCracken (1998) describe irregularly-shaped, steeply to moderately-dipping shoot-like orebodies within a volume bounded by two steeply dipping reverse faults (Figure 4.31) . The footwall fault is the regional D1 fault that juxtaposes Kuridala Formation 'Town Beds' with the Mount Elliott host metasedimentary 'Elliott Beds'. The hanging wall fault is a north-northwest-trending 'crush zone' sub-parallel with bedding and with widths up to 15m that potentially converges with the footwall D1 fault to the south. The Corbould orebodies to the west of Mount Elliott comprises a number of moderately to shallowly north-dipping lenses, the lowermost one of which is localised along the metabasalt contact (Figures 4.26, 4.27 & 4.28)

The host carbonaceous metasiltstones and phyllites are the intermediate unit of a east-northeast-dipping and -facing package between the basal metabasalt to its west and overlying fine-grained, carbonaceous phyllites and schists to the east (Figure 4.31).

The SWAN resource in contrast plunges crudely to the north at about 70° (see gradeshells on Figure 4.20) and is largely confined to a volume of brecciation that lies within the upper Staveley Formation calc-silicates and shadows the also-crudely, steeply-plunging SWAN Diorite (Figures 4.20 to 4.30).

The SWAN anticline is mapped on surface (Figures 4.20, 4.24 & 4.25) but is NOT well defined in the drilled volume although Gunter (2015) shows a moderately steeply-plunging anticlinal axis that she suggests also parallels the mineralised volume.

Structural History

The structural history of the rocks hosting the Mount Elliott-SWAN deposits and environs is not conclusively resolved but recent tectono-stratigraphic interpretations (Murphy et al., 2017) can be summarised as follows:

- Deposition of (1) interbedded calcareous sandstone-siltstone Staveley Formation between ca1725-1710Ma, (2) graded, quartz-rich Roxmere Quartzite sedimentation ca1710Ma, (3) fine-grained, variably

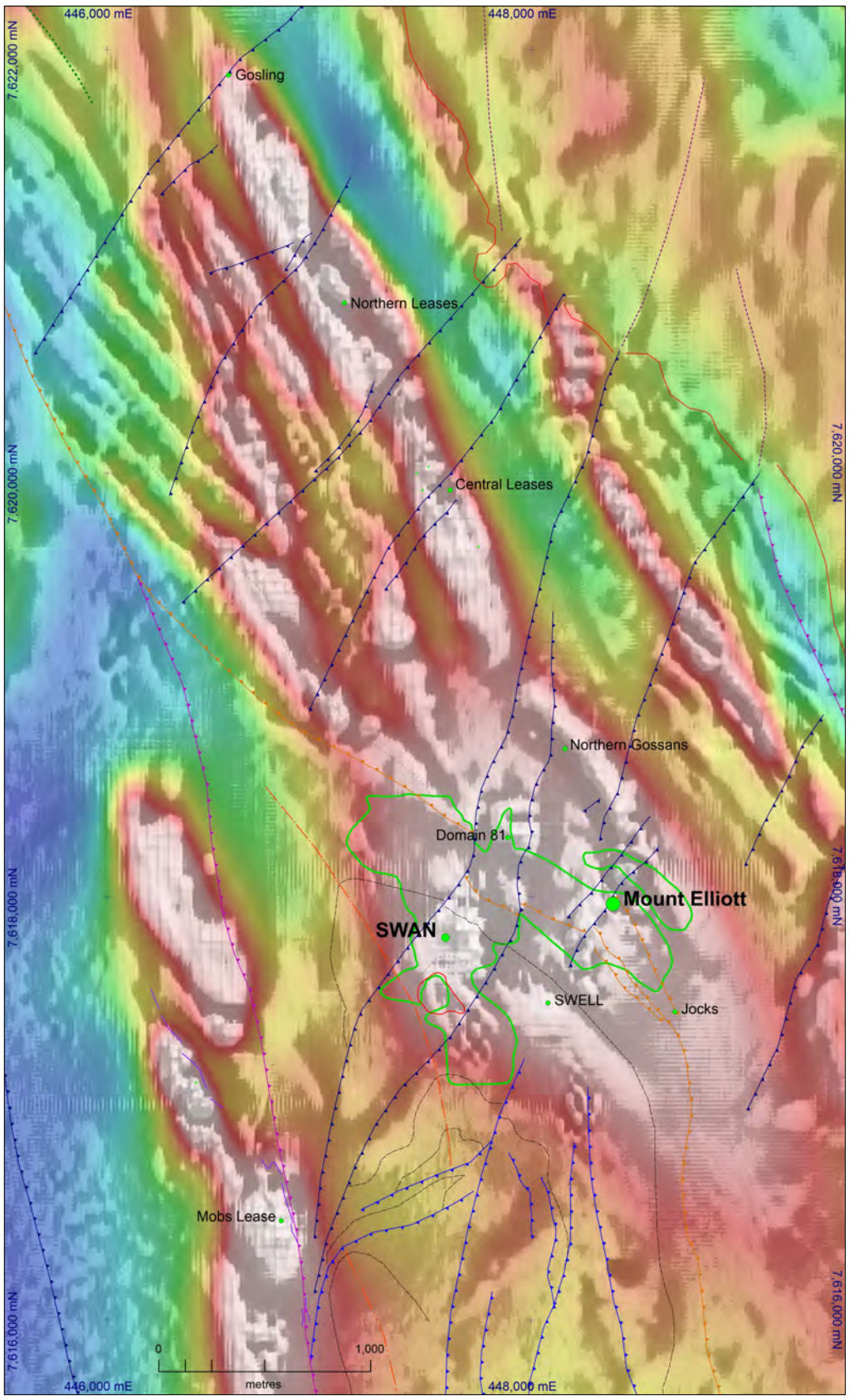

Figure 4.21 Detailed (50m & 25m line spacing) Chinova vrmi magnetics of grey-scale rtp-2vd draped over recent '1370' Cloncurry coloured rtp highlighting strong magnetic character of mafic lithologies but also broad anomalism associated with Mount Elliott-SWAN-SWELL mineralisation. Structural skeleton overlain. Same view as Figure 4.20. Map Projection GDA94 (MGA54)

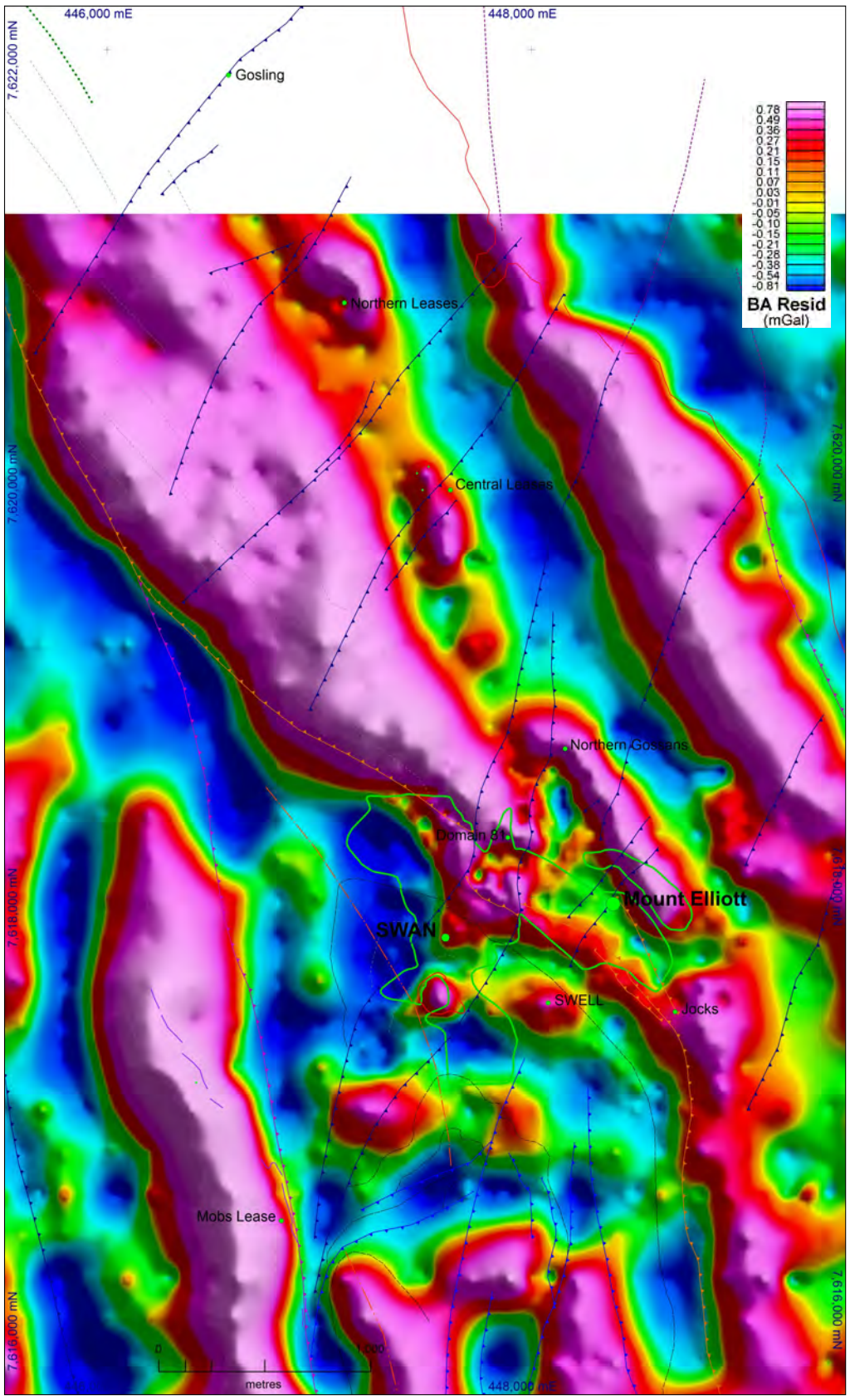

Figure 4.22 Merged detailed (100x100m & 50x50m over Mount Elliott) 2012 Residual Bouguer Anomaly ground gravity data highlighting significant gravity highs associated with mafic lithologies and potentially moderate density anomalism with SWAN mineralisation. Lack of density anomalism with Mount Elliott potentially due to mined out ore. Structural skeleton overlain. Same view as Figure 4.20. Map Projection GDA94 (MGA54)

carbonaceous, Kuridala Formation turbidites ca1710-1680Ma, (4) coarser-grained New Hope Sandstone turbidites accompanied by increasingly significant mafic sill emplacement ca1680-1665Ma, and (5) fine-grained, carbonaceous, Answer Slate and Toole Creek Volcanics accompanied by further increasing mafic input in the form of basaltic flows and doleritic sills ca1665-1650Ma.

- Thin skinned, Isan D1 orogeny with north-northwest-directed shortening ca 1590-1570Ma is associated with the allochthonous thrust emplacement and internal ramping of the Eastern Fold Belt Staveley to Toole Creek packages (Murphy et al., 2017). In the Mount Elliott-SWAN region, the metabasaltic and carbonaceous metasedimentary package hosting Mount Elliott-Corbould is interpreted to be in D1 overthrust juxtapositioning with D1 footwall Staveley and Kuridala Formation units. The steeply-plunging SWAN antiform is potentially a D1 footwall fold formed in a subhorizontal east-west'ish orientation. Little (1997) describes an early S0-parallel fabric preserved crenulated in garnet porphroblasts.
- Isan D2 deformation associated with east-west shortening that regionally produces north-south fold axes, is interpreted to locally rotate the shallow D1 thrust and fold geometries to steep easterly dips (Murphy et al., 2017) and produces the main fabric, an intense, moderately to steeply east-northeast dipping S2 foliation (Little, 1997).
- A regional, west-vergent D2 reverse fault through the Mob's Lease prospect is interpreted by Murphy et al. (2017) to stack the folded Staveley-Roxmere-Kuridala packages.
- The timing of SWAN Diorite remains unconstrained but geological relations suggest that if it was originally a steeply-plunging, pipe-like intrusive its timing would have to be post-D2.
- Little (1997) describes a shallowly dipping S3 crenulation of S2 but with no associated mesoscopic folding. Gunter (2015) reports possible variable F3 fold plunges in the Corbould-Mount Elliott area.
- Strongly boudinaging of the metadolerite sills north and east of Mount Elliott is interpreted to reflect late Isan D4 deformation partitioning adjacent to a solidifying Squirrel Hills Granite during northwest-directed shortening (Murphy et al., 2017). Extensive iron formation alteration around the metadolerite boudins (Figure 4.20) suggests a D4 timing for iron-oxide metasomatism (and mineralisation).
- Late northeast to north-northeast trending D4 faults are well imaged in the magnetics (Figure 4.21). They express variable transpressive geometries in response to northwest-directed late Isan D4 shortening. Gunter (2015) interprets Domain 81 mineralisation to be hosted in one of these structures. They are brittle in nature and are interpreted by Murphy et al. (2017) to span a significant time period during and after Squirrel Hills Granite intrusion and solidification.

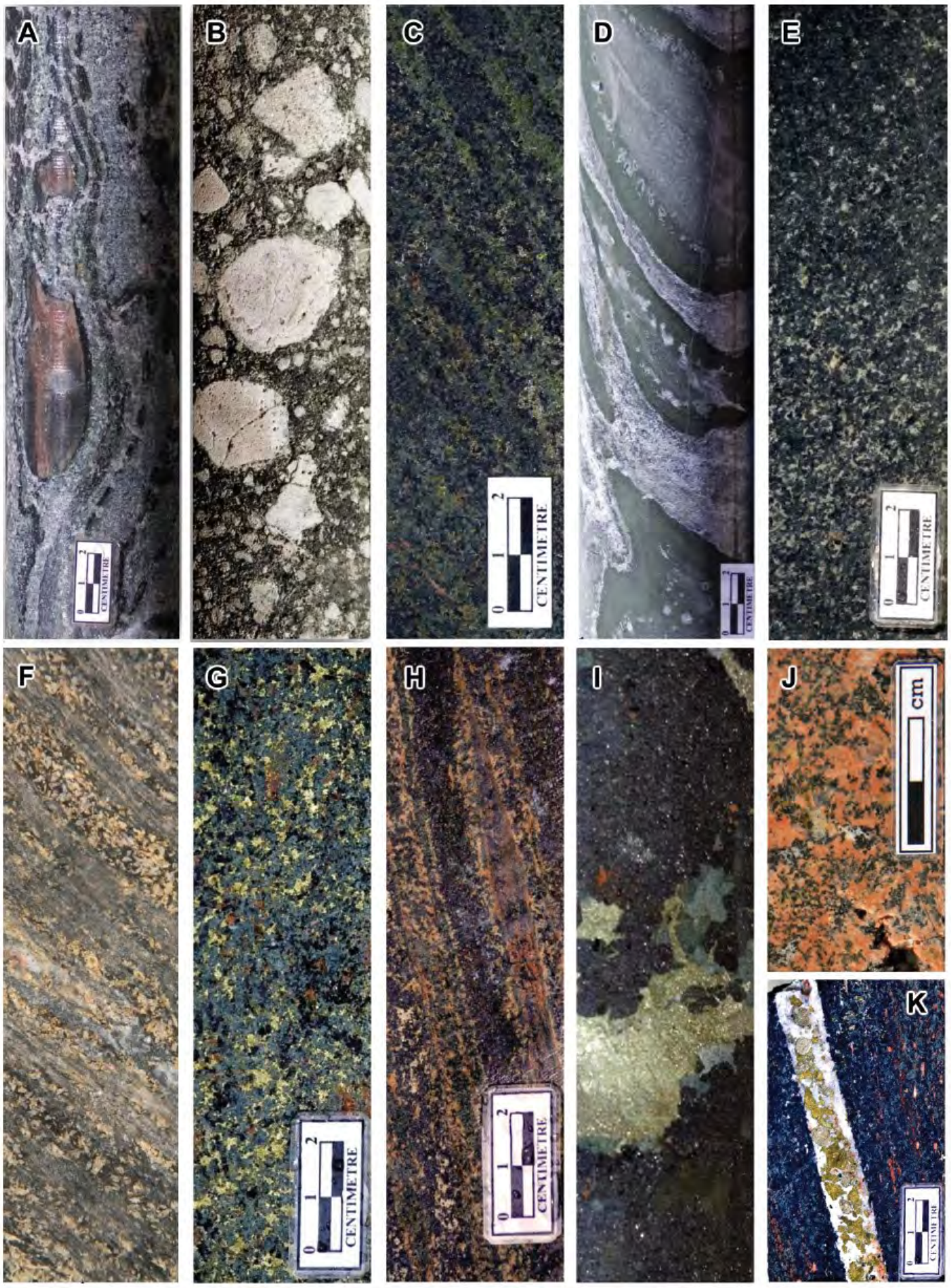

Figure 4.23 Key lithologies, alteration and mineralisation styles from the Mount Elliott-SWAN deposits. **A** - Layered fine- and coarse-grained calc-silicates from the footwall of the SWAN zone; **B** - SWAN Breccia, polymictic, fragment to matrix supported breccia, host to the majority of the SWAN zone mineralisation; **C** - Banded calc-silicate from the eastern margin of the calc-silicate unit; **D** - Banded, vesicular basalt from the Kuridala Formation; **E** - SWAN diorite, from adjacent to the SWAN breccia; **F** - Altered, muscovite-chlorite schist of the "Town Beds" immediately above the contact between the Kuridala and Staveley Formations; **G** - High-grade mineralisation hosted by the SWAN breccia; **H** - Mineralisation hosted by banded calc-silicates; **I** - Coarse-grained pyroxene-chalcopyrite-magnetite-calcite and anhydrite from Mount Elliott; **J** - Late felsic dyke; **K** - Late stage, coarse-grained, carbonate-chalcopyrite-pyrite and molybdenite veining from SWAN (from Brown & Porter, 2010)

Nature of Controlling Structure

Both the SWAN and Mount Elliott-Corbould deposits are hosted by brittle breccias that post-date much or all of the ductile Isan deformation and associated structuring (Little, 1997; Fortowski & McCracken, 1998; Murphy et al., 2017). Garrett (1992) noted variable S2 orientations within Mount Elliott breccia clasts.

At Mount Elliott, coarse (mega)breccias comprise angular fragments of altered metasediment from 10cm to 20m in size host ore (Brown & Porter, 2010) with coarse grained sulphide mineralisation filling voids of similar sizes (Brown & Kirwin, 2009).

SWAN is hosted within a fracture and breccia network largely developed within the banded and massive Staveley Formation calc-silicates. The breccia varies from crackle to matrix-supported, with angular to rounded clasts from centimeters to meters in diameter (Brown & Porter, 2010).

A number of structural controls on brecciation hosting mineralisation have been suggested:

- Fortowski and McCracken (1998) after Garrett (1992) suggest fracturing and brecciation of more competent rocks hosting Mount Elliott ore was initiated within the footwall of the 'crush zone' that marks the north-eastern extent of ore (Figure 4.31) during its reverse faulting.
- Wang and Williams (1996) suggest that the series of shallowly to steeply east-dipping, breccia-controlled ore lenses at Mount Elliott form within a reverse wrench couple between the hanging wall 'crush zone' and the footwall fault (Figure 4.31).
- Little (1997) emphasised extensional brecciation associated with a dilational jog focussed along Jocks Fault, a linkage structure between the major footwall fault and a hanging wall shear (Figure 4.32) that is potentially the down-dip extension of Garrett's (1992) 'Crush Zone'.
- Duncan et al. (2014) from a plan view interpretative map suggest brittle structural control for Mount Elliott-SWAN mineralisation associated with post-ductile, late-orogenic dextral transpressive movements across a sinistral fault jog along the north-northwest striking Mount Elliott Fault.
- Gunter (2015) while acknowledging a lack of clear control on SWAN high grade ore highlights the gross parallelism of brecciation, mineralisation and the plunge of the SWAN fold axis.
- Murphy et al. (2017) suggest that during (post peak-metamorphic) northwest-directed Isan D4 shortening, deformation partitioning (between the rigid SWAN Diorite and the weak Kuridala Formation schists) drives the brittle brecciation within the upper Staveley Formation calc-silicates that localises SWAN mineralisation. They interpret that later in D4 the brittle, north northeast-trending faults cut the SWAN system (diorite, brecciation and mineralisation; Figures 4.25-4.30).
- Gunter (2015) suggests Domain 81 mineralisation is hosted within brecciated metabasalt/amphibolite controlled by the north northeast-trending Domain 81 Fault (Figures 4.25, 4.28, 4.29) which suggests prolonged mineralisation-related fluid flow into late D4 faults that cut earlier formed mineralisation.

WALLROCK ALTERATION

General Characteristics

SWAN and Mount Elliott-Corbould mineralisation is associated with pervasive, pre-breccia, post-peak metamorphic, hematite-stained albite-silica alteration commonly associated with bleaching of carbonaceous, fine-grained metasedimentary lithologies and the calc-silicate alteration of Staveley For-

Figure 4.24 (opposite top) Projected section through the Mount Elliott-SWAN mineral system showing the Mount Elliott-Corbould historic development and stoping, the drilling (coloured by intercept eqwt% Cu) and the Chinova Leapfrog isotropic shells (Gunter, 2015) for 0.6 eqwt%Cu using a 0.5 eqwt%Cu cut-off, the SWAN Diorite, the brecciated volume and the projected 0.3 eqwt%Cu gradeshell.

Figure 4.25 (opposite bottom) Cross section 7618000N through the Chinova Leapfrog model (Gunter, 2015) showing the location of important lithological contacts and structures (see text), gradeshells and highlighting in SWAN the relationship between brecciation as a carapace around the SWAN Diorite and the focus of mineralisation in the upper portions of the Staveley Formation calc-silicates (see also Level Plans). Section location shown on Figure 4.26.

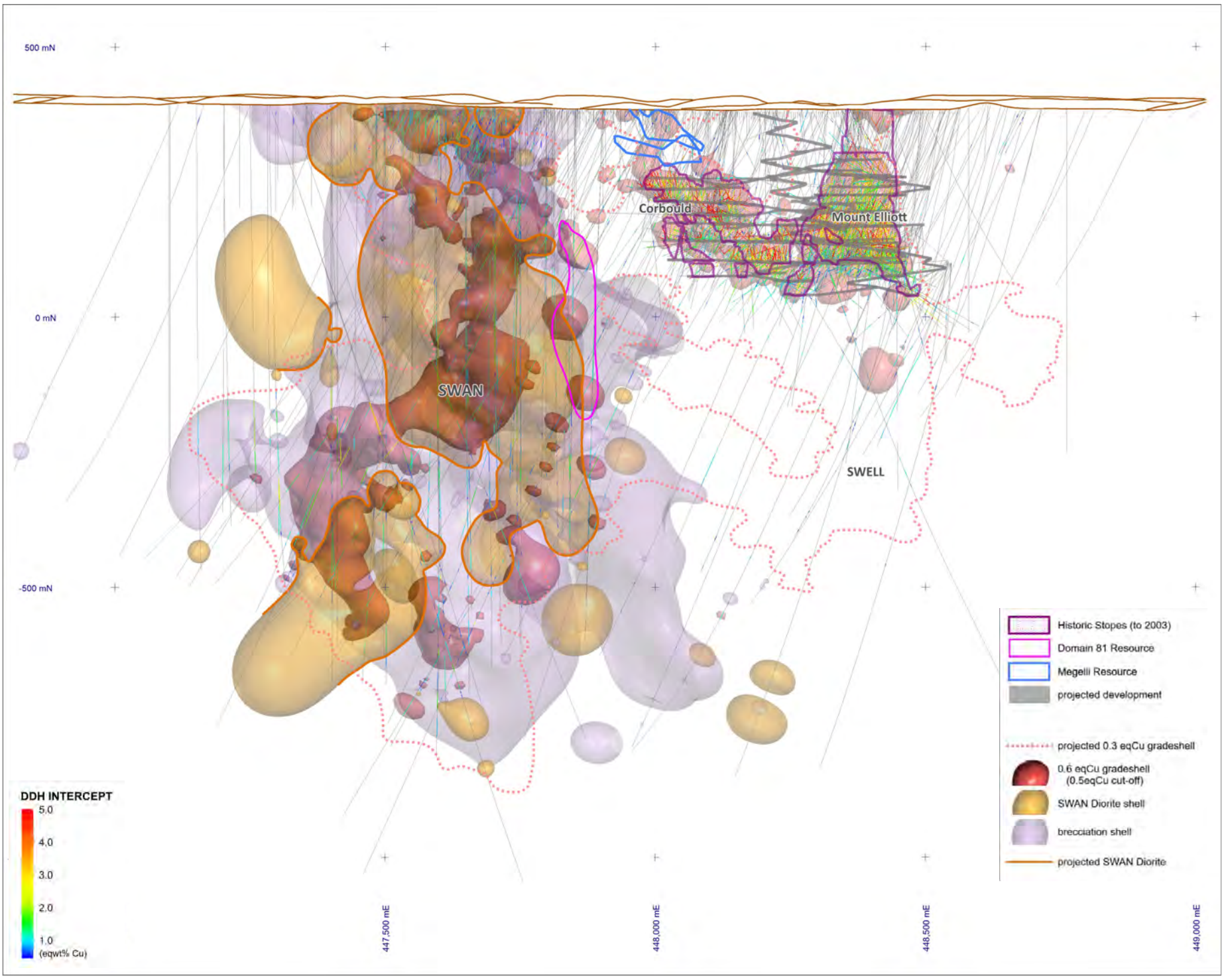
500 mN
0 mN
-500 mN
Corbould
Mount Elliott
SWAN
SWELL
Historic Stopes (to 2003)
Domain 81 Resource
Megelli Resource
projected development
projected 0.3 eqCu gradeshell
0.6 eqCu gradeshell (0.5eqCu cut-off)
SWAN Diorite shell
brecciation shell
projected SWAN Diorite
DDH INTERCEPT
5.0
4.0
3.0
2.0
1.0
(eqwt% Cu)
447,500 mE
448,000 mE
448,500 mE
449,000 mE

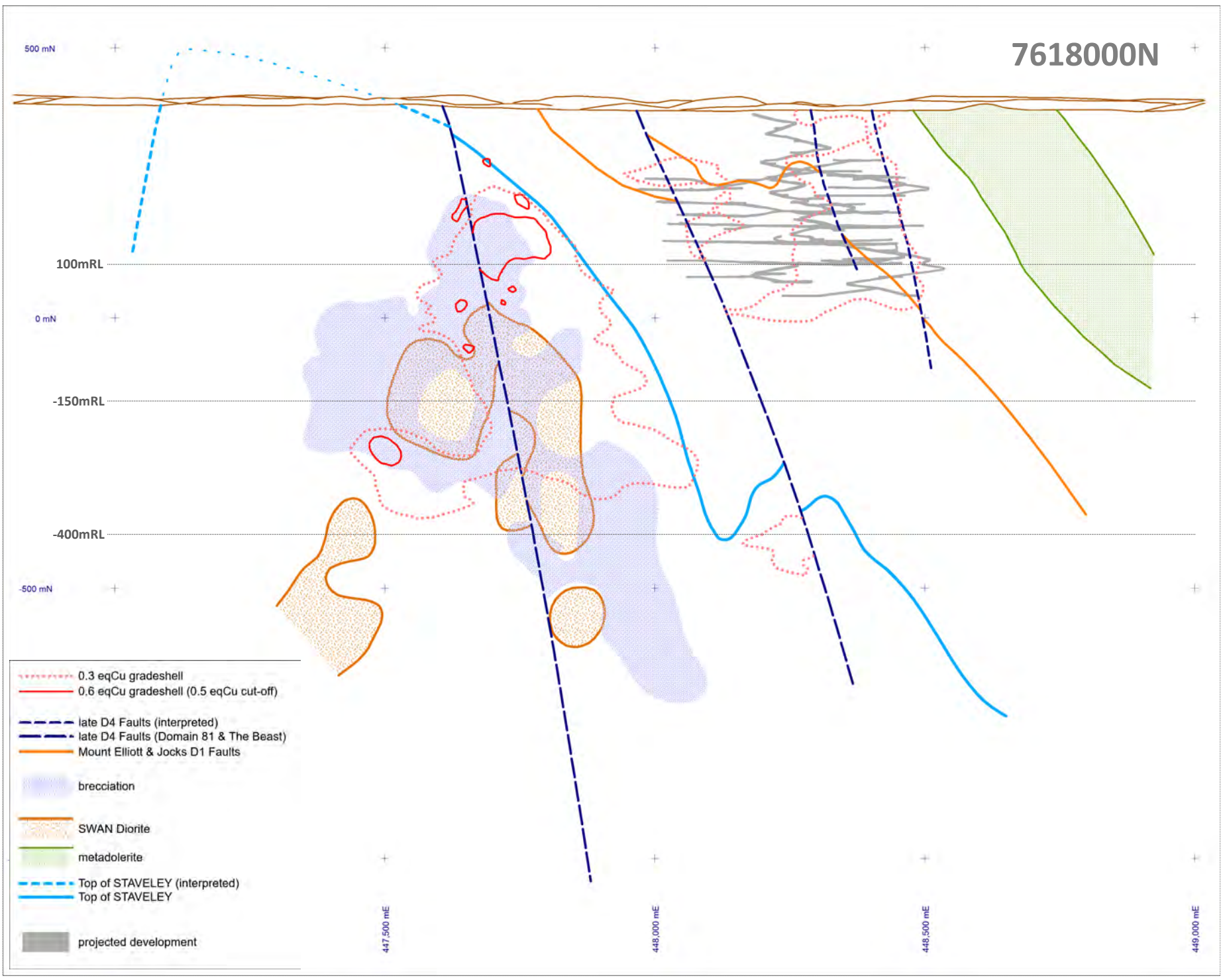
7618000N
500 mN
100mRL
0 mN
-150mRL
-400mRL
-500 mN
0.3 eqCu gradeshell
0.6 eqCu gradeshell (0.5 eqCu cut-off)
late D4 Faults (interpreted)
late D4 Faults (Domain 81 & The Beast)
Mount Elliott & Jocks D1 Faults
brecciation
SWAN Diorite
metadolerite
Top of STAVELEY (interpreted)
Top of STAVELEY
projected development
447,500 mE
448,000 mE
448,500 mE
449,000 mE

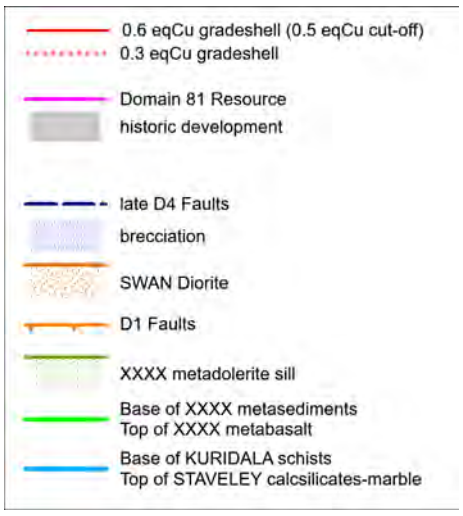

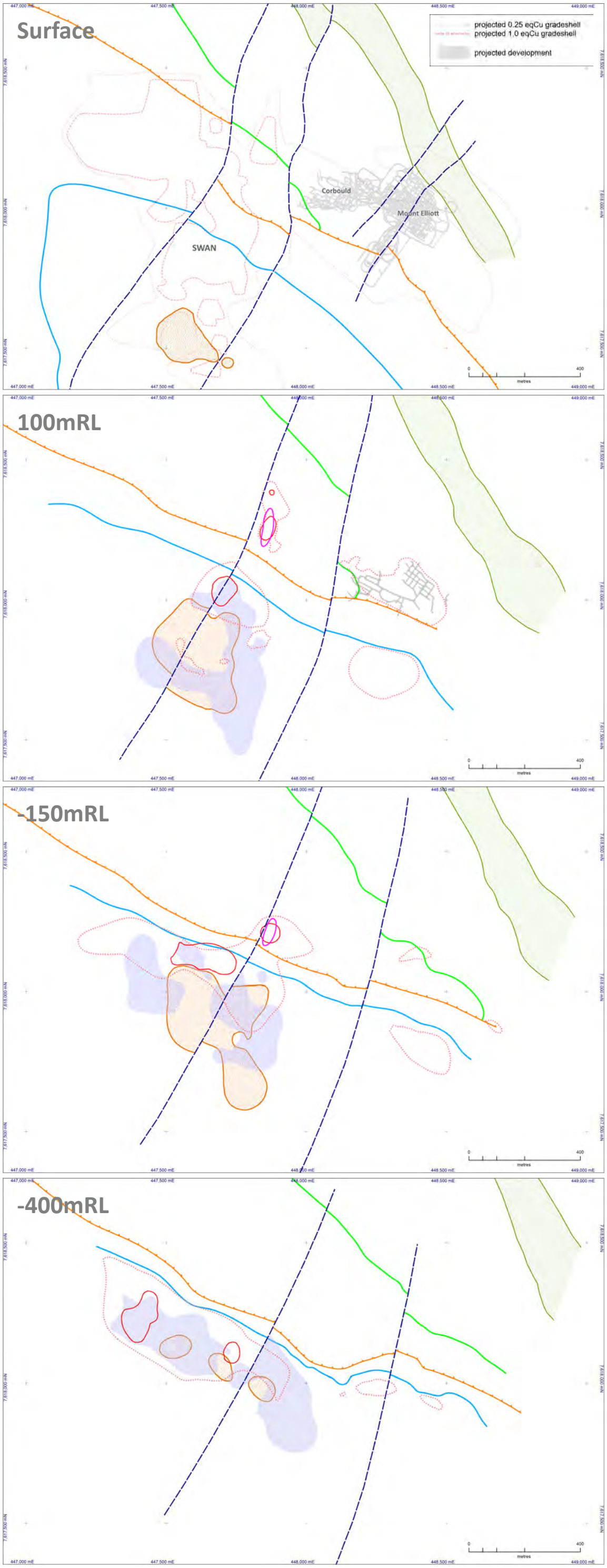

Figure 4.26 (opposite), **4.27** (top) to **4.30** (bottom) Level Plans (surface x2, 100mRL, -150mRL, -400mRL) through the Mount Elliott-SWAN mineral system highlighting the east-plunging geometry of the metabasaltic wedge west of, and beneath, the Mount Elliott-Corbould deposits; and at SWAN, the overall steep north plunge of the system, the largely antithetic (but overlapping) spatial relationship between the SWAN Diorite and calc-silicate brecciation and the positioning of SWAN mineralisation within and around brecciation but focused between the SWAN Diorite and the stratigraphic top of Staveley Formation. Level plans generated from the Chinova Leapfrog isotropic shell models (Gunter, 2015). The local parallelism of the footwall Staveley and Kuridala Formation packages and angular discordance of the hanging wall metabasalt, metasediment and metadoleritic sill package across the Mount Elliott D1 Fault is highlighted in the level plans. Coloured geology in the upper Surface map as for Figure 4.20.

mation calcareous siltstone-sandstones. Brown and Porter (2010) suggest that these are regional scale sodic-calcic alteration effects focused along regional scale high strain corridors. At the deposit scale this sodic alteration is overprinted by multiple pulses of more calcic and potassic alteration controlled by more focused brecciation with each pulse comprising earlier diopside-scapolite evolving to actinolite with mineralisation (Brown & Porter, 2010).

Zonation

Fortowski and McCracken (1998; after Garrett (1992) and McLean & Benjamin (1993)) describe a zoned alteration system at Mount Elliott. This zonation scheme is presented in Figure 4.31 with the annotated zones mineralogically detailed in Table 4.3. Wang and Williams (2001) have documented a zonal paragenetic sequence broadly consistent with the Garrett (1992)-McLean & Benjamin (1993) and Little (1997) schemes.

Outer Zone: Fracture and fabric-controlled, white to pinkish, bleaching due to biotite and graphite destruction. The development of quartz-(hematitic) albite-sericite-calcite (±scapolite ±pyrite ±pyrrhotite ±fluorite) intensifies inward with minor K feldspar on fractures and foliations. This alteration overprints and destroys metamorphic mica, ferromagnesian silicates and graphite and is demonstrably post-peak metamorphic in timing. Little (1997) sees this early silica-albite alteration focused within and above the footwall fault by a fracture network within the metasediments.

Mid Zone: Stronger alteration is reflected by the texturally-destructive addition of clinopyroxene (diopside-hedenbergite) and/or amphibole (actinolite-tremolite)-scapolite with increasing open space, fracture and breccia-controlled hematitic albite-clinopyroxene infill. Veined alteration intensifies to a network and finally into a breccia matrix.

Inner Zone: Massive replacement of hema-

titic albite-altered metasediment by K feldspar -calcite-clinopyroxene ±andradite garnet overprinted by coarse-grained 'skarnoid' clinopyroxene-actinolite-scapolite-calcite-magnetite (±andradite ±tourmaline ±allanite ±apatite ±biotite ±K feldspar) and retrograde fracture and breccia-controlled, chlorite-epidote-calcite-chalcopyrite-pyrite-magnetite. The amphiboles are Na- and K-rich; the scapolite, Na- and Cl-rich.

Little (1997) documents a strong reverse reactivation, structural control on the Footwall Zone massive 'skarn' focused along the footwall fault and associated milled breccias. The Upper Zone mineralisation, that includes the shallower Mount Elliott workings, are ascribed to an outer zone or mid zone 'skarn' carapace controlled by a fracture network developed above the dilational Jocks Fault zone (Figure 4.42).

HALOS

Extent

The original superficial extent of Mount Elliott-SWAN mineralisation has been impossible to determine due to surface disturbance related to historic mining and smelting activities. Searle (1952) reported a gossan zone over Mount Elliott 110ft x 50ft comprising 'malachite, azurite, chrysocolla and red and black oxides of copper'.

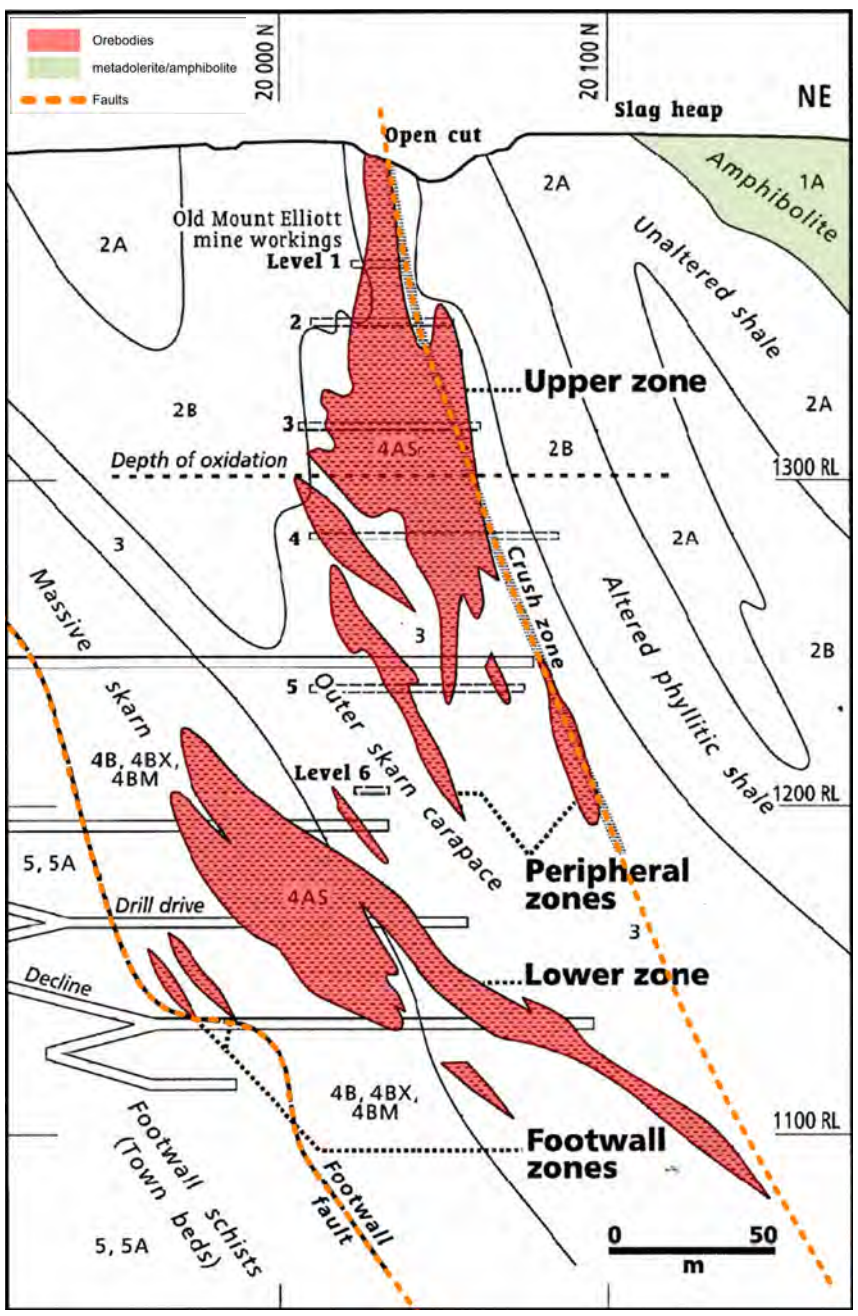

Figure 4.31 Cross section through the Mount Elliott deposit from Fortowski & McCracken (1998) showing irregular, moderate to steeply-plunging orebodies within a zoned 'skarn' type alteration system developed between two major fault zones (see text for further description). Numbered annotation refers to mineralogical zones of Fortowski & McCracken (1998; Table 4.3). The footwall fault is a major D1 structure regionally juxtaposing blocks of significantly contrasting lithologies. Approximate section location shown on Figure 4.26.

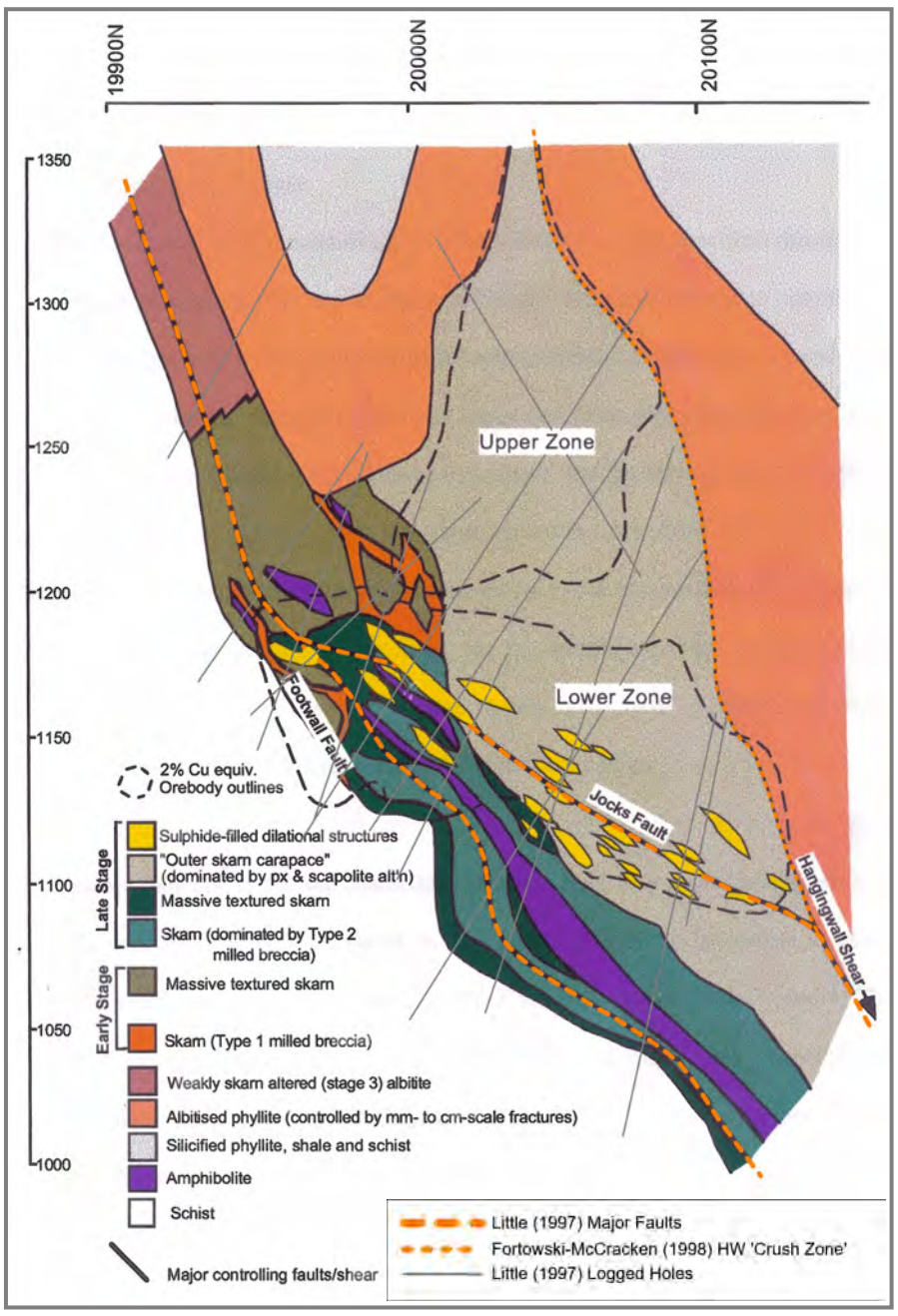

Figure 4.32 Similar cross section through the Mount Elliott deposit from Little (1997) with deeper geometries. The section highlights the reverse dilational jog along Jocks Fault controlling Lower Zone mineralisation and the lithological, alteration and 'skarn' assemblages defined by Little. The footwall fault is a major D1 structure regionally juxtaposing blocks of significantly contrasting lithologies. Section location approximately as for Figure 4.31 and shown on Figure 4.26.

Geophysical Expression

The detailed Chinova magnetic and gravity (Figures 4.21 & 4.22) and '1370' Cloncurry radiometric Uranium (Figure 4.34) data over the Mount Elliott-SWAN region highlight:

- The strong magnetic and gravity response of the mafic lithologies including the SWAN Diorite.
- A broad domain of magnetic anomalism is associated with Mount Elliott-SWAN-SWELL mineralisation at depth. Brown and Porter (1998) warn that slag dumps, waste dumps, infrastructure and the removal of much of the high grade ore complicate the Mount Elliott magnetic response.
- An independent magnetic anomaly over SWAN combines the magnetic response of the SWAN Diorite and SWAN alteration.
- No gravity expression of Mount Elliott is evident perhaps due to the removal of ore.
- SWAN mineralisation has a moderate gravity expression that is distinct from that of the SWAN Diorite.
- SWAN and Mount Elliott mineralisation appears to have a strong radiometric Uranium responses with the Mount Elliott response potentially compromised by surfical waste (Brown & Porter, 1998). Uranium anomalism continues northward, associated with iron formation mantling the boudinaged metadolerites.

Geochemical Expression

Due to the surficial disturbance of past mining and smelting, an Auger regional soil survey was undertaken in the 1980s by Amoco. Minus 80# Cu, Ag and Co data is available and presented in Figures 4.35-4.37. Gold was apparently not analysed. This auger soil geochemistry highlights:

- Significant Cu anomalism (>900ppmCu) over SWAN, Domain 81 and immediately northwest of Mount Elliott
- Very significant Cu-Co anomalism (>900ppmCu, >80ppmCo) associated with the iron formations mantling the boudinaged metadolerites north-northwest of Mount Elliott . Despite significant exploration drilling no Cu-Au mineralisation has been identified in the Central and Northern Lease areas.
- Silver shows no relationship with known mineralisation. Silver anomalism at the southern end of the survey may be associated with a carbonaceous metasiltstone within the upper Staveley Formation.

Lithogeochemistry

No lithogeochemical studies have been undertaken in the Mount Elliott-SWAN regions.

TIMING OF MINERALISATION

Relative Timing

All workers (Searle, 1952; Garrett, 1992; McLean & Benjamin, 1993; Wang & Williams, 1996, Fortowski & McCracken, 1998; Brown & Porter, 2010; Duncan et al., 2014; Murphy et al., 2017) are in agreement that Mount Elliott and SWAN mineralisation is fracture and breccia-controlled and overprints the main Isan foliation-forming and metamorphic event (post-peak metamorphic). Murphy et al. (2017) suggest late Isan D4, deformation partitioning control adjacent to a solidifying Squirrel Hills Granite implying a broad synchronicity between mineralisation and Williams-Naraku-aged intrusion.

Absolute Ages

Ar-Ar dating of pre-mineralisation actinolite (Wang & Williams, 2001) and biotite at Mount Elliott (Perkins & Wyborn, 1998) returned ages of 1510±3Ma and 1496±4Ma respectively. More recent Re-Os molybdenite dating (Duncan et al., 2011) returned consistent dates of 1513±5Ma at Mount Elliott and 1515±6Ma at SWAN. A pre-ore calc-silicate alteration U-Pb titanate age at Mount Elliott of 1530±11 is also reported by Duncan et al. (2011).

These mineralisation and alteration ages are all within error of the 1514±4Ma age of the adjacent Squirrel Hills Granite (Pollard & McNaughton, 1997) and imply a close genetic relationship.

Table 4.3: Mount Elliott alteration, lithology and mineralogy. Zones (Units) annotated on Figure 4.31

Unit	Rock type	Mineralogy	Mineralisation	Comment
1A, 1B	Amphibolite-metadolerite	hbl, pl, bi, mt	py	1A sill, to 100 m thick; 1B is thin dykes
2A	Carbonaceous phyllite, metasiltstone	bi, pl, qz, gr, and	py,po	Unaltered. Occasional schist zones.
2B	Altered phyllite	pl, bi, qz, ksp, ca, fl	py	Outermost alteration halo.
3	Altered phyllite	hab, qz, sca, ca, cpx	py, po, cp, chr, ml, at, cup, tn, cu, cc	Outer skarn carapace. Hosts Upper zone orebody and part Lower zone.
4B	Undifferentiated skarn	hab, cpx, ca	py	
4BX	Massive skarn pseudobreccia	cpx, hab, ca, ksp, trm, mt	py, po, cp	Host rock completely altered. Part host of Lower zone orebody.
4BM	Massive skarn pseudobreccia, magnetite rich	mt, hab, sca, cpx, ca	py, cp	Common in deeper levels below the Lower zone.
4AS	Coarse massive skarn + sulphide	cpx, ca, mt, ap, sca	cp, po, py,bn, cc	High grade crosscutting veins.
4AI	Coarse zoned skarn	cpx, ca, ap, mt, qz, amt, gyp	py	Vugs often lined with cpx, ca, qz, amt or gyp.
1C	Metabasalt	hlb, pl mt, bi, sca		Often altered to scapolite-biotite rock.
5A	Altered schist	hab, bi, qz, ksp		Intense silicification, feldspathisation.
5	Schist	bi, qz, mu and se, pl (stl, tml, gn)		Quatz boudins common. Stl, tml and gn reported.
1D	Microdiorite	hab, ca, bi, qz		Crosscuts all the above units as dikes.
6	Calc-silicate	cpx, hab, ca mt	py, cp, cu, cc, chr, ml	SWAN prospect.
6M	Calc-silicate, magnetite rich	mt, cpx, ca, hab	py, cp	Often zones with >30% mt. SWELL prospect.

amt -amethyst, and-andalusite, ap-apatite, at-atacamite, bi-biotite, bn-bornite, ca-calcite, cc-chalcocite, chr-chrysocolla, cp-chalcopyrite, cpx-clinopyroxene, cu-native copper, fl-fluorite, gn-garnet, gr-graphite, gyp-gypsum, hab-hemitite-dusted albite, hbl- hornblende, ksp-potassium-feldspar, ml-malachite, mt-magnetite, mu-muscovite, pl-plagioclase, po-pyrrhotite, qz-quartz, sca-scapolite, se-sericite, stl-staurolite, tml-tourmaline, tn-tenorite, trm-tremolite.

Figure 4.33 (right) Detailed geology of the Mount Elliott-SWAN region. Map area and Legends as for Figure 4.20. Map Projection GDA94 (MGA54)

Figure 4.34 (far right) Mount Elliott-SWAN zoom of detailed 100m line-spacing, 2018 '1370' Cloncurry Uranium Radiometric Image. Structural skeleton overlain. Same map area as Figure 4.33. Map Projection GDA94 (MGA54)

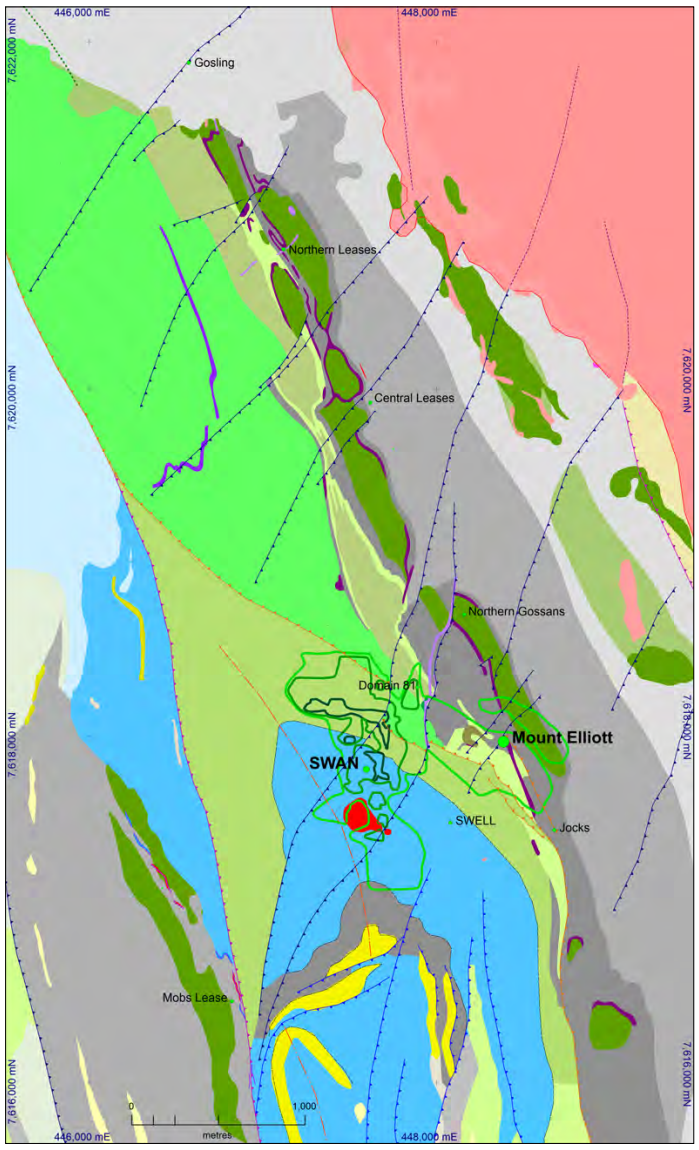

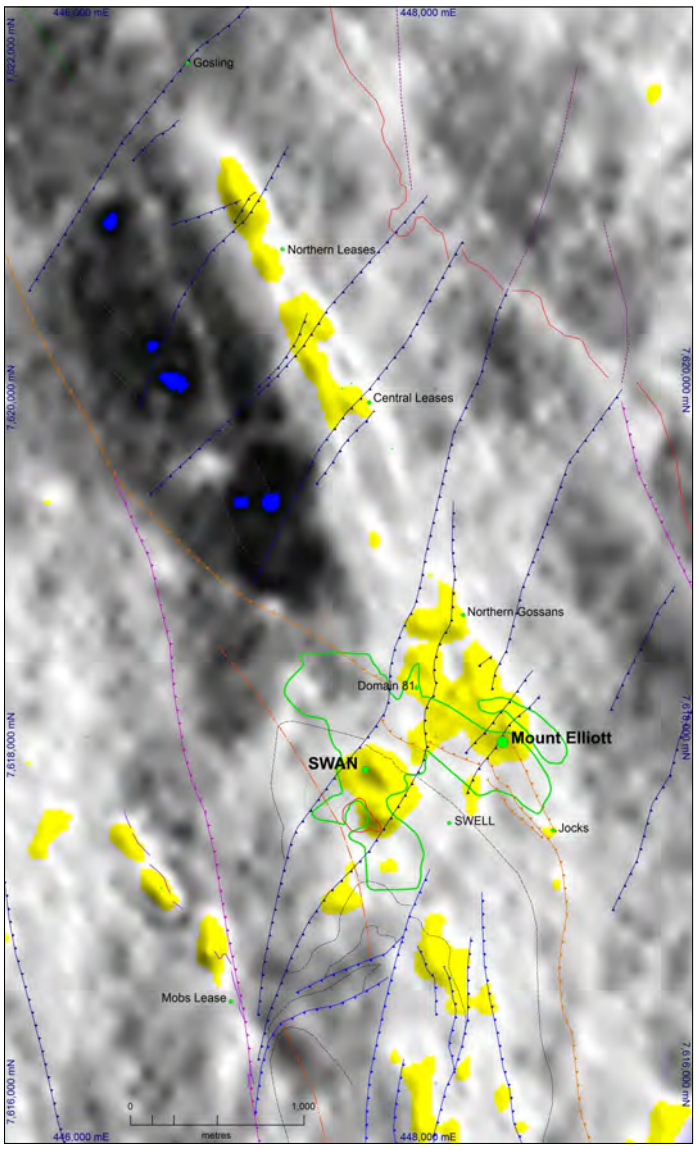

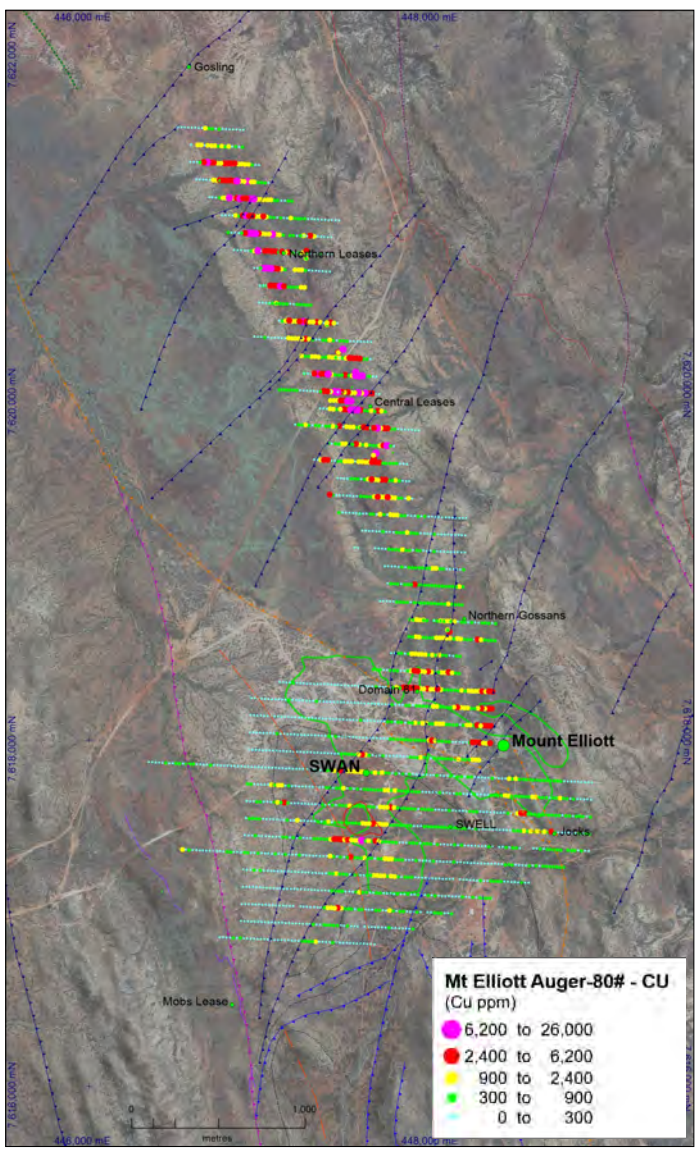

Figure 4.35 (below) Mount Elliott-SWAN region -80# soil auger Copper on Worldview image draped over DEM. Map area as for Figure 4.33. Map Projection GDA94 (MGA54)

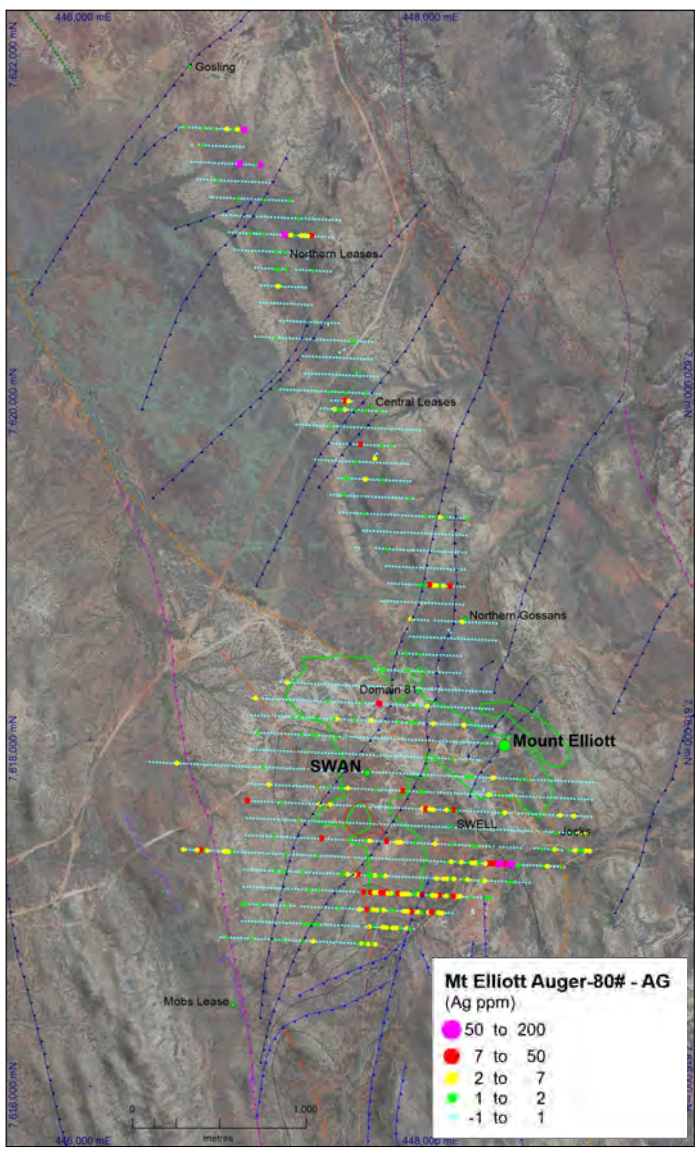

Figure 4.36 (below centre) Mount Elliott-SWAN region -80# soil auger Silver on Worldview image draped over DEM. Map area as for Figure 4.33. Map Projection GDA94 (MGA54)

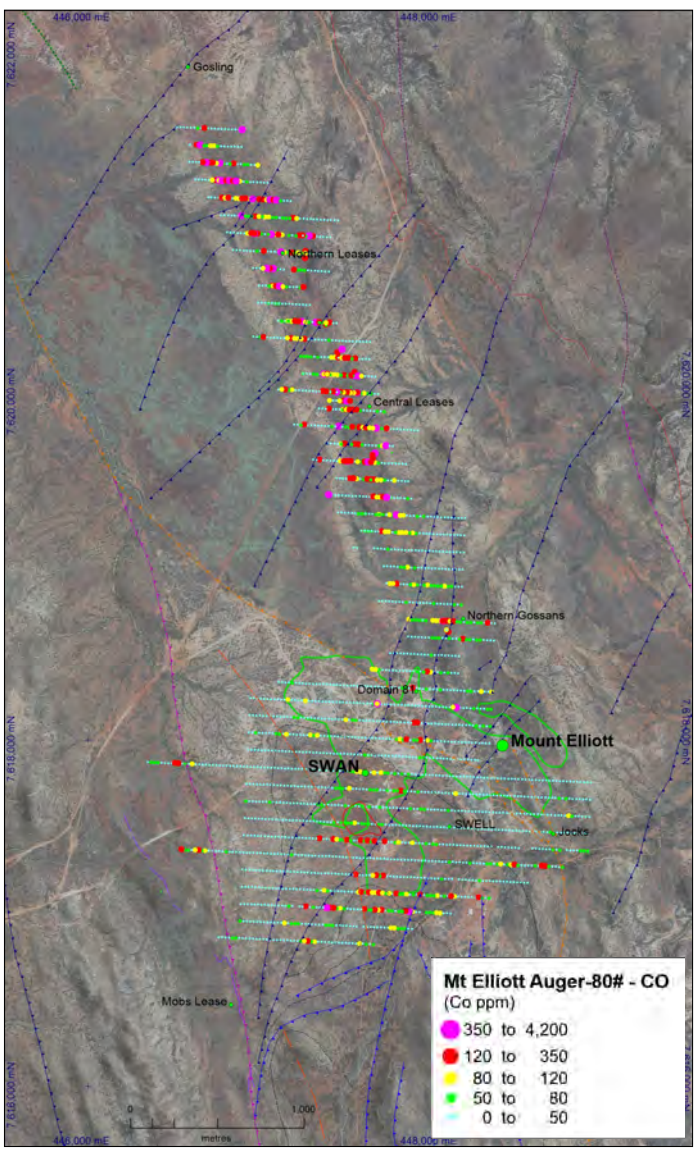

Figure 4.37 (below right) Mount Elliott-SWAN region -80# soil auger Cobalt on Worldview image draped over DEM. Map area as for Figure 4.33. Map Projection GDA94 (MGA54)

GENETIC MODELS

Direct intrusion-related skarn models have predominated despite the immediate lack of causative intrusions at Mount Elliott and SWAN (Garrett, 1992; McLean & Benjamin, 1993; Wang & Williams, 1996; 2001; Little, 1997; Fortowski & McCracken, 1998) due to the coarse-grained 'skarnoid' mineral assemblages at Mount Elliott. All genetic commentators agree on the distinct fracture and breccia control on mineralisation and its late-orogenic, post-peak metamorphic timing.

More recent workers (Brown et al., 2009; Brown & Kirwin, 2009; Brown & Porter, 2010; Duncan et al., 2011; 2014; Murphy et al., 2017) have highlighted IOCG affinities of the Mount-Elliott-SWAN system and re-interpreted 'skarnoid' mineralogies as sodic-calcic alteration in the 'IOCG' spectrum of assemblages.

Murphy et al. (2017) highlight the common threads in the world-wide family of 'IOCG-style' deposits which fit the Mount Elliott-SWAN system which comprise strong brittle structural control, synchronous but not-immediately-adjacent voluminous magmatism, Cu-Au mineralisation, iron-oxide (magnetite ±hematite) association, district- to local-scale, alkali alteration (sodic-calcic (Na-(Ca)) & potassic (K)) and a distinctive (but variably mixed) suite of minor elements (Ag, REE, U, Mo, F, P, Ni, As, Co, Ba).

EXPLORATION

Discovery Method

The outcropping Mount Elliott gossan was discovered in 1889 by a prospector, James Elliott.

A coincident geochemical anomaly and circular magnetic anomaly that was targeted by Union Miniere and Anaconda Australia and that became SWAN was first drilled in the early 1970s.

Merlin-Mount Dore Cu-Au-Mo-Re Deposits

Figure 4.38 Five Diamond Drill Rigs drilling Merin in November 2008. View looking south with Roxmere Quartzite ridge on right and Mount Dore Granite on left. Photo from Doug Kirwin, 2009.

PRODUCTION AND DIMENSIONS

Historic Production and Resources

High grade, surface-enriched copper was mined from Mount Dore in the early 1900s with a reported 15.74 tonnes of oxide ore mined for a total of 5.81 tonnes of copper (Lazo & Pal, 2009; Beardsmore, 1992).

Some modern drilling was conducted in 1957 with one hole intersecting Mount Dore mineralisation at depth, returning 8.8m@1.3%Cu at a depth of 49.7m (Lazo & Pal, 2009).

Exploration by Cyprus and Arminco after 1975 drilled around 30 diamond drillholes and an unspecified number of percussion holes into the southern portion of Mount Dore. Beardsmore (1992) reports a resource to 300m (open to depth) from Nisbet (1980 from this drilling

Mount Dore: 40Mt@1.08%Cu, 6.5g/tAg

Ivanhoe Cloncurry Mines Ltd acquired the Mount Dore leases in late 2003 from the receivers of Selwyn Mines Limited. Between 2003 and 2008 Ivanhoe completed 19,273m of drilling on Mount Dore and announced a copper resource of

Mount Dore: 80Mt@0.6%Cu
(Lazo & Pal, 2009)

In mid-2008, during a reverse circulation drilling campaign delineating near surface copper to the north of the known Mount Dore mineralisation, strong molybdenite mineralisation was intersected. From mid-2008 to October 2009, Ivanhoe drilled a further 24,865m into the Merlin molybdenite zone.

In 2010, an Independent Technical Appraisal reported a Merlin JORC resources using a 0.3%Mo cut-off (SRK, 2010) of

Indicated: 5.2Mt@1.0%Mo, 16.0ppmRe, 0.2%Cu, 3.7ppmAg

Inferred: 3.5Mt@0.8%Mo, 14.2ppmRe, 0.3%Cu, 4.4ppmAg

During 2010, Ivanhoe completed nominal 50m infill drilling of Merlin. In 2011 Preliminary economic analyses of both the Merlin Mo-Re and Mount Dore oxide Cu projects were completed, and in 2012, a Merlin Mining Feasibility Study by Lycopodium Consultants (2012) was finalised.

Detailed current measured, indicated and inferred resources for Merlin and Mount Dore are presented in Table 4.2. Total resources quoted by Chinova are

Merlin: 6.4Mt@1.5%Mo, 26ppm Re, 0.3%Cu

Mount Dore: 110.8Mt@0.55%Cu, 0.5g/tAu
(Chinova Resources, 2014, 2017)

Mineralised bodies

Merlin Mo mineralisation occurs in a series of moderately east dipping lenses comprising breccia to fracture-controlled mineralisation with thickness from less than 5m up to ~20m and with overall dimensions of ~1050m strike, ~450m downdip extent and up to ~80m overall stacked thickness (Valk, 2014). Mount Dore Cu mineralisation also sits within a moderately east dipping volume with dimensions ~2200m strike, ~500m downdip extent and ~150m thickness.

Figure 4.39 Merlin massive molybdenite breccia. 0.9m @46.4%Mo, 446g/tRe. Hole MDQ0264. Kirwin (2009)

HOST ROCKS

Resource Stratigraphy

Despite the relatively poor exposure at Merlin -Mount Dore aside from the Roxmere Quartzite ridge (locally 'SQT') and Mount Dore Granite, a complete east-dipping stratigraphic sequence is well preserved in the extensive diamond drilling at Merlin-Mount Dore (Hinman, 2012a).

Both the Merlin and Mount Dore resources are hosted on or close to the stratigraphic transition between the Staveley Formation and the Kuridala Formation.

Staveley Formation to the west comprises banded calc-silicates and interbedded calcareous sandstones-siltstones. Close to the stratigraphic top of Staveley Formation, drilling reveals a gradational sedimentalogical transition via a dominating and cleaning (quartz-richer) siltstone-component into a rhythmically-cycled, quartz-rich, sandstone-siltstone-dominated Roxmere Quartzite (Hinman, 2012a). The Roxmere Quartzite has a thickness up to 40m. Four or five major fining-upward, gradational cycles have be identified within the Roxmere Quartzite despite the strong Isan D2-D4 deformation overprint (Figures 4.44 4.45; Hinman, 2012a). The upper contact of the Roxmere Quartzite is similarly sedimentalogically gradational upwards into a further small thickness of Staveley Formation calc-silicates and/or calcareous sandstones-siltstones (Figures 4.40, 4.44, 4.45).

The sharper sedimentalogical and redox-contrasting transition into Kuridala Formation phyllites, phyllitic schists, phyllitic siltstones and carbonaceous metasiltstones is locally preserved in the drilling but is more commonly structurally modified due to the more phyllitic nature of the Kuridala Formation lithologies. Kuridala Formation lithology is significantly variable along strike with the package dominated by phyllitic lithologies around Merlin (Figure 4.45) but by carbonaceous metasiltstone to the south at Mount Dore (Figure 4.44).

Folded, hematite-dominated iron formations in the upper Staveley Formation southwest of Mount Dore (Figure 4.40) can be tracked northwards in the magnetics (Figure 4.41) and appear to have higher magnetite components in the calc-siliate lithologies.

Host Rocks

Merlin is hosted by Staveley Formation calc-silicates and Kuridala Formation carbonaceous metasiltstones, very commonly within breccias formed along stratigraphic and structural contacts of the two lithologies (Figures 4.45, 4.47 H-K; Hinman, 2012a; Murphy et al., 2017).

The calc-silicates have a banded texture comprising fine-grained, hematite-dusted, K-feldspar and albite-altered metasiltstone interbedded with fine to coarse-grained calcite, actinolite, quartz, magnetite and minor epidote and apatite. The carbonaceous metasiltstone comprises 60% quartz, 30% muscovite, 5% biotite and 5% graphite. The overlying phyllite has a well developed foliation and comprises 55% quartz and 45% subhedral to euhedral muscovite (Falkner & Phillips, 2017).

Mount Dore is hosted by the Kuridala Formation within a variably bleached carbonaceous metasiltstone-shale package (Figure 4.44, Figures 4.47A-G). Bleaching has made lithological determination problematic in the Mount Dore deposit but true phyllitic litho-types in both the lowermost and upper parts of the Kuridala Formation package at Mount Dore (Figure 4.44) are characterised by a very high mica content and a very strong schistosity (commonly kinked in the footwall of the Mount Dore Granite overthrust). This schistosity is generally lacking from the carbonaceous metasiltstones, bleached or not (Figures 4.47B, C). The bleached metasiltstones are composed of recrystallised quartz grains with a micro mosaic texture with occasional incipient alteration K-feldspar and fine white mica.

The Mount Dore Granite while not directly hosting mineralisation comprises a medium to coarse-grained assemblage of quartz, K-feldspar, plagioclase, ±biotite, ±hornblende, ±titanate, ±apatite, ±zircon (Falkner & Phillips, 2017).

METAMORPHISM

Metamorphic Grade

Regional metamorphism at Merlin-Mount Dore reached upper greenschist to amphibolite facies grade. Jaques et al. (1982) identified some biotite-zone, upper greenschist to lower amphibolite facies grade rocks in parts of the Staveley Formation but predominately andalusite-almandine-staurolite zone, amphibolite facies grade throughout the bulk of the Kuridala-Selwyn region. Peak metamorphism occurred during Isan D2 deformation prior to Cu-Au mineralisation.

INTRUSIVE ROCKS IN REGION

Granitoids

The Mount Dore Granite is an outlier, highly radiogenic intrusion of the Williams-Naraku Suite. The granite has been dated at 1516±10Ma (Pollard & McNaughton, 1997) and 1517±7Ma (Babo et al., 2017). The truncated intrusion is the unmineralised, structural hanging wall to both the Merlin and Mount Dore resources.

Mafic Intrusives

Metadoleritic-amphibolitic sills intrude the fine grained Kuridala Formation metasediments south of the Mount Dore Granite (Figure 4.40). They are regarded as being approximately syn-depositional with their hosting sediments, are metamorphosed to hornblende-plagioclase mineralogy (Brown & Porter, 2010) and are folded during Isan Orogeny.

Figure 4.40 (opposite left) Detailed geology of the Merlin-Mount Dore region compiled from historic and company mapping and interpretation. Extent of mineralisation has been vertically projected. Mapping and interpretation attribution as in Figure 4.5. Structural interpretation from Deep Mining Queensland (Murphy et al., 2017). Legend below. Map Projection GDA94 (MGA54)

Figure 4.41 (opposite right) Detailed Chinova vrmi magnetic image: greyscale rtp-2vd draped over coloured rtp highlighting stronger magnetic character of calc-silicate altered Staveley Formation and the Kuridala metadolerites and the absence of magnetic response associated with either Merlin or Mount Dore. Structural skeleton overlain. Same view as Figure 4.40. Map Projection GDA94 (MGA54)

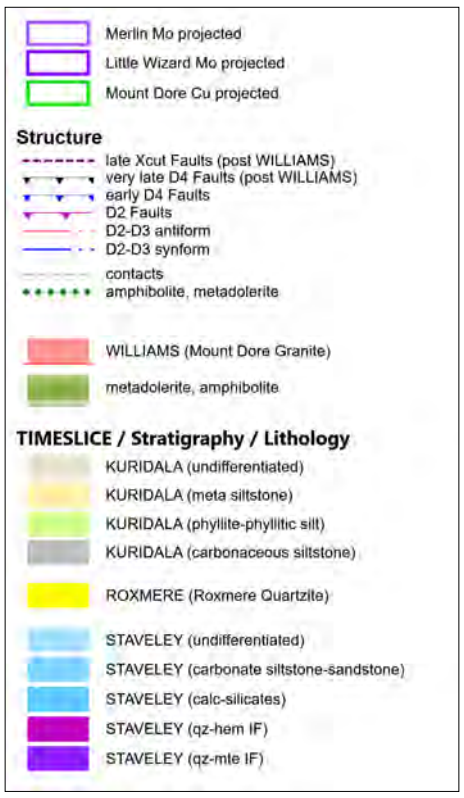

Figure 4.42 (opposite left) Local zoom of detailed 100m line-spacing, 2011 Heli-TEM EM Amplitude Channel 15 highlighting Kuridala carbonaceous meta-siltstone responses dipping beneath (and striking south of) the Mount Dore Granite and a depletion in EM conductivity response around Merlin-Mount Dore perhaps reflecting bleaching of carbonaceous metasediments. Cultural responses southwest of Ballarea. Structural skeleton overlain. Same map area as Figure 4.40. Map Projection GDA94 (MGA54)

Figure 4.43 (opposite right) Merged 2012 Chinova Residual Bouguer Anomaly ground gravity data highlighting a lack of density anomalism directly related to mineralisation apart from a potential low density domain associated with the oxide-rich southern portion of Mount Dore. Structural skeleton overlain. Same view as Figure 4.40. Map Projection GDA94 (MGA54)

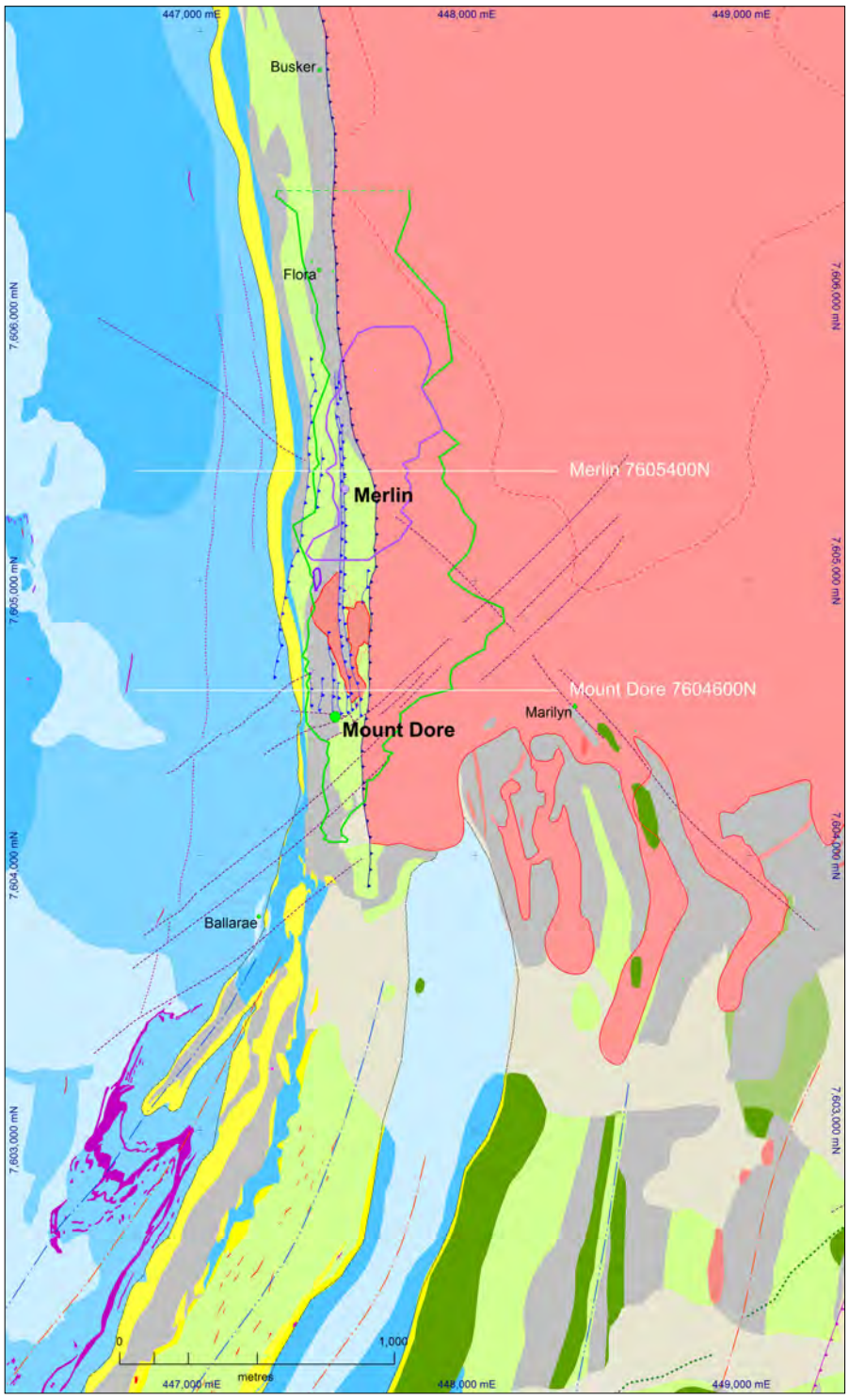
447,000 mE
448,000 mE
449,000 mE
Busker
Flora
Merlin
Merlin 7605400N
Mount Dore
Mount Dore 7604600N
Marilyn
Ballarae
7,606,000 mN
7,605,000 mN
7,604,000 mN
7,603,000 mN
0
1,000
metres

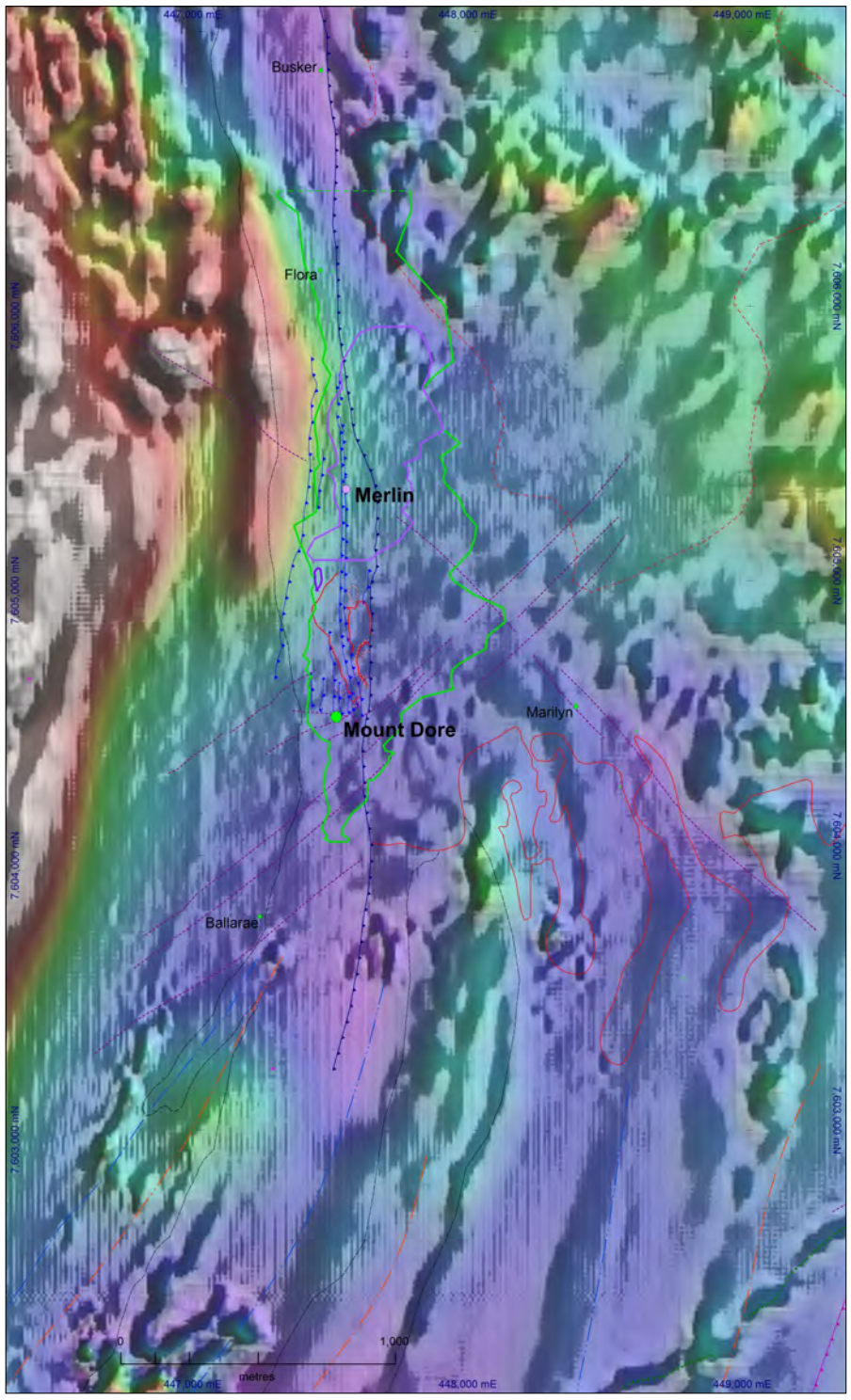
Busker
Flora
Merlin
Mount Dore
Marilyn
Ballarae
7,606,000 mN
7,605,000 mN
7,604,000 mN
7,603,000 mN
0
1,000
metres
447,000 mE
448,000 mE
449,000 mE

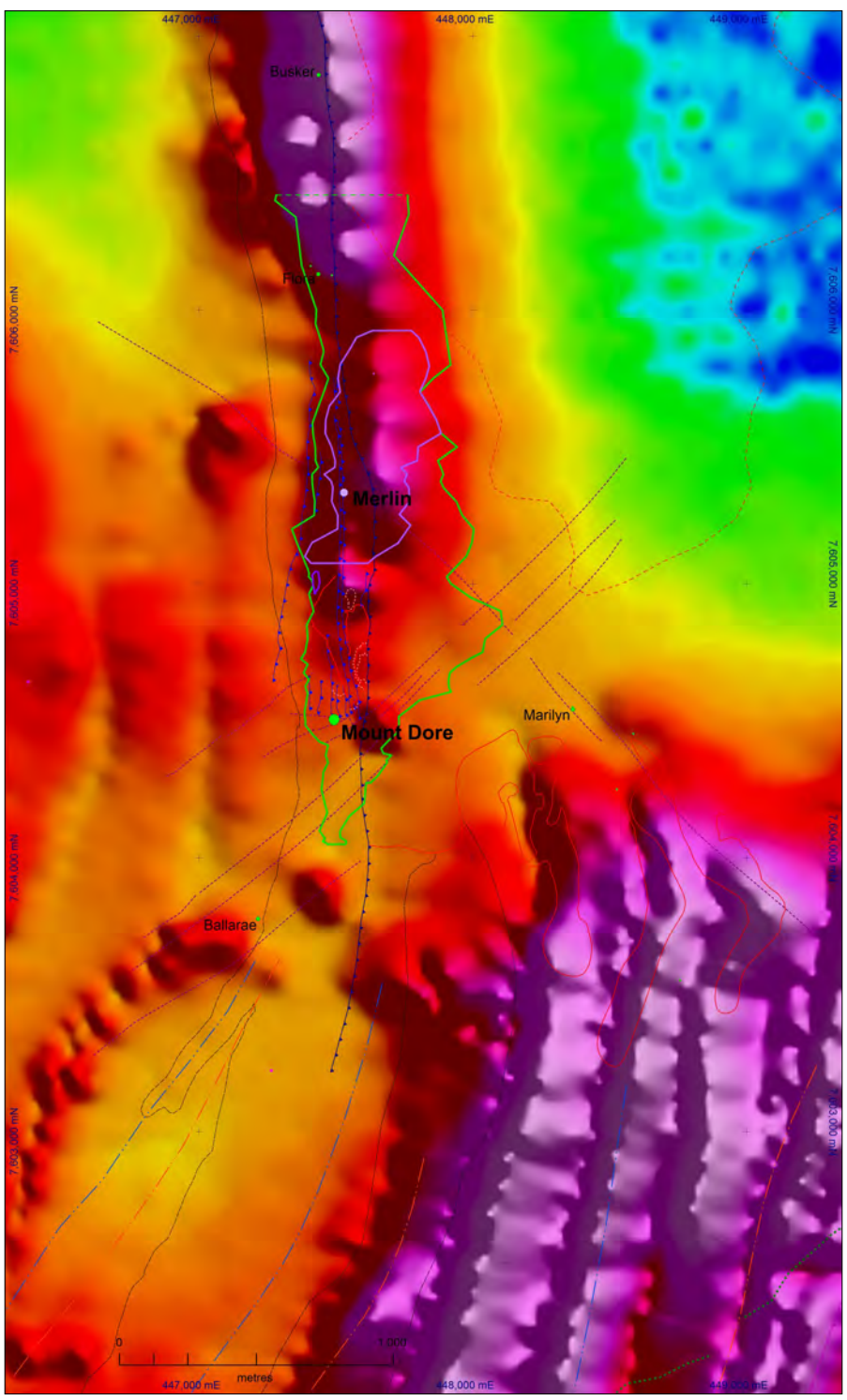
447,000 mE
448,000 mE
449,000 mE
Busker
Flora
Merlin
Mount Dore
Marilyn
Ballarae
7,606,000 mN
7,605,000 mN
7,604,000 mN
7,603,000 mN
0
1,000
metres

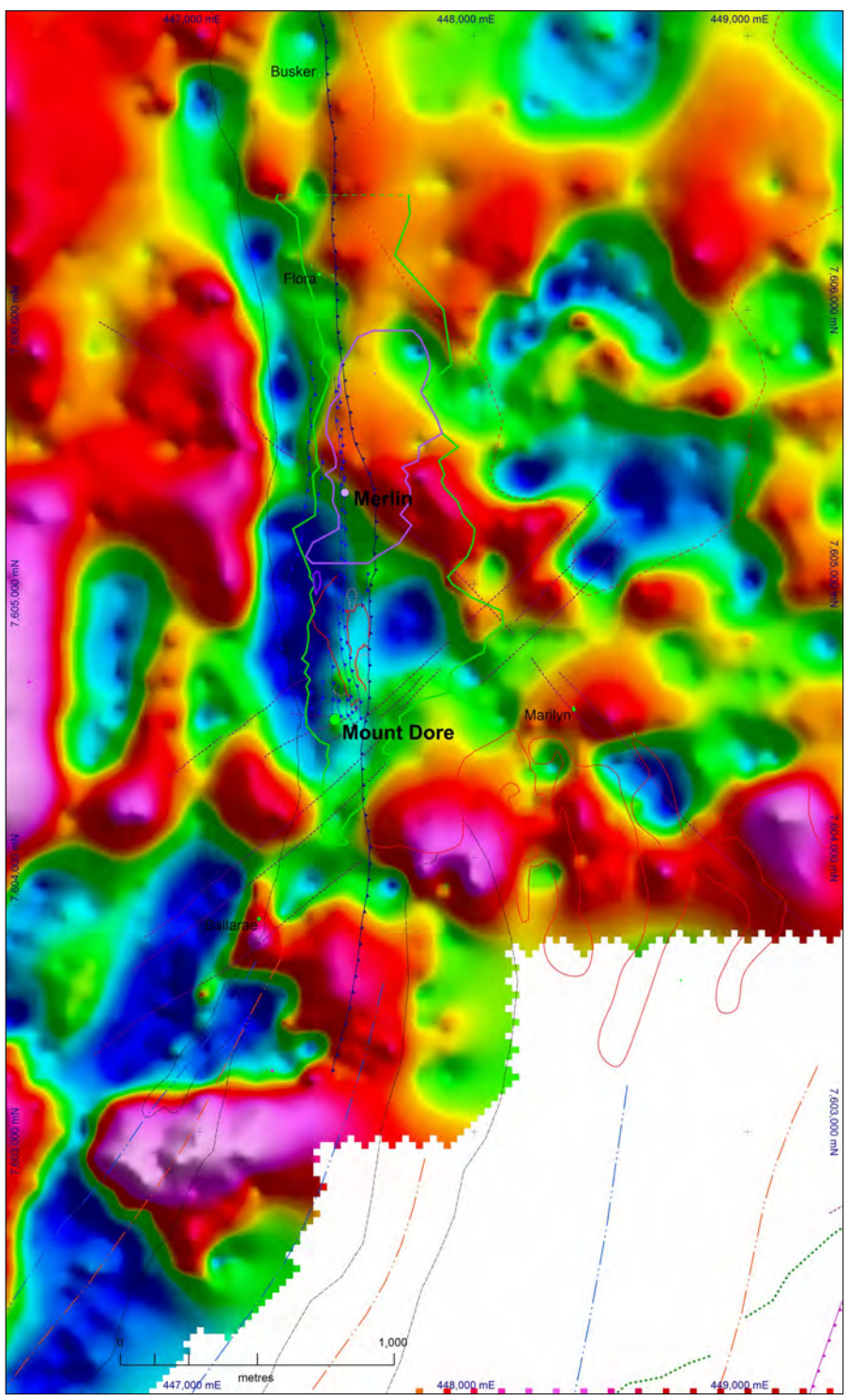
Busker
Flora
Merlin
Mount Dore
Marilyn
Ballarae
7,606,000 mN
7,605,000 mN
7,604,000 mN
7,603,000 mN
0
1,000
metres
447,000 mE
448,000 mE
449,000 mE

STRUCTURAL CHARACTERISTICS

Structural Setting

Outcrop is sparse at Merlin-Mount Dore between the Roxmere Quartzite 'SQT' ridge and the Mount Dore Granite but a number of discrete, small-displacement thrusts have been mapped (Figure 4.40; Hinman, 2012a) which correlate well with drillcore structures. Some of these demonstrably cross cut stratigraphy at very low angles, have tightly-associated Mo soil geochemistry (Figure 4.45 and 4.54) and are the updip expression of mineralisation-controlling structures at depth.

Importantly these control structures are small-scale structures with small displacements that would not (and do not) feature on regional scale structural maps. The only significant fault is the Mount Dore Granite overthrust fault which is demonstrably post-mineral and post-Mount Dore Granite and not related to mineralisation in a process sense.

Both the Merlin and Mount Dore resources lie close to the stratigraphic transition between the Staveley and Kuridala Formation packages. Two sections are presented here through Mount Dore (Figure 4.44) and Merlin (Figure 4.46) that were generated from detailed drillcore structural analysis (Hinman, 2012a; Murphy et al., 2017) and which demonstrate the structural setting and controls on the Cu-Au and Mo-Re resources.

The following uses the Isan structural nomenclature outlined in the previous Regional Deformation section and is consistent with that of Murphy et al., (2017).

Mount Dore 7,604, 600N (Figure 4.44)

- The drilling reveals the well-preserved, sedimentologically-gradational stratigraphy from Staveley Formation calc-silicates in the west, up into the Roxmere Quartzite, through some more calc-silicates, and into Kuridala Formation phyllites , phyllitic schists and carbonaceous meta-siltstones.
- The Mount Dore Kuridala Formation section is dominated by carbonaceous meta-siltstones that host most of the Cu-Au mineralisation.
- The early D4 reverse faulting ,which meshes well with surface-mapped faults (Figure 4.40), is complex, curvilinear and anastomosing. The faulting is in general slightly steeper than bedding and results in small displacements that would only be discernible in 1:500 scale mapping (or better) and detailed drill section analysis …. and would certainly not register in regional scale maps or interpretations.
- Brittle fracture and breccia damage zones around the reverse faults are well developed within the carbonaceous silts and along re-activated contacts, in particular, shallower dipping surfaces and contacts that are well oriented to extend subvertically in the transpressive northwest-directed shortening of early D4.
- Better developed mineralisation (higher grade shoots) are likely to have shallowly north-dipping plunges parallel to re-activating (vertically-extending) pre-existing fold plunges and the intersection of bedding and the early D4 faulting (see insert in Figure 4.44).
- The brittle, fracture and breccia, damage zones host the Cu-Au mineralisation largely within the carbonaceous meta-siltstones. The minor phyllitic volumes at Mt Dore host significantly less mineralisation due their highly schistose nature and ductile (non-brittle) re-activation in D4.
- The Mount Dore Granite overthrust Fault starkly contrasts with the mineralisation-controlling, early D4 faults. It is highly planar, it is post-mineral deforming both mineralisation and alteration, it juxtaposes internal, coarse-grained granite with the Mount Dore package and has a significant, mappable throw. This fault is the only demonstrable 'Mount Dore Fault' despite previous interpretations of the 'SQT' ridge (Lazo & Pal, 2009; Brown & Porter, 2010; Duncan et al., 2011, 2014) and the entire volume between the Roxmere Quartzite and Mount Dore Granite (Faulkner & Phillips, 2017) as the Mount Dore Fault.
- Late (post mineralisation and post-granite=post-Williams Suite) cross-cutting faulting shows minor off-setting of the sectional architecture. This fault zone is parallel to a regional northeast-trending joint set at Merlin-Mount Dore and produces a wide zone of late brittle deformation that marks the southern termination of the definable Mount Dore resource (Figure 4.40)

Merlin 7,605,400N (Figure 4.45)

- The Merlin drilling also reveals a well-preserved, sedimentologically-gradational stratigraphic transition from Staveley Formation calc-silicates in the west, up into and out of the ROXMERE Quartzite via some non-calcareous siltstones, through some more calc-silicates, and into Kuridala Formation phyllites , phyllitic schists and carbonaceous meta-siltstones.
- In contrast with the Mount Dore section, the Merlin Kuridala Formation section is dominated by phyllites and phyllitic siltstones with only a relatively thin carbonaceous meta-siltstone package sitting above the upper Staveley Formation calc-silicates. Some other minor carbonaceous meta-siltstones are interbedded within the phyllitic package (see also Figure 4.40)
- The early D4 faulting is again complex, curvilinear and anastomosing and is characterised by brittle fracture and breccia damage zones in the Staveley Formation calc-silicates and Kuridala Formation carbonaceous meta-siltstones, but by ductile (sometimes mylonitic) tight structures within the phyllitic lithologies.
- Brittle fracture and breccia zones host the Mo mineralisation, firstly along a central, early D4 reverse fault along which calc-silicate and carbonaceous siltstone is brecciated, and secondly, along normal stratigraphic calc-silicate - carbonaceous meta-siltstone contacts that are activated during D4 shortening and brecciate in both the footwall and hanging wall of the central mineralised D4 structure (see Figure 4.46).
- Better developed Mo mineralisation (higher grade shoots) have shallowly north-dipping plunges parallel to the intersection of bedding and the early D4 faulting. A clear and high grade example is where the footwall brecciated calc-silicate - carbonaceous meta-siltstone contact converges and merges with the D4 fault damage zone at -50mRL (Figure 4.45).
- The Mount Dore Granite overthrust Fault is again absolutely planar, is post-mineral and juxtaposes internal, coarse-grained Mount Dore granite with the Merlin package. It alone at Merlin-Mount Dore has a significant, mappable throw but is post-mineral.
- Reactivation of the structures hosting fracture and breccia-controlled Mo mineralisation at this post-Mount Dore Granite, late D4-time, deforms the weak Mo mineralisation to form the Mo-matrix breccias for which Merlin is well known (Figures 4.47J, K)
- Minor Cu mineralisation exists where early D4 structures intersect carbonaceous meta-siltstone higher in the package. This suggests different metal precipitation might simply be a function of different physio-chemical environments and that different timings for Cu-Au and Mo-Re mineralisation within the Merlin-Mount Dore system might be illusionary.
- Late cross-cutting faults cut the entire sequence including granite and result in minor offsets of the sectional architecture, and do potentially produce off-sets of ore that will have mine stope design significance.

Figure 4.44 (opposite top) Mount Dore Cross Section 7,604,600N from detailed drillcore structural analysis (Hinman, 2012) highlighting fault damage zone control on Cu-Au mineralisation largely hosted within variably bleached, Kuridala Formation carbonaceous metasiltstones (see text for detail)

Figure 4.45 (opposite bottom) Merlin Cross Section 7,605,400N from detailed drillcore structural analysis (Hinman, 2013) highlighting fault and contact reactivation damage zone control on Mo-Re mineralisation along re-activated stratigraphic and structurally juxtaposed Staveley Formation calc-silicates and Kuridala Formation carbonaceous metasiltstones (see text for detail)

Mount Dore

7,604,600N

Structure
- very late Xcut Fault (post WILLIAMS)
- late D4 Reverse Fault (post WILLIAMS)
- early D4 Mylonite (syn WILLIAMS)
- early D4 Reverse Fault (syn WILLIAMS)
- early D4 damage zone - mylonitic / shear
- early D4 damage zone - brecciation

Lithology
- contact breccia - tourmalinised
- MOUNT DORE GRANITE
- KURIDALA PHYLLITE-PHYLLITIC SILT
- KURIDALA BLACK SILT
- ROXMERE QUARTZITE
- STAVELEY SILT
- STAVELEY CALC-SILICATE

Mineralisation
- Cu mineralised BRECCIA
- Mo mineralised BRECCIA

DDH Assay
- Mo ppm
- Cu percent

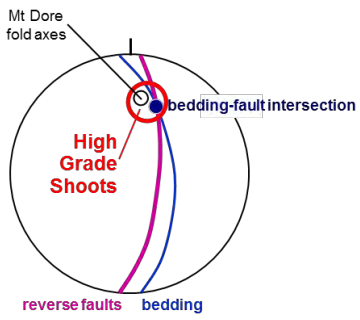

400mRL
300mRL
200mRL
100mRL
0mRL
-100mRL
-200mRL
447,200mE
447,300mE
447,400mE
447,500mE
447,600mE
447,700mE
447,800mE
447,900mE
448,000mE

Merlin

7,605,400N

Soil Geochem Anomalism
- Mo anomalism
- Cu anomalism

- projected development

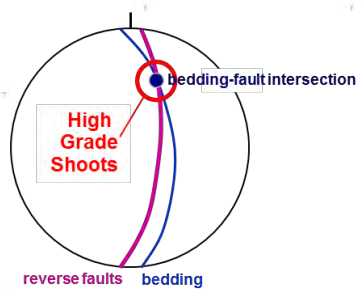

Structural History

The structural history of the rocks hosting the Merlin-Mount Dore resources is summarised below

- Deposition of (1) interbedded calcareous sandstone-siltstone Staveley Formation between ca1725-1710Ma, (2) cyclically-graded, quartz-rich Roxmere Quartzite sedimentation ca1710Ma, (3) fine-grained, variably carbonaceous, Kuridala Formation turbidites ca1710-1680Ma with relatively minor mafic sill emplacement.
- During thin skinned, Isan D1 orogeny with north-northwest-directed shortening ca1590-1570Ma the entire Staveley Formation to Toole Creek Volcanic succession is allochthonously thrust emplaced over older successions. North to north-northwest-directed thrusting is associated with internal ramping within the allochthonous block. D1 is expressed along the Starra line of deposits but not directly at Merlin-Mount Dore.
- Isan D2 deformation driven by east-west shortening, at Merlin-Mount Dore produces north-south folding with sub-horizontal F2 fold axes preserved south of the Mount Dore Granite, rotates the Staveley-Kuridala Formation host packages to moderate east dips and produce strong S2 fabrics in clay-richer lithologies. Peak metamorphism occurs during D2 deformation.
- Some small-scale, folds at Mount Dore with variable north to north-northeast fold axes have been mapped and logged in drillhole sections (Beardsmore, 1992; Hinman, 2012a; Figure 4.44) as potential D3 folds. Beardsmore (1992) notes coarse D3 crenulation of S2 fabrics but their association with F3 folds is not made clear. Later crenulation and kinking of S2 fabrics is also associated with the Mount Dore Granite overthrust.
- D4 reverse to transpressive faulting is generally steeper than bedding, slightly more north-northeasterly striking than stratigraphy and brittle in character (Figures 4.40, 4.44, 4.46). Fracture and breccia networks associated with these D4 small-displacement-but-high-damage structures control primary Cu-Au and Mo-Re mineralisation (Hinman, 2012a). In phyllitic, post-peak-metamorphic lithologies these structures are ductile and tight and can be locally mylonitic in character.
- Mount Dore Granite intrusion at depth is interpreted to be broadly synchronous with D4 deformation. Small slithers of fine-grained intrusion exhibiting marginal brecciation and touminalisation are preserved within the D4-faulted Kuridala Formation packages (Figures 4.40, 4.44) west of the post-mineral and overthrust main body of coarse-grained Mount Dore Granite.
- Post-mineralisation and post-granite solidification, a portion of the main body Mount Dore Granite overthrusts Merlin-Mount Dore mineralisation from its crystalliation location at depth below (or adjacent to) the Merlin-Mount Dore system. Re-activation associated with this overthrusting mills the mineralised fracture and breccia networks along D4 faults to form the very high grade, molybdenite-matrix breccias for which Merlin is renowned (Figures 4.39, 4.47J, K). Deformation of earlier formed molybdenite has important implications for Re-Os dating (see Absolute Ages below) and paragenetic relationships.
- Late conjugate faulting with steep to moderate dips and northwest and northeast orientations is coherent with late jointing throughout the Selwyn region. Some of these faults have significant displacement that may impact ultimate mine geometries at Merlin and Mount Dore.

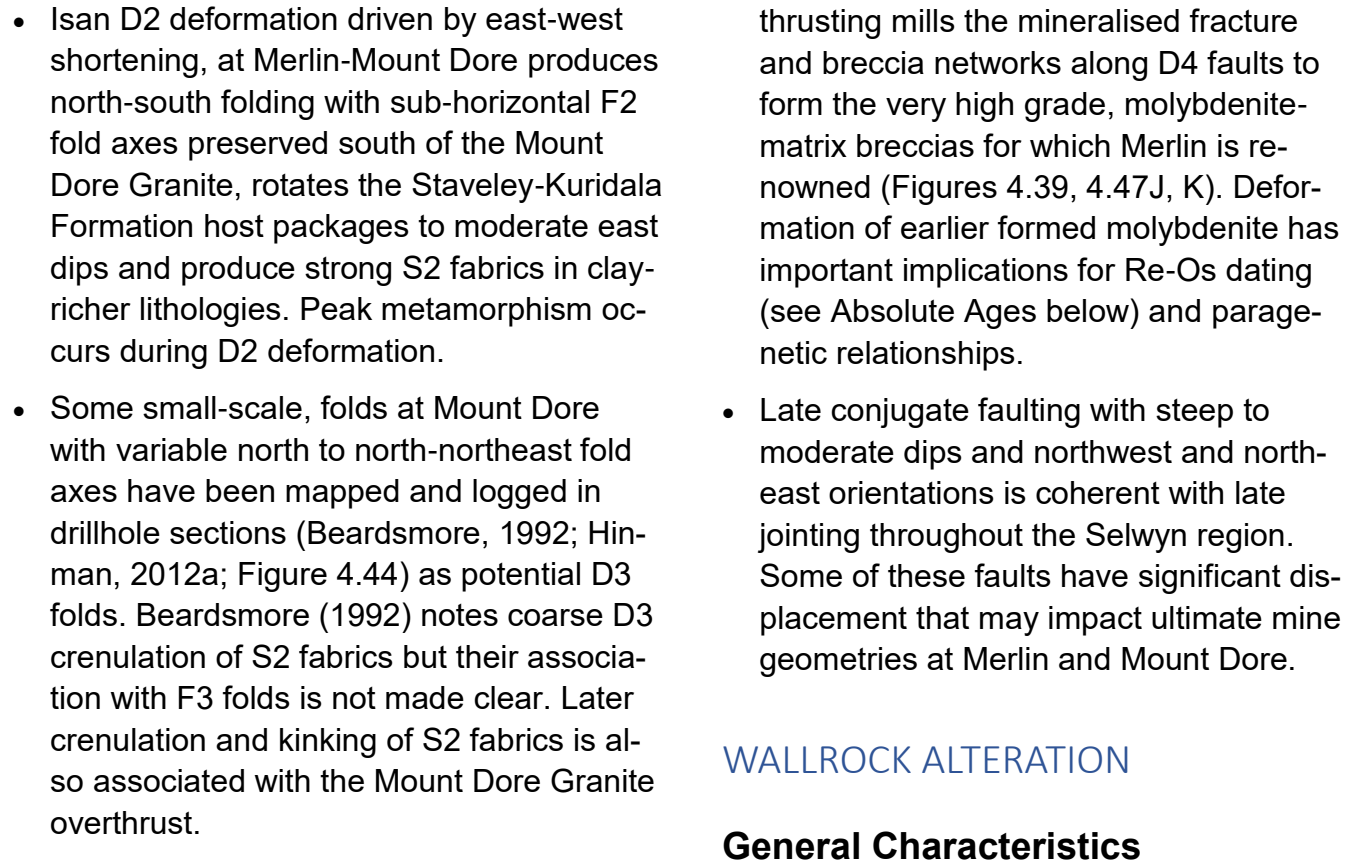

Figure 4.46 Merlin Long Section showing cumulative grade products through projected lenses and existing development. From Faulkner & Phillips, 2017.

Figure 4.47 (opposite) Merlin-Mount Dore mineralised rock specimens, core and slabs. **A**- Mount Dore copper oxides at Mount Dore surface workings (Goss, 2009); **B**- Fracture controlled copper oxides in carbonaceous meta-siltstone MDHQ07 87m (Goss, 2009); **C** - Variably bleached laminated carbonaceous meta-siltstone (Nunn, 2012); **D**- Mount Dore breccia showing rounded, variably bleached, albite-silica-altered, meta-sedimentary clasts with chalcocite, chrysocolla and native Cu mineralisation MDQ0088 223.9m (Kirwin, 2009): **E**- Variably albite-K-feldspar-altered, meta-siltstone clast breccia with strong chalcocite mineralisation MDQ0088 270.0m (Kirwin, 2009); **F**- Albite-K-feldspar-altered, meta-siltstone breccia with strong chalcocite mineralisation (Kirwin, 2009); G- Silica-albite altered banded calc-silicate with fracture and replacement-controlled chalcopyrite mineralisation MDQ0149 244.6m (Kirwin, 2009); **H**- Silica-albite-K feldspar-altered banded calc-silicate with fracture/stylolite-controlled molybdenite mineralisation MDQ0149 249m (Kirwin, 2009); **I**- Silica-albite altered siltstone with fracture network-controlled molybdenite mineralisation MDQ0149 232m (Kirwin, 2009); **J**- Molybdenite-matrix breccia with silica-hematite-dusted albite (quartz-K feldspar) altered, sub-rounded clasts MDQ0147 233.1m; 8.1%Mo, 151ppmRe (Kirwin, 2009); **K**- Molybdenite-matrix breccia with silica-hematite-dusted albite (quartz-K feldspar) altered, sub-rounded clasts MDQ0147 238.4m; 12.4% Mo, 305ppmRe, 0.6%Cu, 0.16g/tAu, 83g/tAg (Kirwin, 2009)

WALLROCK ALTERATION

General Characteristics

Both Merlin and Mount Dore mineralisation is associated with pervasive, pre-brecciation, post-peak metamorphic, ±hematite-stained, ±scapolitic silica-albite alteration associated with bleaching of carbonaceous, fine-grained metasedimentary lithologies (Lazo & Pal, 2009; Nunn et al., 2012) and the actinolite-diopside-epidote ±biotite ±magnetite ±scapolite ±garnet calc-silicate alteration of Staveley Formation calcareous siltstone-sandstones (Lazo & Pal, 2009; Duncan et al., 2014; Figures 4.47C to K). Sodic-calcic alteration is less evident in the less brecciated and less permeable, highly schistose phyllitic lithologies.

Overprinting fracture, vein and breccia-controlled and pervasive replacement crystalline K feldspar-quartz alteration accompanies copper mineralisation at Mount Dore (Lazo & Pal, 2009; Figure 4.47E) and is present in Merlin breccia clasts (Figures 4.47H, J & K). Intense, replacive quartz-K feldspar alteration has been misidentified as granite and logged as ‘pseudo-granite’ but represents intense potassic alteration associated with mineralisation (Greene, 2011).

Supergene alteration at Mount Dore has a complex, strongly down-dip-fingering geometry controlled by the fracture and breccia-controlling structures (Hinman, 2012a) and is well developed at the southern end of the resource. Secondary copper minerals include chrysocolla, cuprite, native Cu, chalcotrichite, pseudomalachite, azurite and malachite (Lazo & Pal, 2009) Down dip and down-plunge hypogene sulphides include chalcocite (Figures 4.47E & F; Kirwin, 2009), chalcopyrite and pyrite.

Zonation

No deposit scale mineral and/or alteration zonation studies have been completed at Merlin-Mount Dore, however, Nunn et al. (2012) undertook geochemical and alteration analyses on the two sections presented here (Figures

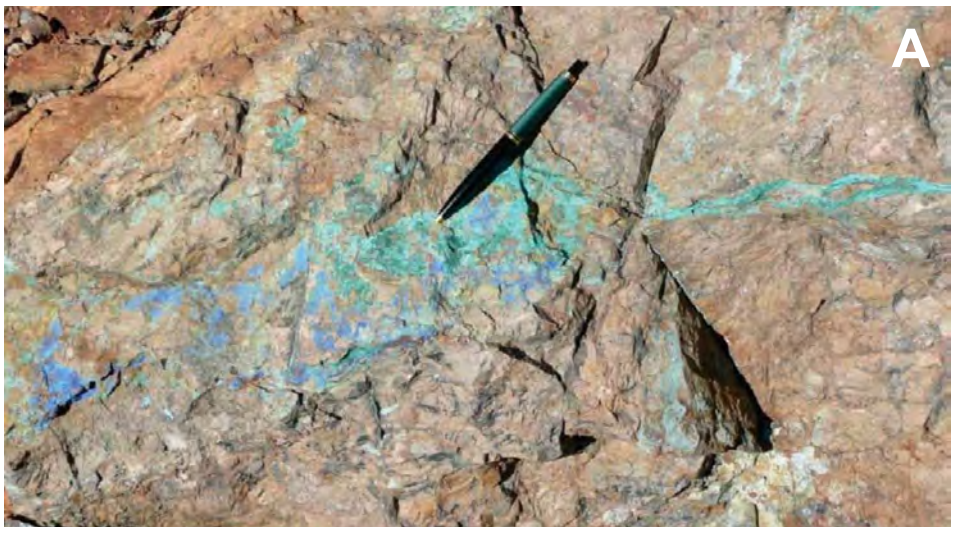
A


B


C

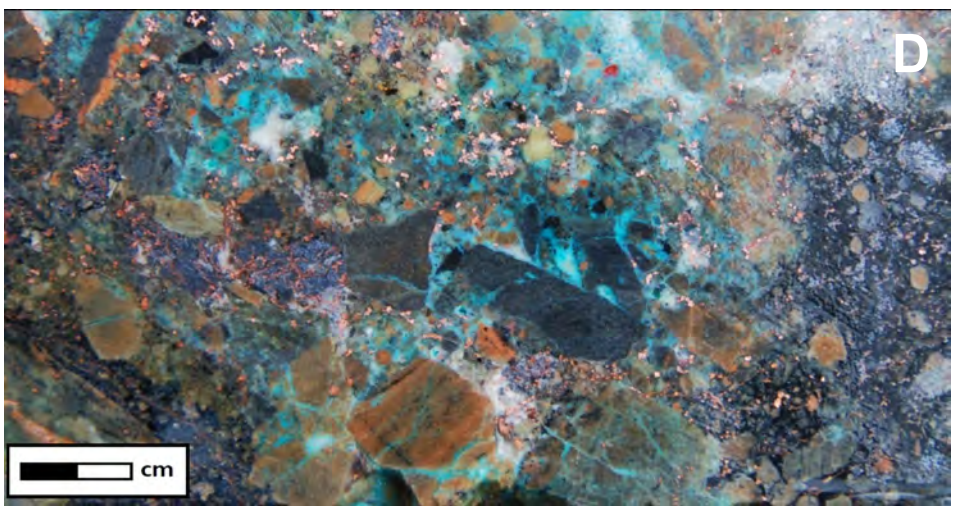
D
cm


E
cm

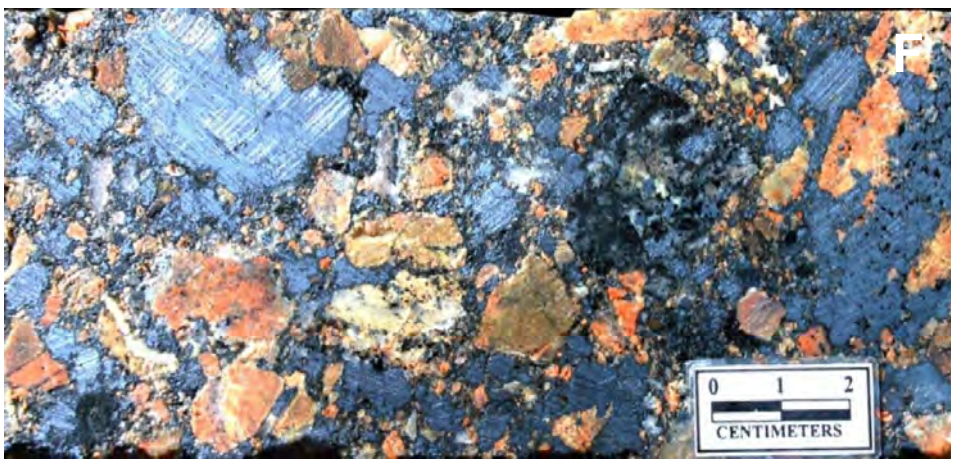
F
0 1 2
CENTIMETERS

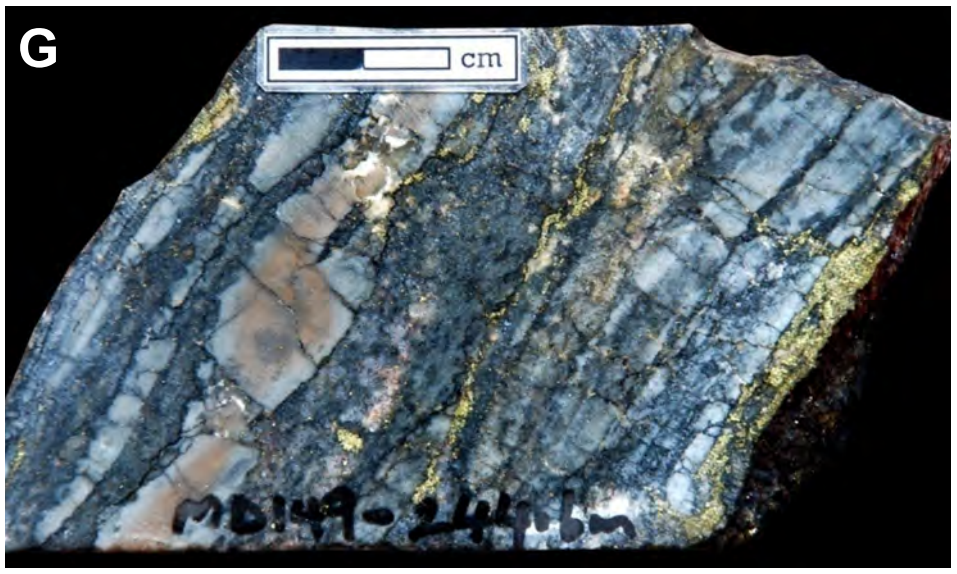
G
cm

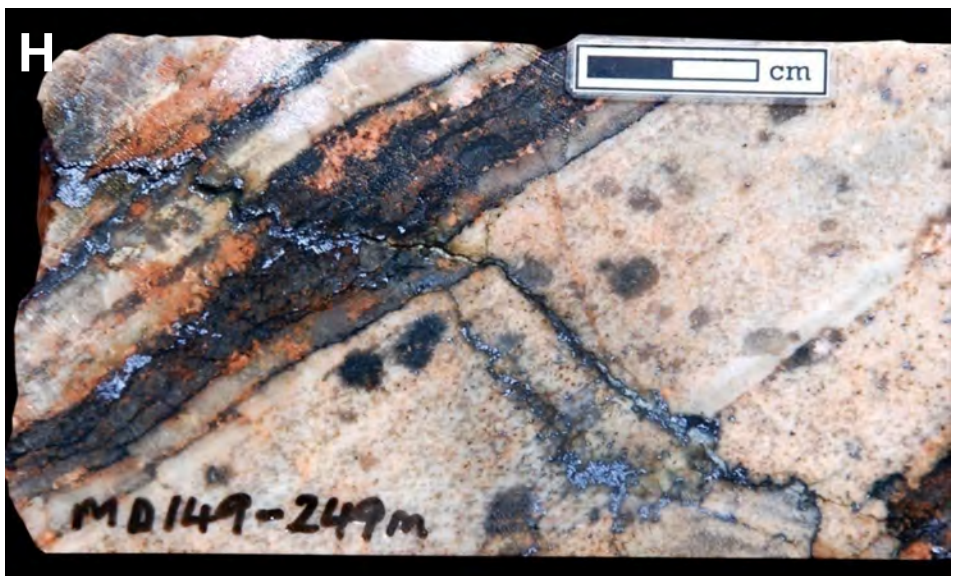
H
cm
MD149-249m

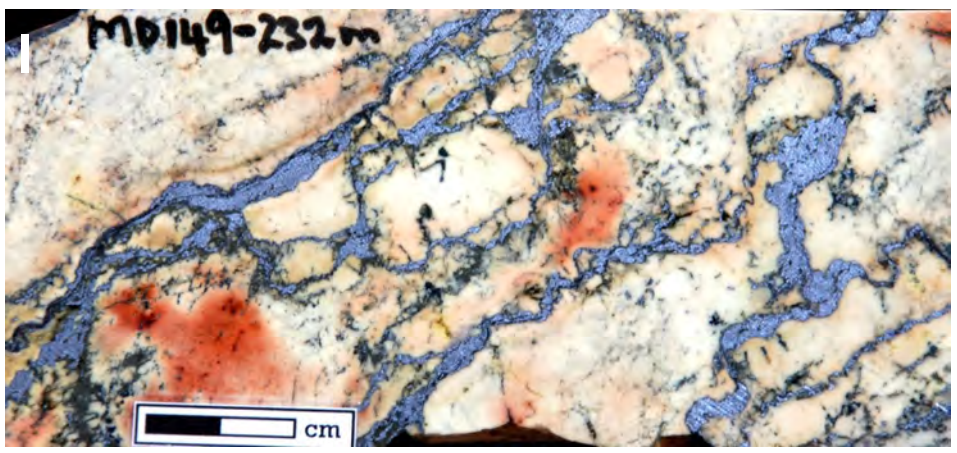
I
MD149-232m
cm

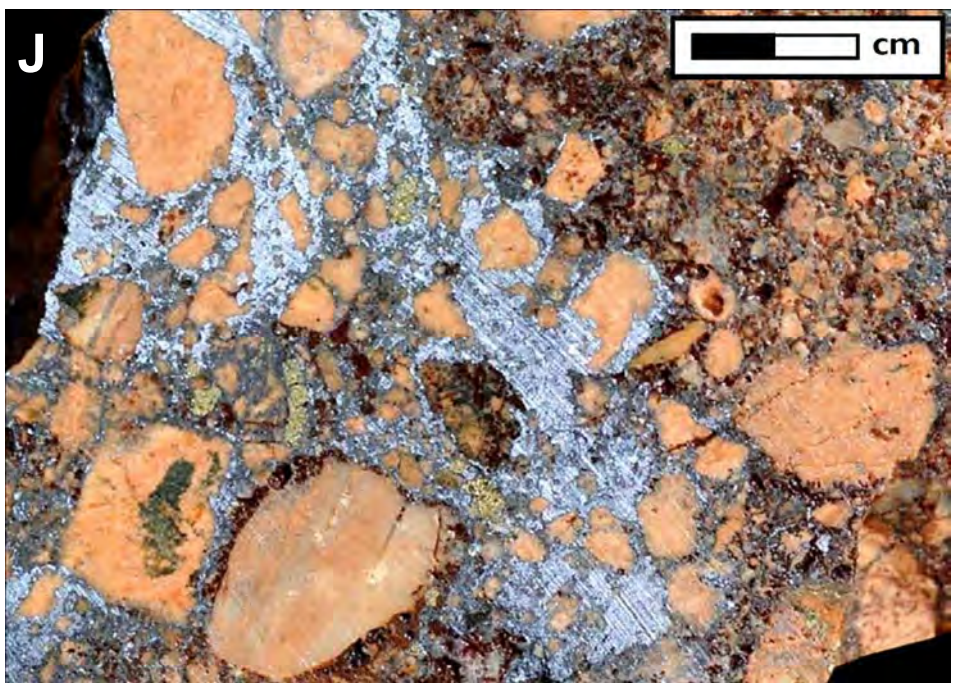
J
cm

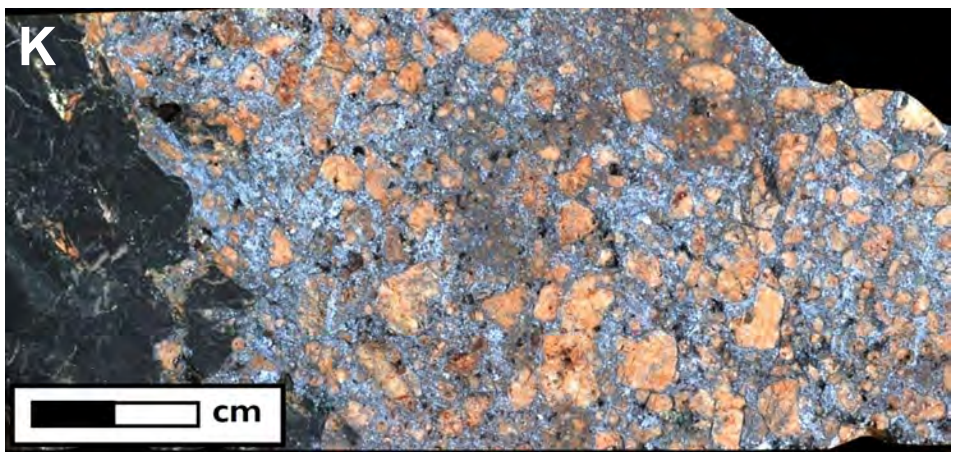
K
cm

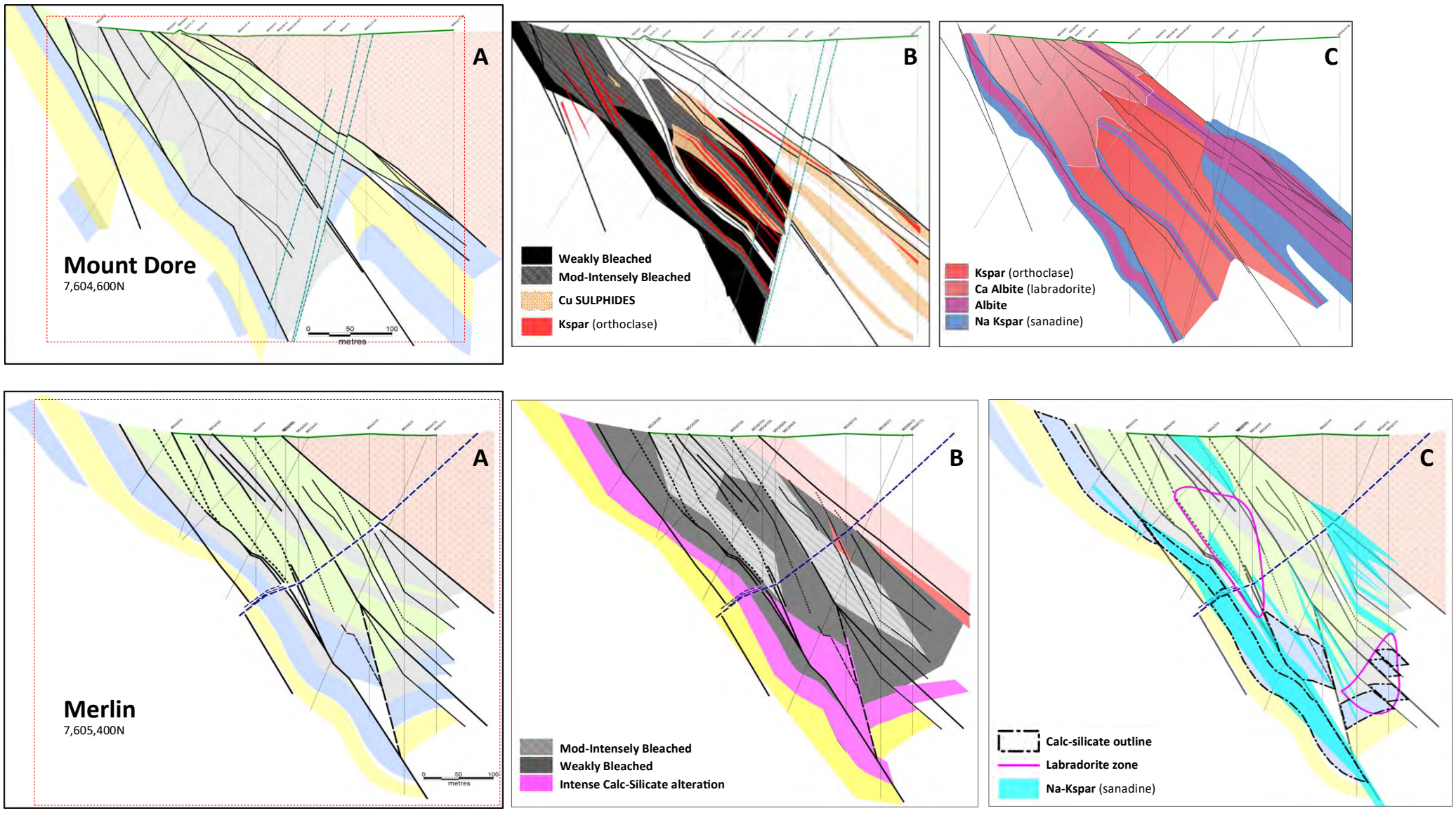

Figure 4.48 (top A-B-C) Mount Dore section alteration zonation (Nunn et al. 2012) **A**- Mount Dore drillcore-logged Section (Figure 4.44 for Legend). **B**- Moderate to intense bleaching of carbonaceous meta-siltstones associated with K feldspar alteration and copper mineralisation. Note absence of calc-silicate alteration of the upper Staveley Formation (cf. Merlin; Figure 4.49B below) **C**- Distribution of feldspar compositions showing K feldspar alteration within the copper-mineralised carbonaceous meta-siltstones (see also Figure 4.44) transitional upwards into a supergene labradorite-dominated zone and with albite-sanadine compositions associated with Stavaley Formation alteration.

Figure 4.49 (bottom A-B-C) Merlin section alteration zonation (Nunn et al. 2012) **A**- Merlin drillcore-logged Section (Figure 4.46 for Legend) **B**- Weak bleaching of carbonaceous meta-siltstones associated with molybdenite mineralisation in and around calc-silicate-carbonaceous siltstone contacts (see Figure 4.46). Strong calc-silicate alteration of the upper Staveley Formation (cf. Mount Dore; Figure 4.48B above). Moderate to intense bleaching on Merlin section attributed to phyllic lithologies. **C**- Distribution of feldspar compositions highlighting strong K feldspar (sanadine) alteration associated with strong molybdenite mineralisation in and around calc-silicate-carbonaceous siltstone contacts (see Figure 4.46) and abrupt updip termination of K feldspar alteration with molybdenite mineralisation.

4.44 & 4.46) aimed at identifying zonation patterns that might define vectors to ore. They undertook the study using an Exoscan™ Fourier Transform Infra-Red (FTIR) spectrometer that acquires spectral information that can be processed to distinguish compositional variations in feldspar mineralogy. In addition they logged relative bleaching and other mineralogical variations.

Although Nunn et al. (2014) have interpreted a reversed paragentic scheme, with sodic alteration overprinting potassic alteration compared with other workers, their mapping of bleaching and feldspar compositions does present some within-section and between-section zonation patterns that vector stronger alteration and suggest directions to potential further ore, and shed light on the relationship between copper and molybdenum mineralisation.

Figures 4.48 & 4.49 present Nunn et al.'s bleaching and feldspar composition data. Important relationships from their work are highlighted below:

- Mount Dore copper mineralisation is associated with moderate to intense bleaching of carbonaceous meta-siltstones.
- Stronger copper mineralisation at Mount Dore is associated with K feldspar (orthoclase) alteration.
- An updip transition from K feldspar to labradorite feldspar compositions at Mount Dore may be associated with supergene alteration effects.
- At Mount Dore, the upper Staveley Formation is NOT calc-silicate altered but exhibits an albite-sanadine alteration overprint.
- In contrast, at Merlin the upper Stavely Formation is intensely calc-silicate altered with a strong K feldspar (sanadine) overprint associated with molbdenum mineralisation.

Nunn et al. (2012) conclude that:

- Primary copper mineralisation occurs within fractures and breccias associated with faulting within the carbonaceous lithologies.
- Deposition of copper mineralisation is interpreted to be the result of mixing of oxidised, sulphur-poor, Na, Cl, (Cu, Mo, Re) -rich brine with reduced, sulphur-rich fluids sourced from the carbonaceous meta -siltstones
- Molbdenum mineralisation occurs at the contacts between calc-silicates and carbonaceous meta-siltstones.
- Deposition of molybdenite is interpreted to be the result of acid, oxidised, sulphur-poor, Na, Cl, (Cu, Mo, Re) -rich brine contacting pH-buffering calc-silicate and reduced sulphur rich fluids source from the Black Shale.

Spatially Merlin Mo-Re mineralisation is completely contained within the Mount Dore Cu system (Figures 4.40 & 4.46). Nunn et al. (2013) and Hinman (2012a) noted at Merlin that structures controlling molybdenite mineralisation appeared to also control copper mineralisation updip where the structure intersected carbonaceous meta-siltstone which suggested the possibility that the same fluid produced Mo and Cu mineralisation in a zoned system controlled by host lithology. Nunn et al.'s work suggested that with respect to calc-silicate alteration Merlin is more proximal compared to Mount Dore where calc -siliates are not well developed.

In contrast, Green (2011) who undertook cathodoluminescence and fluid inclusion studies on the intense K feldspar-quartz (pseudo granite) alteration at Merlin, interprets the unusual Merlin Mo system to post-date and overprint the fringes of the Mount Dore Cu IOCG system. Green (2011) highlighted a distinctive lack of carbonate and CO_2-bearing fluid inclusions at Merlin that are generally characteristic of IOCG Cu-Au systems. Two distinct fluid systems and alteration parageneses are proposed by Green (2011), viz

Mount Dore: potassic, silicic, carbonate and chloritic alteration stages with chalcopyrite-pyrite ore

Merlin: potassic, silicic and phyllic alteration stages with molybdenite only ore

HALOS

Extent

The superficial extent of Mount Dore secondary copper mineralisation was relatively small with surfical workings over a few 10s of square meters. Merlin mineralisation is completely blind. No studies focused on the aerial extent of lithogeochemical alteration have been completed at Merlin and Mount Dore.

Geophysical Expression

The detailed Chinova magnetic, gravity, heliTEM and radiometric U^2/Th data over Merlin-Mount Dore are presented in Figures 4.41 to 4.43 and Figure 4.51.

No particular magnetic or gravity expressions are directly linked with Merlin or Mount Dore mineralisation apart from potential low densities associated with the oxide-rich, supergene, southern, up-plunge portion of Mount Dore (Figure 4.43). Variations in calc-silicate alteration of the Staveley Formation are evident in the magnetics (Figure 4.41) west and northwest of Merlin.

A diminution in EM response (Figure 4.42) over both Merlin and Mount Dore in the Kuridala Formation reflects graphite-destruction associated with albite-quartz alteration bleaching of the carbonaceous meta-siltstones. It appears to be a direct geophysical expression of alteration at Merlin-Mount Dore and has an extent approximately equivalent to the extent of mineralisation at depth (Figure 4.42).

Uranium anomalism enhanced by radiometric U^2/Th (Figure 4.51) highlights significant anomalism over Mount Dore and a second stronger zone west of the Mount Dore Granite Overthrust between Flora and Busker.

Geochemical Expression

Copper, gold and molbdenum soil geochemistry over Merlin-Mount Dore are presented in Figures 4.52 to 4.54. The following geochemical responses are highlighted:

- The southern extent of Mount Dore shows strong soil Cu anomalism (>300ppmCu; Figure 4.52) over a broad area. Murphy et al. (2017) interpret this to reflect the up-plunge surface projection of the Mount

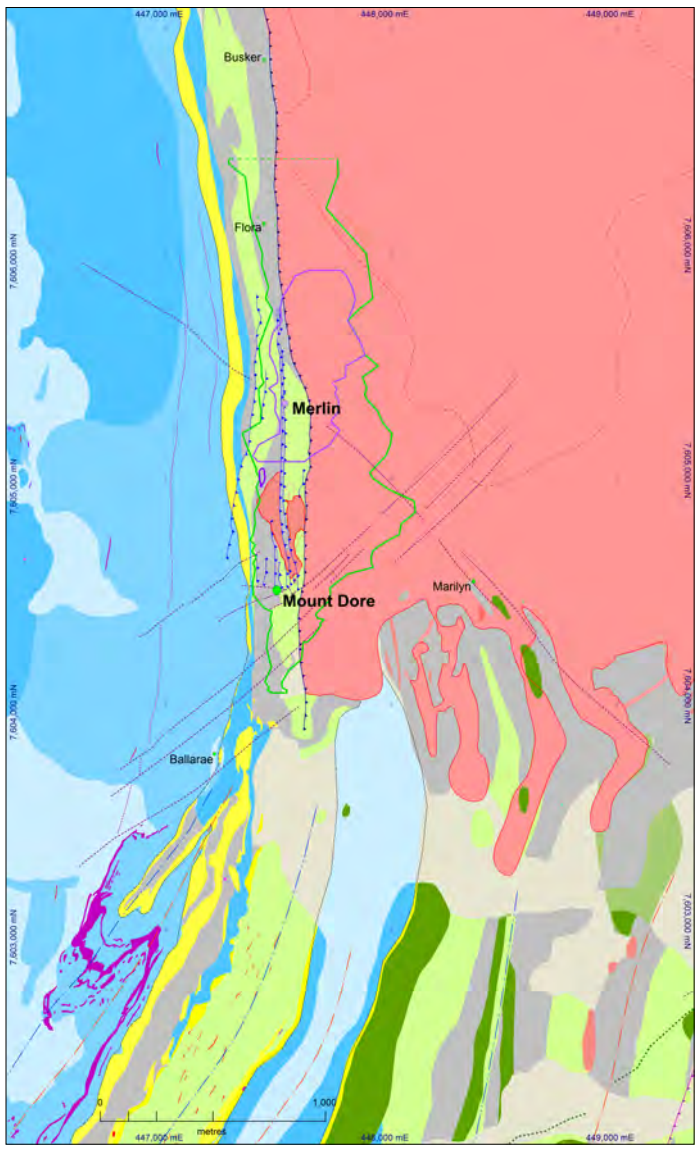

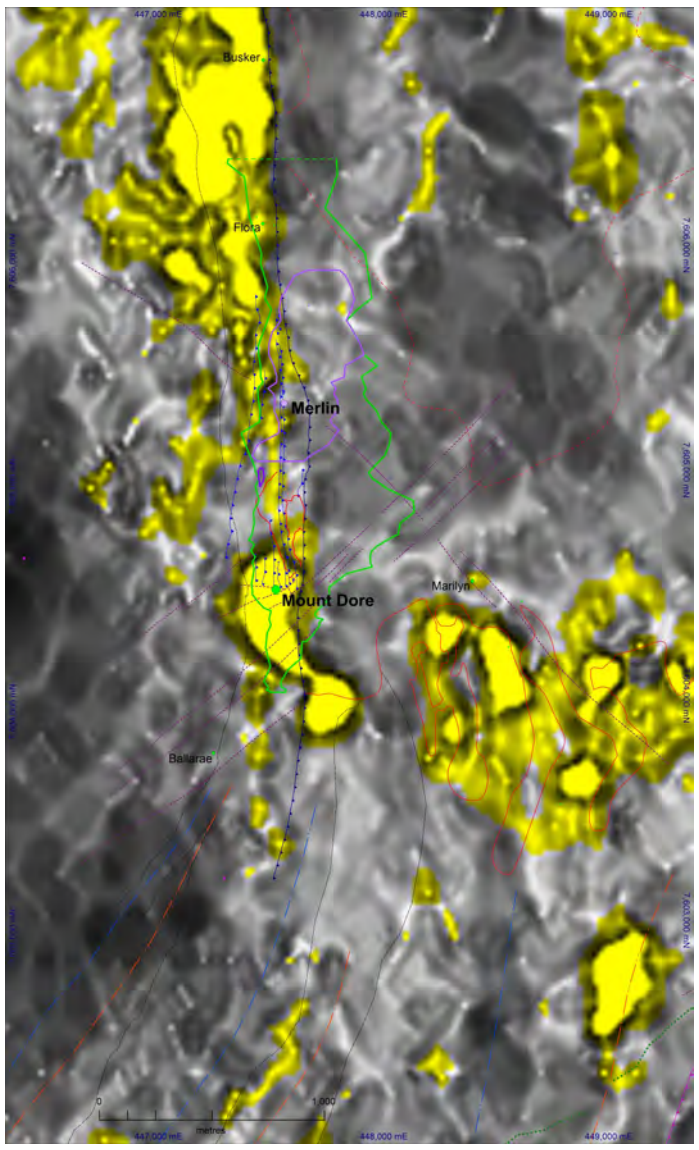

Figure 4.50 (right) Detailed geology of the Merlin-Mount Dore area. Legend as for Figure 4.40. All maps in panel same view with structural skeleton. Map Projection GDA94 (MGA54)

Figure 4.51 (far right) Merlin-Mount Dore U^2/Th from detailed 2018 '1370' Cloncurry Radiometrics highlighting anomalism over Mount Dore and between Flora and Busker.

Figure 4.52 (below) Merlin-Mount Dore -80# soil Copper on Worldview image draped over DEM highlighting strong soil Cu anomalism at southern end of shallow north-plunging Mount Dore system and a second region of strong anomalism between Flora and Busker.

Figure 4.53 (below centre) Merlin-Mount Dore -80# soil Gold on Worldview image draped over DEM showing no Au anomlism over Mount Dore but anomalism between Flora and Busker.

Figure 4.54 (below right) Merlin-Mount Dore -80# soil Molbdenum on Worldview image draped over DEM highlighting extreme Mo anomalism west of the Roxmere Quartzite ridge southwest of Merlin and minor anomalism updip of known Merlin mineralisation.

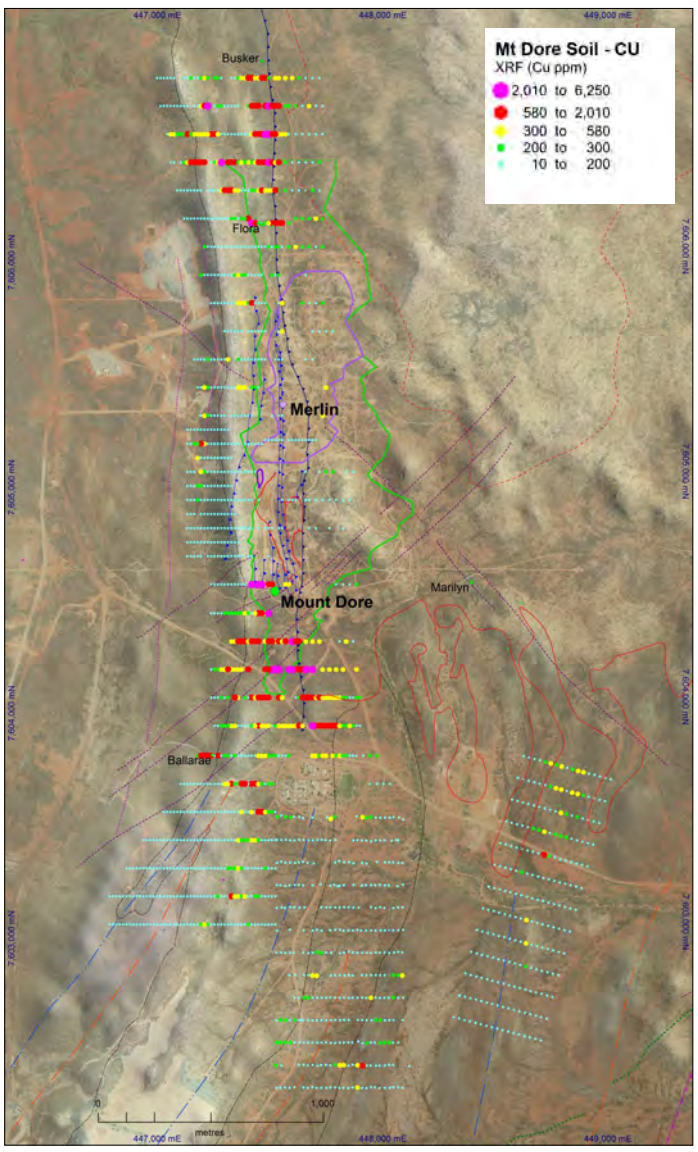

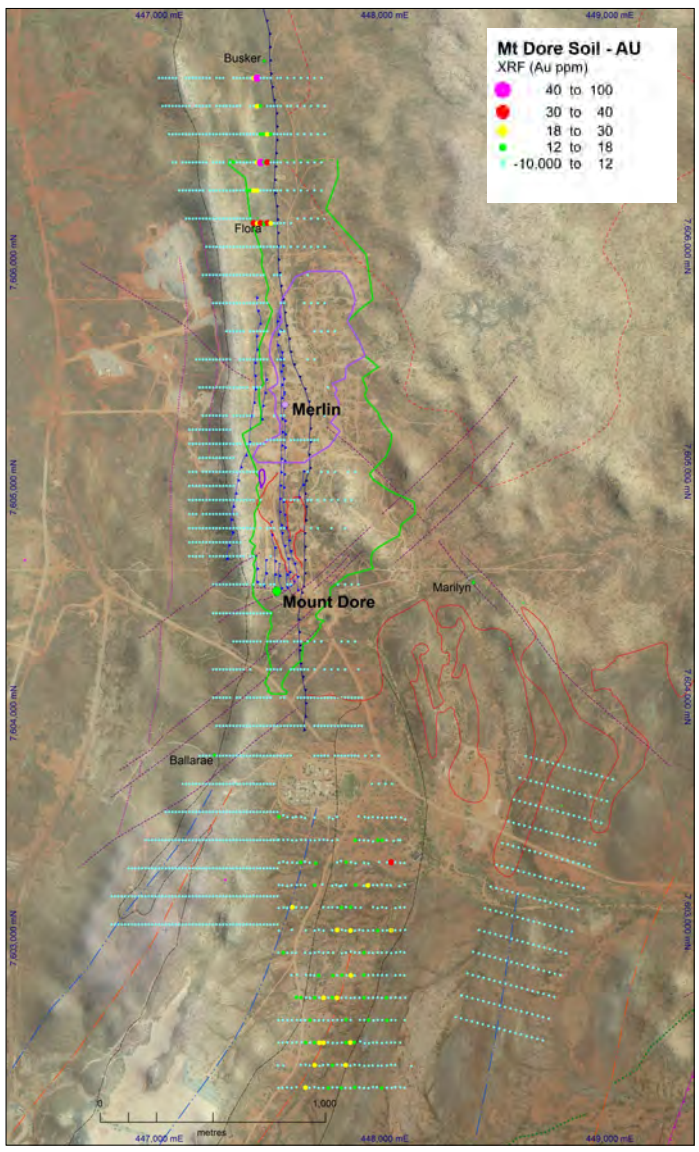

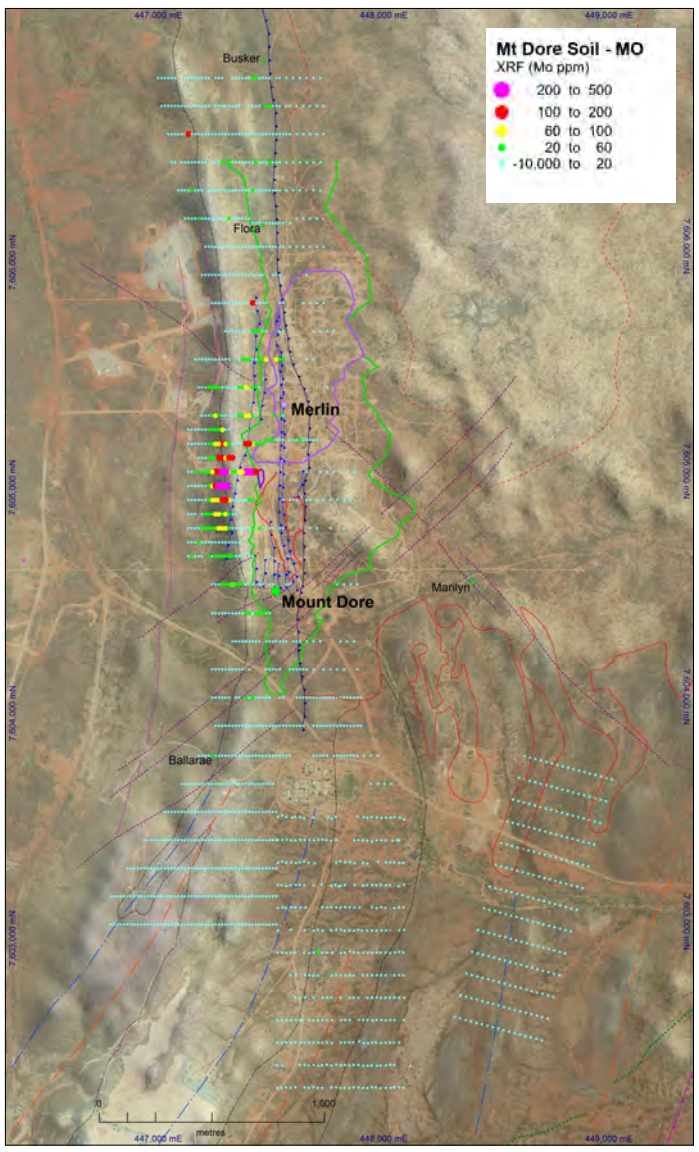

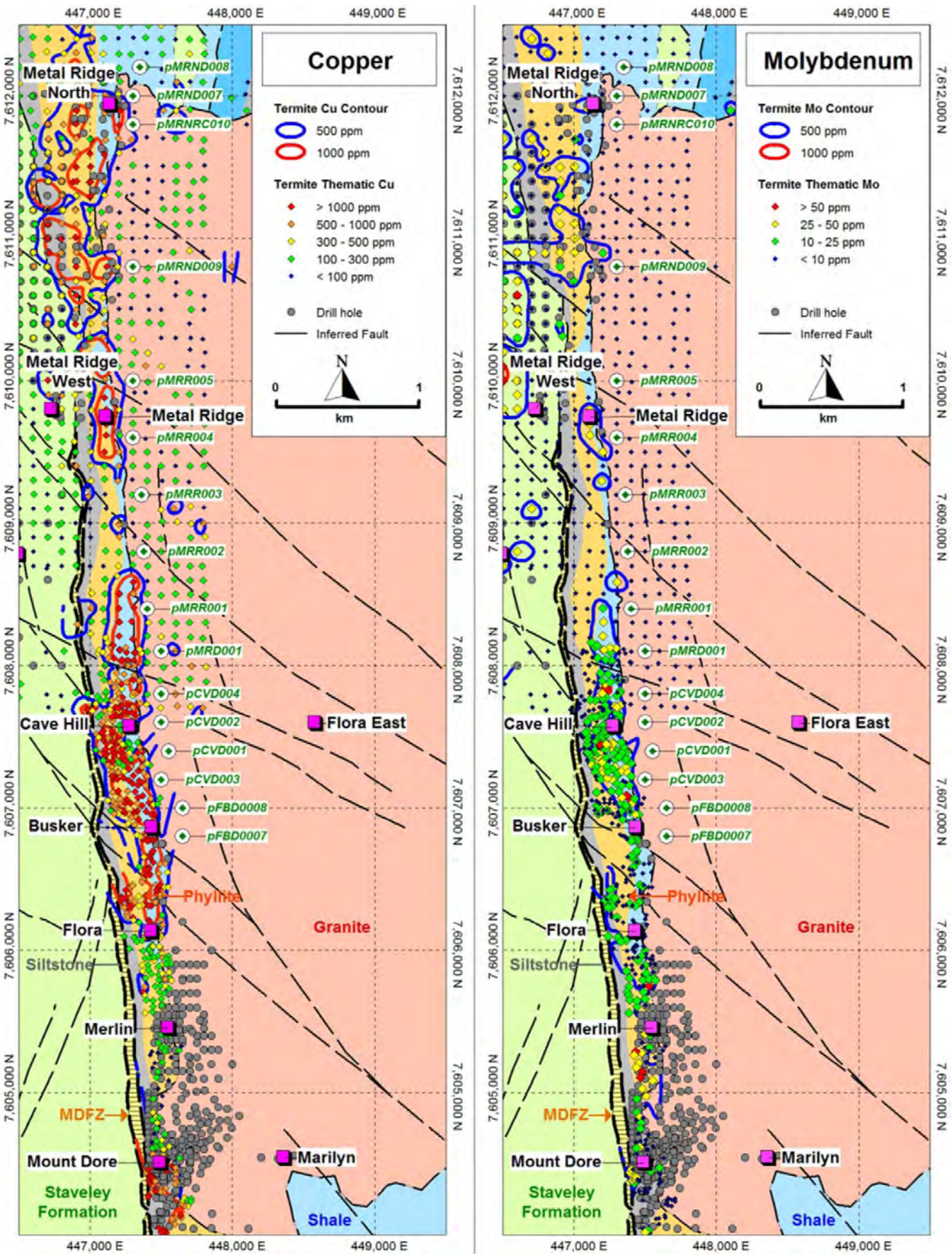

Figure 4.55 Termite mound copper and molybdenum geochemistry north of Mount Dore to Metal Ridge North highlighting strong Cu and Mo anomalism between Flora and north of Cave Hill. Map Projection GDA94 (MGA54)

Dore system (Figure 4.44)

- Merlin shows moderate-strong soil Mo anomalism (>60ppmMo) closely associated with structures that control Mo mineralisation at depth (Figures 4.54 & 4.46). Stronger soil Mo anomalism (>100ppmMo) west of the Roxmere Quartzite ridge has not been linked to additional mineralisation.
- Strong soil Cu-Au anomalism between Flora and Busker (Figures 4.52 & 4.53; coincident with strong U anomalism, Figure 4.51) has not been linked to additional mineralisation.

Termite mound sampling has also been completed along the entire strip adjacent to the Mount Dore Granite north of Mount Dore to Metal Ridge North. Figure 4.55 presents the termite mound copper and molbdenum results. Strong anomalism in termite mound samples is present between Flora and north of Cave Hill.

Lithogeochemistry

No lithogeochemical studies apart from the sectional work done by Nunn net al. (2012) outlined above have been undertaken in the Merlin-Mount Dore region.

TIMING OF MINERALISATION

Relative Timing

All workers (Beardsmore, 1992; Lazo & Pal, 2009; Kirkby, 2009; Greene, 2011; Hinman, 2012a; Duncan et al., 2014; Murphy et al., 2017; Babo et al., 2017; Falkner & Phillips, 2017) are in agreement that both Merlin and Mount Dore mineralisation are hosted in breccia and fracture networks formed during reverse to transpressive faulting that post dates metamorphism, Isan D2(-D3) deformation and early sodic-calcic alteration.

Significant differences in the timing of final breccia formation (in particular the ultimate formation of the distinctive moly-matrix breccias at Merlin) and the emplacement and tectonic role of the Mount Dore Granite exist.

Many workers (Kirkby, 2009; Green, 2011; Duncan et al., 2014; Falkner & Phillips, 2017) have emphasised strain partitioning between the Mount Dore Granite and the Roxmere Quartzite ‘SQT’ ridge focusing strain to produce the brecciation that hosts both Merlin and Mount Dore mineralisation. Hinman (2012a) and Murphy et al. (2017) point out (1) the anomalously planar nature of the granite overthrust reverse fault in significant contrast with the curvilinear breccia-controlling structures in the Merlin-Mount Dore systems, and (2) the demonstrably post-mineral and post-potassic alteration timing of coarse-grained Mount Dore Granite juxtapositioning with the Merlin-Mount Dore systems. They argue that the current geometry of the Mount Dore Granite is largely post-mineral but that an earlier granite geometry may have impacted strain partitioning.

Babo et al. (2017) argue largely on the basis of Re-Os dating that the moly-matrix breccias at Merlin pre-date fracture controlled molybdenite mineralisation. On geological grounds, Hinman (2012a) argues that damage zone, fracture and breccia networks along controlling reverse (transpressive) faults originally control primary molybdenite mineralisation, but that later re-activation of these structures (during the overthrusting of the Mount Dore Granite) results in the production of the milled moly-matrix breccias of Merlin (see Absolute Age discussion below).

Absolute Ages

Duncan et al. (2011, 2014) reported Re-Os geochronology on molybdenite samples from Mount Dore and Merlin. Mount Dore samples returned ages 1497±6Ma, 1501±5Ma, 1508±5Ma, and1503±5Ma (av **~1502Ma**) and Merlin samples 1503±5Ma and 1502±7Ma (av **~1503Ma**) with one outlier from a moly-matrix breccia at **1552±6Ma**.

Babo et al. (2017) reported Re-Os geochronology on Merlin breccia-hosted molybdenite, fracture/stylolite-hosted molybdenite and disseminated molybdenite. The vein, stylolitic and disseminated molybdenite returned ages of 1523±6Ma, 1521±6Ma and 1520±6Ma with a weighted average of **1521±3Ma** while the moly-matrix breccias returned older dates of 1539±6Ma, 1541±6Ma, 1533±6Ma, 1529±6Ma, and 1534±6Ma with a weighted average of **1535±6Ma**.

Babo et al. (2017) interpret the ages to fit with a paragentic sequence of earlier breccia-hosted Mo mineralisation and later (younger) fracture/stylolitic and disseminated mineralisation. This is at odds with the moly-matrix breccia timing relationships suggested by Hinman (2012a).

Murphy et al. (2017) caution about the conflict between well documented, post-peak-metamorphic, geological timing relationships (Adshead, 1995; King 2012) and a significant-

ly older ‘syn-metamorphic’, Re-Os molybdenite date at Osborne of 1595-1600Ma (Gauthier et al., 2001). Murphy et al., suggest that the dating of deformed molybdenite (eg in the moly-matrix breccias at Merlin) is problematic due to disturbed Re-Os systematics associated with Re loss associated with recrystallization during deformation. Little work has been done on the quantitative distributions of Re and Os in deformed molybdenite, but suspect ages abound in the literature (McCandless et al., 1992) in which Re loss results in erroneously older age determinations.

Published work on Merlin molybdenites by Sharma et al. (2016) highlighted highly significant, inclusion clearing in molybdenite that was deformed, but was unable to identify Re loss (or other elemental systematics) in the cleared, deformed molybdenite.

The older age determinations for deformed molybdenite in the Merlin moly-matrix breccias (both Duncan et al., 2014 & Babo et al., 2017) compared with simple fracture, stylolitic and disseminated molybdenite is not in accord with the geological relationships that would have the moly-matrix breccias derived from a reworking of denser fracture and network-controlled, primary molydbenite mineralisation initially formed at the same time but in closer proximity to the controlling structure.

GENETIC MODELS

While all workers agree on the post-peak metamorphic, brittle control on Merlin and Mount Dore mineralisation (see above) and there is general consensus that Mount Dore Cu-Au mineralisation has IOCG credentials, considerable puzzlement surrounds the Mo-Re Merlin deposit. Kirkby (2009) favours a molybdenum-rich IOCG model (‘Merlin-style IOCG’) due to its spatial and temporal association with a granitic batholith and its brittle structural control. Greene (2011) proposes a more direct magmatic model.

Duncan et al. (2014), on the basis of U, Th, F and Rb enrichment in the associated ca1500Ma intrusions, suggests Merlin may be genetically aligned with Climax-type porphyry molybdenum deposits.

Considerable disagreement as to the relative timing of Merlin Mo-Re and Mount Dore Cu-Au mineralisation exits. Lazo & Pal (2009) conclude that the Merlin Mo-Re mineralisation overprints an earlier Mount Dore Cu-Au system. Greene (2011) agrees noting: (1) different alteration stages associated with Mo-Re and Cu-Au mineralisation, and (2) a clear overprinting relationship between earlier Cu-Au alteration stages and a distinct and separate hydrothermal event characterized by an initially-supercritical ore fluid that produces the Mo-Re-associated ‘pseudo-granite’ intense K feldspar-quartz alteration. Greene (2011) favours a direct magmatic origin for the Merlin ore fluid with deposition of Mo due to phase separation, decreasing pressure and temperature and mixing with an ambient saline fluid containing reduced sulphur.

In contrast Nunn et al. (2012) propose Cu-Au and Mo-Re precipitation from the same oxidised, sulphur-poor, Cu-Mo-Re-rich brine under different physio-chemical conditions but along the same structural network. Mount Dore copper precipitation is interpreted to be the result of mixing of oxidised, sulphur-poor, Na, Cl, (Cu, Mo, Re) -rich brine with reduced sulphur-rich fluids sourced from the carbonaceous meta-siltstones entirely within the carbonaceous meta-siltstones. Deposition of molybdenum is interpreted to be the result of the same acid, oxidised, sulphur-poor, Na, Cl, (Cu, Mo, Re) -rich brine contacting pH-buffering calc-silicate and reduced sulphur rich fluids source from the carbonaceous meta-siltstones along the contact of the calc-silicates and carbonaceous meta-siltstones.

Age dating of earliest-formed molybdenite at Merlin (1503Ma; Duncan et al., 2014 and 1521Ma; Babo et al., 2017) and Mount Dore (1502Ma; Duncan et al, 2011) are broadly contemporaneous and within error of the age of the Mount Dore Granite (1516Ma; Pollard & McNaughton, 1997). Duncan et al’s (2011, 2014) age dating allows for a close genetic relationship between intrusion and mineralisation and does not support a very significant time gap (~6Ma quoted errors) between copper and molbdenum mineralisation.

EXPLORATION

Discovery Method

Outcropping Mount Dore copper oxides were discovered by prospecting in the early 1900s. Merlin was discovered at depth in 2008 during the progressive northward drill out of the Mount Dore resource.

Starra Line Au-Cu Deposits

Figure 4.56 Starra Line looking north from Starra244, Starra251 and Starra257 with open cut workings to ridge in middle distance over Starra 276. Photo taken prior to 276 development. Photo from Morrison, 2012.

PRODUCTION AND DIMENSIONS

Historic Production and Resources

The following early history of the Starra deposits draws heavily on Kary & Harley (1990). The 'Selwyn hematites' were assessed for iron ore potential in 1956 by the BMR and were discovered to contain anomalous copper. Follow up drilling by Enterprise Exploration Pty Ltd encountered sub-economic copper (gold not anlaysed) in four diamond drill holes in the areas now referred to as Starra (previously Selwyn Areas) 244 and 257.

In the late 1960s, Anaconda Australia Inc completed extensive mapping and rockchip sampling to define a significant gold anomaly including 70m@4g/tAu but did no further work (Kary & Harley, 1990). In the early 1970s during regional exploration for Pegmont-style Pb-Zn, Newmont Australia Ltd carried out further rockchip sampling along the ironstones and drilled several holes at Starra 244 with only anomalous gold reported.

In 1975 Cyprus Minerals carried out regional exploration that lead to a focus on SWAN (adjacent to Mount Elliott) and Mount Dore. In 1978, they re-focused on gold exploration along the 'Selwyn hematites'. Further rockchip sampling along the ironstone ridges identified areas of interest at Starra 244, 251, 257 (Figures 4.56 & 4.57) and 222. Detailed mapping by John Leishmann from the late 1970s to the 1990s remain the foundation of geological relationships in the Selwyn region. Between 1978 and the commencement of mining in 1988, Cyprus drilled 314 airtrac, 80 reverse circulation, 29 rotary percussion and 259 diamond drill holes to define a pre-mining resource

Selwyn Areas: 5.3Mt@5g/tAu, 1.98%Cu
(Kary & Harley, 1990)

In addition, Cyprus did extensive geophysics (ground magnetic, IP, ground SiroTEM, downhole SiroTEM) none of which satisfactorily distinguished mineralised from unmineralised ironstones.

Mining of high grade gold (and copper) continued to March 1999 and Sleigh (2002) reports total historic production from five Selywn Deposits (222, 244, 251, 257 and 276) to 2002 as

Selwyn Areas: 6.84Mt@4.6g/tAu, 2.1%Cu
(Sleigh, 2002)

Selwyn Mines Ltd purchased title over the Selwyn (Starra) Line of Deposits, Mount Elliott-SWAN and Mount Dore regions in 1999 (Sleigh, 2002). During 2000-2001, Selwyn Mines Ltd reviewed the Starra Line resources and highlighted significant lower grade resources enclosing the high grade shoots. Sleigh (2002) quotes resources at different (eq%Cu) cut-off grades

(1.5eq%Cu) 29Mt@2.5g/tAu, 1.4%Cu

Figure 4.57 2012 Starra Line Long Section with mined resources (red), underground development (yellow), probable resources in 2012 (blue) and drilling from Starra222 in the south to Starra 276 in the north.

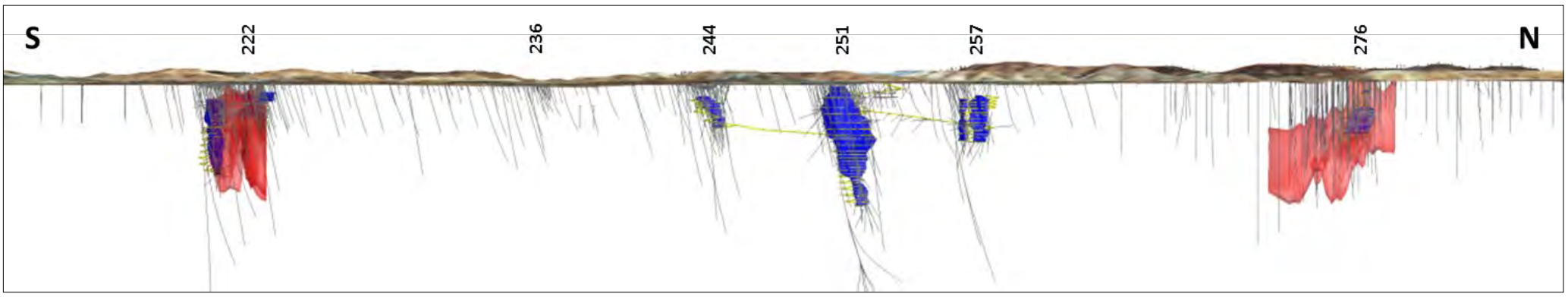

(1.0eq%Cu) 49Mt@1.76g/tAu, 1.05%Cu

(0.5eq%Cu) 95Mt@1.1g/tAu, 0.74%Cu

Within a global resource to 300m of

253Mt@0.48g/tAu, 0.34%Cu

Mining continued until 2002 with total production between 1992 and 2002 quoted as

11.4Mt@3.2g/tAu, 2.1%Cu
(McGeough and Faulkner, 2017)

Low metal prices forced mine closure in 2003 and Ivanhoe Australia Ltd purchased the Mining Leases in late 2003. Ivanhoe Australia subsequently purchased Osborne Mines from Barrack Mines Ltd in 2010 and during 2011 and 2012 Ivanhoe located promising extensions to Starra 276 and Starra 222 as potential feed for the Osborne mill (Morrison, 2012).

Some production from Starra 276 and 222 was undertaken during 2013 and 2014 but figures are not available (see Figures 4.63-4.66).

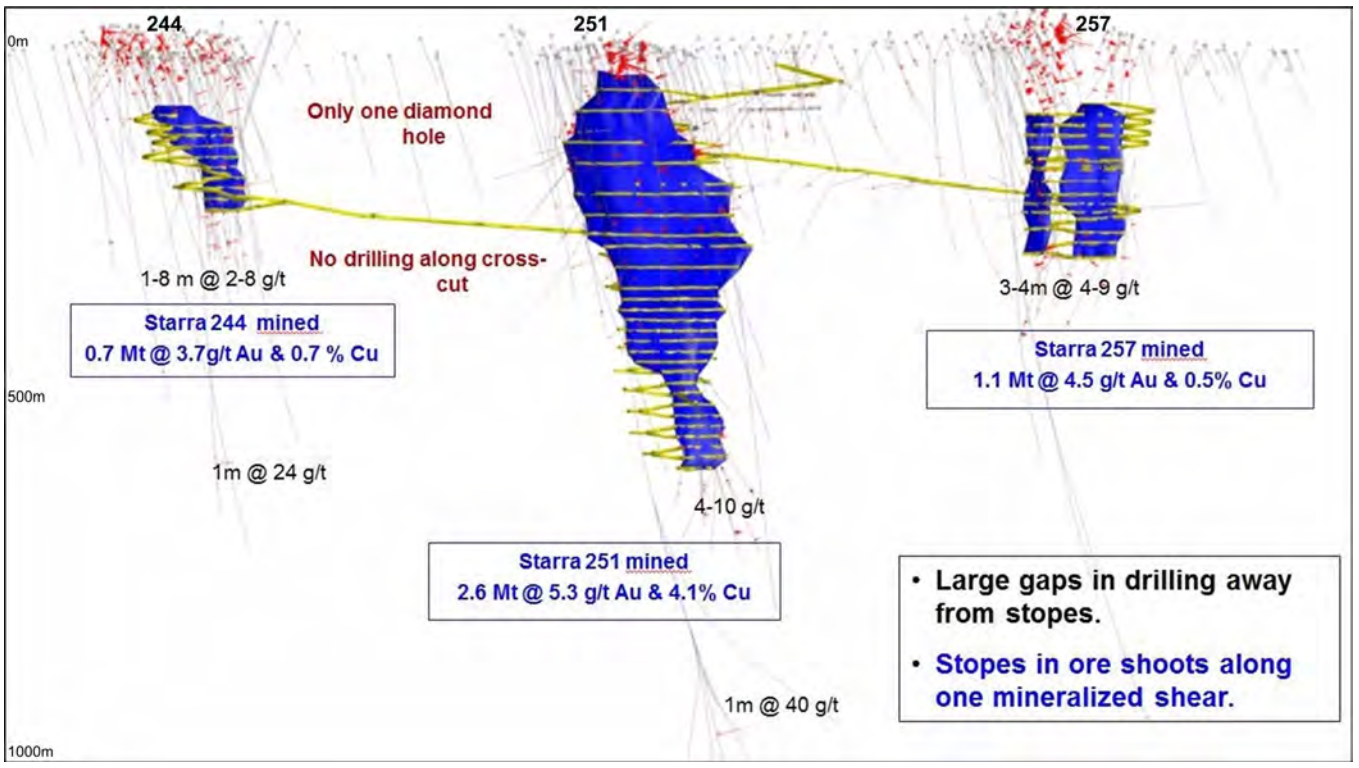

Figure 4.58 Starra 244, 251 and 257 historic stoping, mine development and mined reserves with intercept widths and grades in down-plunge drilling. Open pits not shown. (from Morrison, 2012)

Mineralised bodies

The mined Starra deposits occurred as steeply north-plunging orebodies (apart from Starra 276: Figure 4.57, 4.58) within a 100-500m wide structure ('Starra Shear') which has been traced north-south for over 10km. Individual shoots have wedge-shaped geometries in plan view with thicknesses varying from 1m to 30m and with strikes from 80m to 300m. Starra 222 has been mined to 460m below surface and Starra 276, around 400m. Detailed descriptions of ore body geometries can be found in Kary and Harley (1990). Figure 4.58 highlights historically mined resources at Starra 244, Starra 251 and Starra 257 and intercept widths and grades in deeper, plunge-extension drilling.

HOST ROCKS

Host Rocks

The Starra deposits are hosted within quartz-magnetite iron formations of the Staveley Formation and associated magnetite-chlorite/biotite-bearing schists that occur along the complexly deformed contact between quartz-mica schists of the Double Crossing Metamorphics and Staveley Formation interbedded calcareous meta-siltstones and arenites (Figure 4.59). Discontinuous lenses and rootless folds of both quartz-hematite and quartz-magnetite iron formation occur within an up to 500m wide, multiply-deformed Starra Shear zone over 10km of strike. Discontinuous ironstones can be traced over a further 60km to the south in Staveley Formation calc-silicates and meta-sediments (Kary & Harley, 1990).

METAMORPHISM

Metamorphic Grade

Laing, Rubenach and Switzer (1988) proposed a metamorphic grade discontinuity across the Starra Shear between lower to upper greenschist grade Staveley Formation and upper amphibolite grade Double Crossing Metamorphics to the west (Figure 4.59). Rotherham (1997) argued that original biotite-scapolite assemblages were intensely metasomatised to chlorite within the Starra Shear and that the original Staveley Formation assemblages within the shear zone also reflect amphibolite facies metamorphism. Rotherham (1997) concluded that the perceived metamorphic grade discontinuity across the major structural zone may not exist.

INTRUSIVE ROCKS IN REGION

Granitoids

West of the Starra line of deposits the Wonga-aged Gin Creek Granite syn-deformationally intrudes the Double Crossing Metamorphics (Figure 4.59). The Gin Creek Granite is massive in its core domains but exhibits significant 'thready' syn-tectonic, intrusive relationships with the Double Crossing Metamorphics over significant volumes. This is mappable in the detailed magnetics (Figures 4.8, 4.9 & 4.59) and reflects both significant sheet-like, syn-deformational intrusion into the Double Crossing Metamorphics as well as significant xenolith remanence within the intrusive (Murphy et al., 2017). The Gin Creek Granite has returned zircon U-Pb ages of 1741±7Ma (Page & Sun, 1998) and 1743±9Ma (Geoscience Australia).

The Mount Dore Granite to the northeast of Starra is a highly radiogenic intrusion of the Williams-Naraku Suite and has been dated at 1516±10Ma (Pollard & McNaughton, 1997) and 1517±7Ma (Babo et al., 2017).

Mafic Intrusives

Metadoleritic-amphibolitic sills intrude both the Double Crossing Metamorphics and the Staveley Formation (Figure 4.59). Their relative and absolute timing is unknown.

STRUCTURAL CHARACTERISTICS

Structural Setting

The Starra line of deposits lie within a wide zone of intense, multiphase deformation, the Starra Shear zone, that has also suffered multistage metasomatism. The Starra Shear zone is typified by gradational increases in strain over 50-100m into the margins of the shear zone; eastward within the footwall Double Crossing Metamorphic quartz mica schists (and metadoleritic/amphibolitic sills) and westward within the hanging wall Staveley Formation calcareous, meta-siltstone-sandstone package.

The shear zone contains remnant and discontinuous, tabular lenses, ribbons and rootless folds of quartz-magnetite and quartz-hematite ironstone with common steeply-plunging geometries (Leishman, 1983). The more dominant, quartz-hematite ironstones are commonly more massive and tabular, but brecciated forms exist (Sleigh, 2002). Both the magnetite and hematite ironstones are typically medium to coarse-grained with only moderately preserved internal fabrics (Sleigh, 2002) suggesting metamorphic re-crystallization post dated their structural dismemberment (Murphy et al., 2017).

The high grade portions of the ore bodies are typically developed as broad, ribbon-like shoots (sometimes in clusters) within more massive magnetite ironstones. Lower grade mineralisation is commonly developed in both the footwall and along strike of high grade zones hosted within the chlorite/biotite-magnetite schists. At Starra 244 and 222 some higher grade zones are entirely schist-hosted (Sleigh, 2002).

Structural History

The structural history of the rocks hosting the Starra line of deposits remains significantly contentious. Many schemes have been suggested, most of which have attempted to

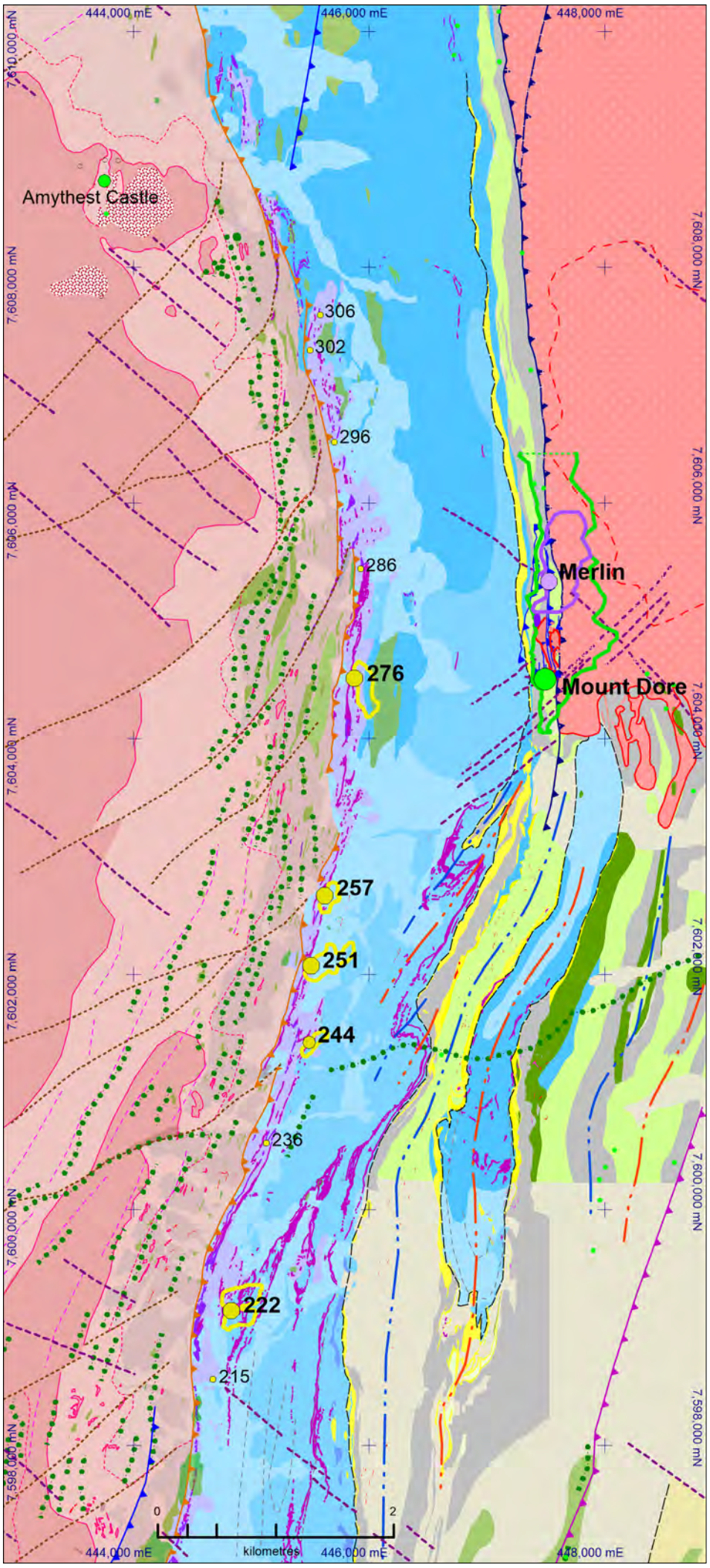

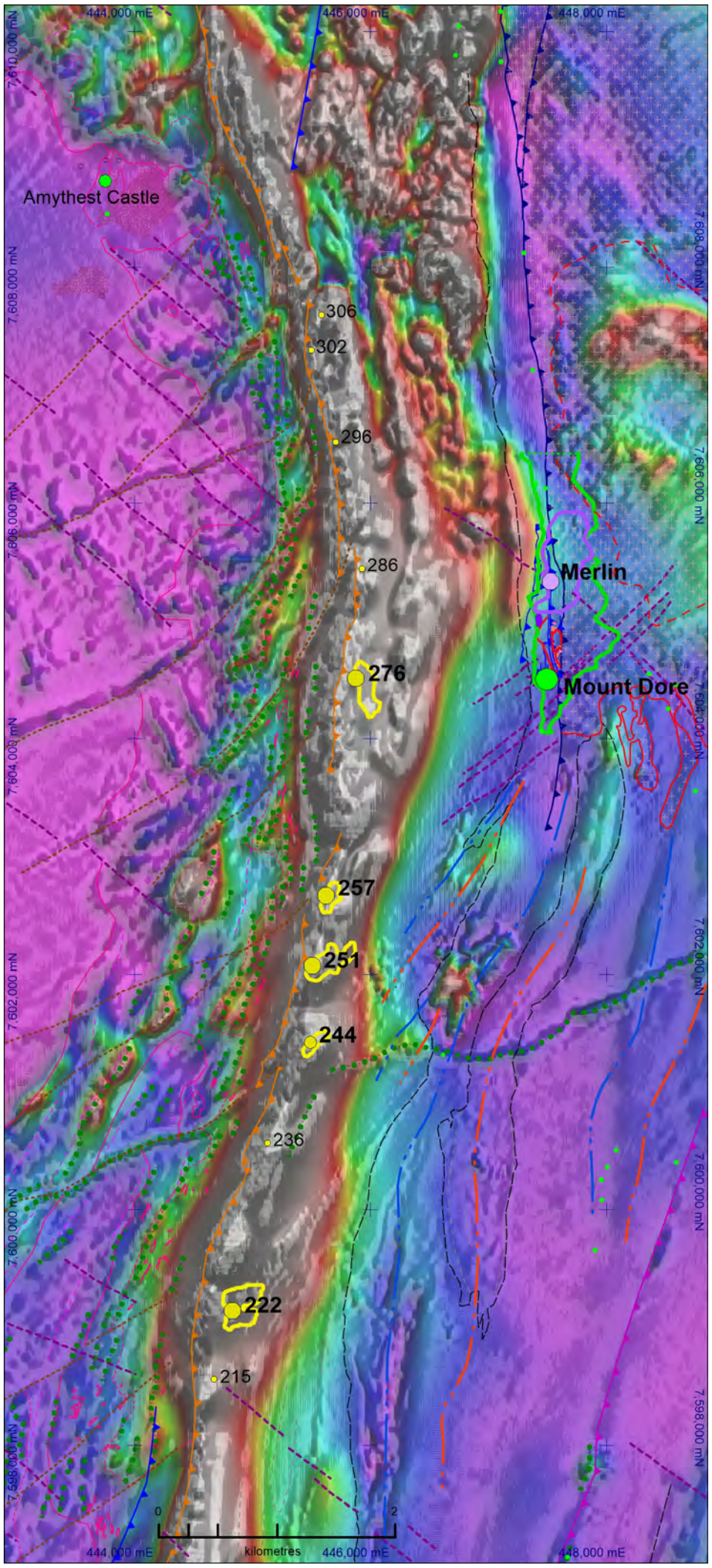

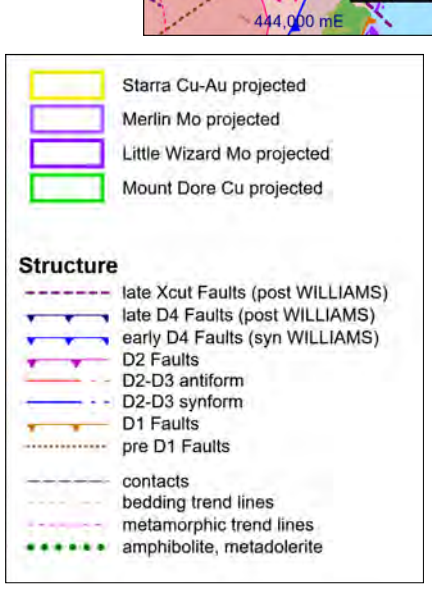

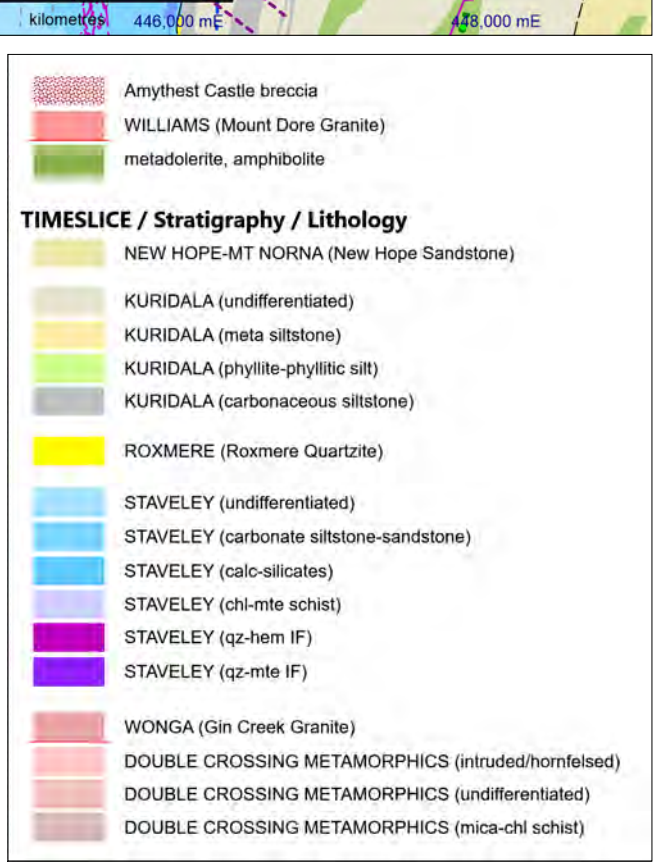

Figure 4.59 (above left) Solid geology compilation-interpretation of the Starra line of deposits and environs from Deep Mining Queensland (Murphy et al. 2017) highlighting the basal D1 thrust and the volume of attenuated iron formation within chlorite-magnetite schists marking the full extent of the Starra Shear Zone. Data attribution presented in Figure 4.59. Map Projection GDA94 (MGA54)

Figure 4.60 (above) Detailed Chinova vrmi greyscale RTP-2VD overlain on coloured RTP highlighting predominant magnetic signature of chlorite-magnetite schist along the Starra Line and the absence of distinctive magnetic expression of know resources. Major deposits & resources vertically projected and structural skeleton overlain. Same map area as Figure 4.59. Map Projection GDA94 (MGA54)

contexturalise the very significant and complex deformation zone that hosts the ironstones and mineralisation and resolve their relative timing. Summaries of various schemes are presented here.

- Switzer (1987) and Laing et al. (1989) interpreted the Starra Shear zone as part of an early, layer-parallel (ie formed subhorizontally), deformation zone that destroyed all pre-existing fabric, including bedding, S0. On the basis of regionally

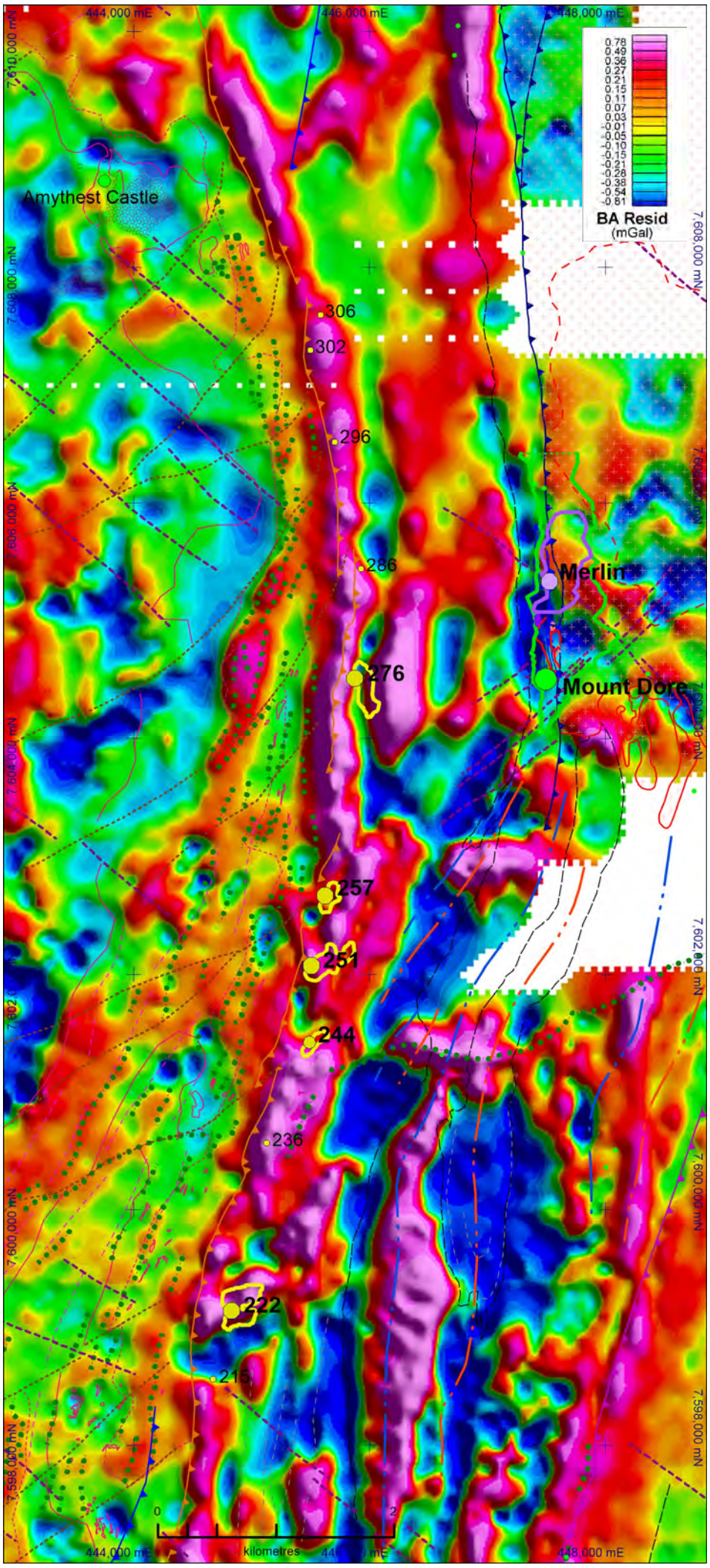

Figure 4.61 Starra line zoom of merged detailed 2012 Residual Bouguer Anomaly ground gravity data highlighting gravity response of massive iron formation and metadoleritic/amphibolite bodies and no specific response of known resources. Major deposits & resources vertically projected and structural skeleton overlain. Same map area as Figure 4.59. Map Projection GDA94 (MGA54)

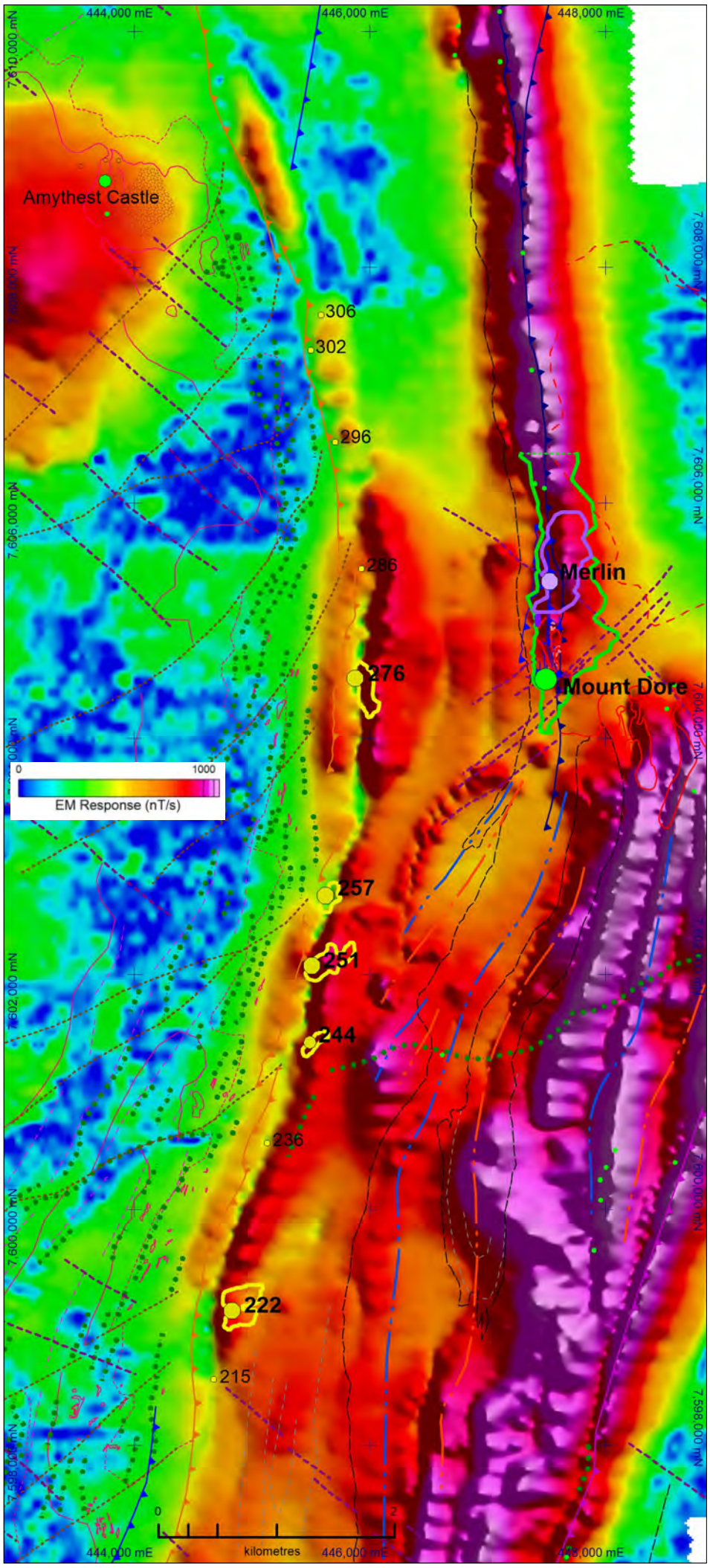

Figure 4.62 Starra line zoom of detailed 100m line-spacing, 2011 Heli-TEM EM Amplitude Channel 15 highlighting reduced chargeability associated with chlorite-magnetite schists marking the Starra Shear and no particular anomalism associated with known resources. Major deposits & resources vertically projected and structural skeleton overlain. Same map area as Figure 4.59. Map Projection GDA94 (MGA54)

opposing shear senses along the Starra line and on the western limb of the regional Gin Creek antiform (Figure 4.4), they argued that the regionally-extensive, D1 shear zone had been folded during Isan D2. Switzer (1987) argued on the basis of shallow northward-plunging, quartz-feldspar mineral rodding within the Gin Creek Granite (now considered earlier Wonga-aged extensional detachment fabrics) that the Staveley Formation had been transported northward over the Double Crossing Metamorphics-Gin Creek Granite block and that the directly-related, regionally-extensive Starra Shear originated as a pre-D2 extensional detachment. The Shear Zone was subsequently folded during D2 (rotated to steep easterly dips at Starra) and re-activated during ongoing Isan deformation. Switzer (1987) proposed a syn-D2 timing of ironstone formation, and Starra line mineralisation was interpreted to have occurred during later brittle re-activation.

- Davidson et al. (1988) also noted a complex deformation history of the Starra ironstones following Switzer's (1987) and Laing et al's (1989) scheme of a major D1 decollemont; folded by regional D2 deformation; minor northeast-trending D3 crenulation without significant macroscopic expression and later D4 brittle-ductile, reverse re-activation associated with Williams batholith emplacement. Davidson et al. (1988), in contrast with Switzer (1987) and Laing et al. (1989), suggested Starra ore and mineralisation was deformed by all the recognizable stages of deformation and proposed an original syngenetic exhalative origin of the gold-copper ores.
- Adshead-Bell(1998), largely on the basis of microstructural observations, identified a

series of successive shallow and steeply oriented deformation events. D1 produced a shallowly-dipping, layer-parallel foliation not attributed to any macro- or regional-scale structuring. D2, in accord with previous workers, was the most pervasive event and resulted in upright, north-northwest-trending, tight to isoclinal folds with steep easterly-dipping axial planes (eg. Staveley-Kuridala Formation folding south of the Mount Dore Granite; Figure 4.59). D3 was again identified as a flat lying crenulation (with top-to-west sense of shear) but attributed with a macroscopic rotation of prior D2 folds. D4 produced a steeply east-dipping foliation similar in orientation to S2 and not easily differentiated from S2 except in zones of significant S3 development. Adshead-Bell (1998) suggests the Starra Shear zone resulted from high strain largely during D4 with west-side-up sense-of-shear. Ironstones resulted from intense iron metasomatic replacement that obliterated composite S2/S4 fabrics syn- to post-D4. Gold-copper mineralisation was controlled by localised shallow-dipping crenulations (D5-D6 of Adshead-Bell, 2000) and associated extensional veins, crackle breccias, boudin necks and tension gashes.

- Duncan et al. (2014) followed Adshead-Bell's (1998) scheme but highlights evidence of pre-D2 (and perhaps pre-D1) ironstone development including: hematite inclusions in syn-D2 andalusite porphyroblasts; a D1 hematite-chlorite fabric folded by D2 (White, 1989); and frequent identification of rotated S2 fabrics in hematite breccia clasts with both hematite and foliated magnetite in the breccia matrix (White, 1989). Duncan (2014) concludes that a component of iron oxide alteration at Starra was pre- or early syn-D2. Duncan (2014) concedes on the basis of magnetic data that the Starra Shear appears to be folded around the F2 Gin Creek antiform and is therefore pre-D2.
- Murphy et al. (2017) have attempted to rationalise previous work with regional relationships and further interpretation. They suggest the Starra Shear is a D1 basal thrust associated with the north to north-northwest-directed, regional, allothchonous placement and internal ramping of the Eastern Fold Belt Staveley to Toole Creek packages over older, previously Wonga-deformed and syn-tectonically intruded packages to the west and north. Originally east-west D1 folding is well preserved (and currently identified) in the immediate footwall and hanging wall domains of major D1 thrusts: in the Snake Creek Anticline area (Rubenach et al., 2008); at the northern end of the Marimo Synform; in the footwall of the Overhang Shear in the Mitakoodi Culmination (O'Dea et al., 2006); and in the hanging wall of the folded Cloncurry Overthrust around Cannington (Hinman, 2018).

Steeply-plunging remnants, ribbons and

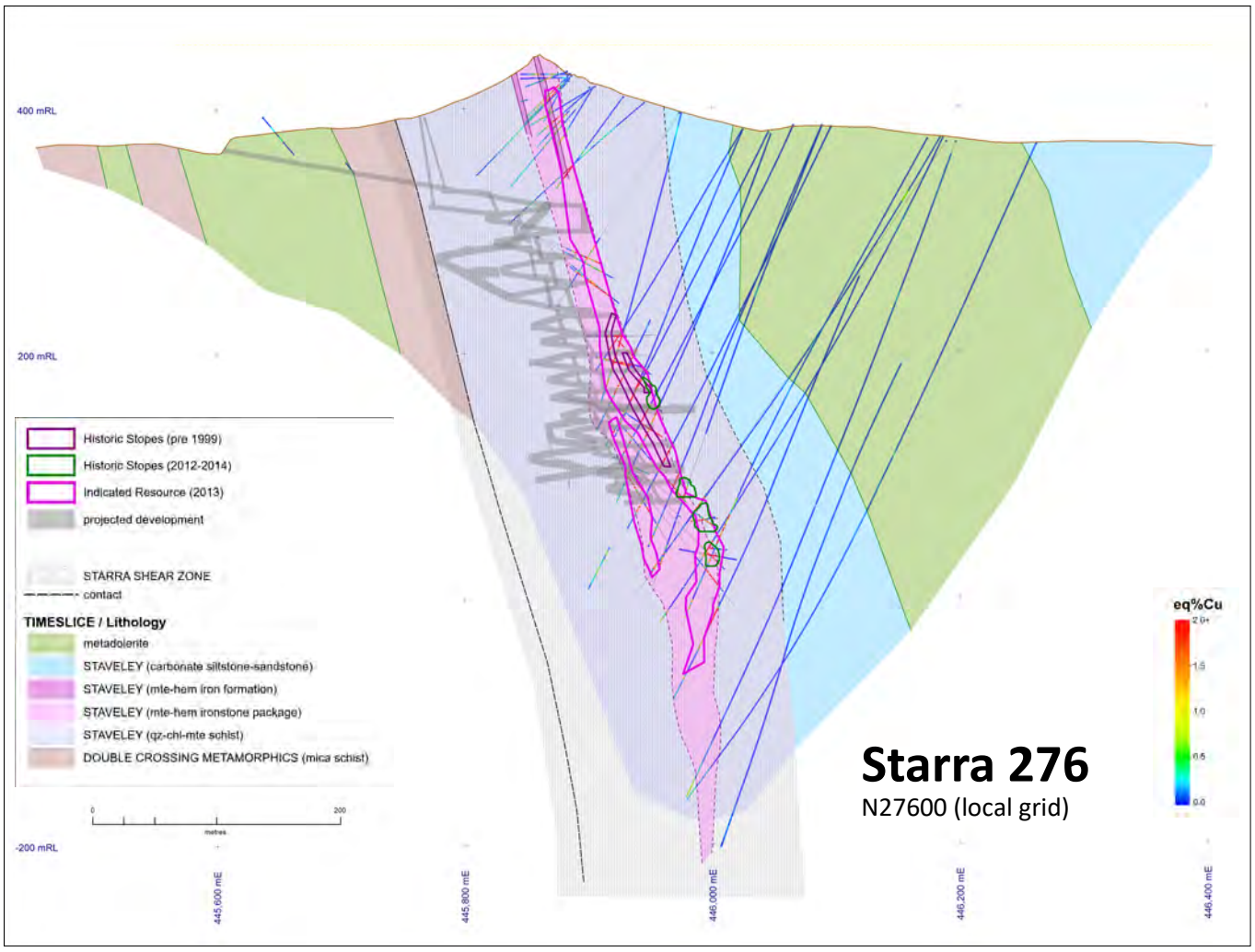

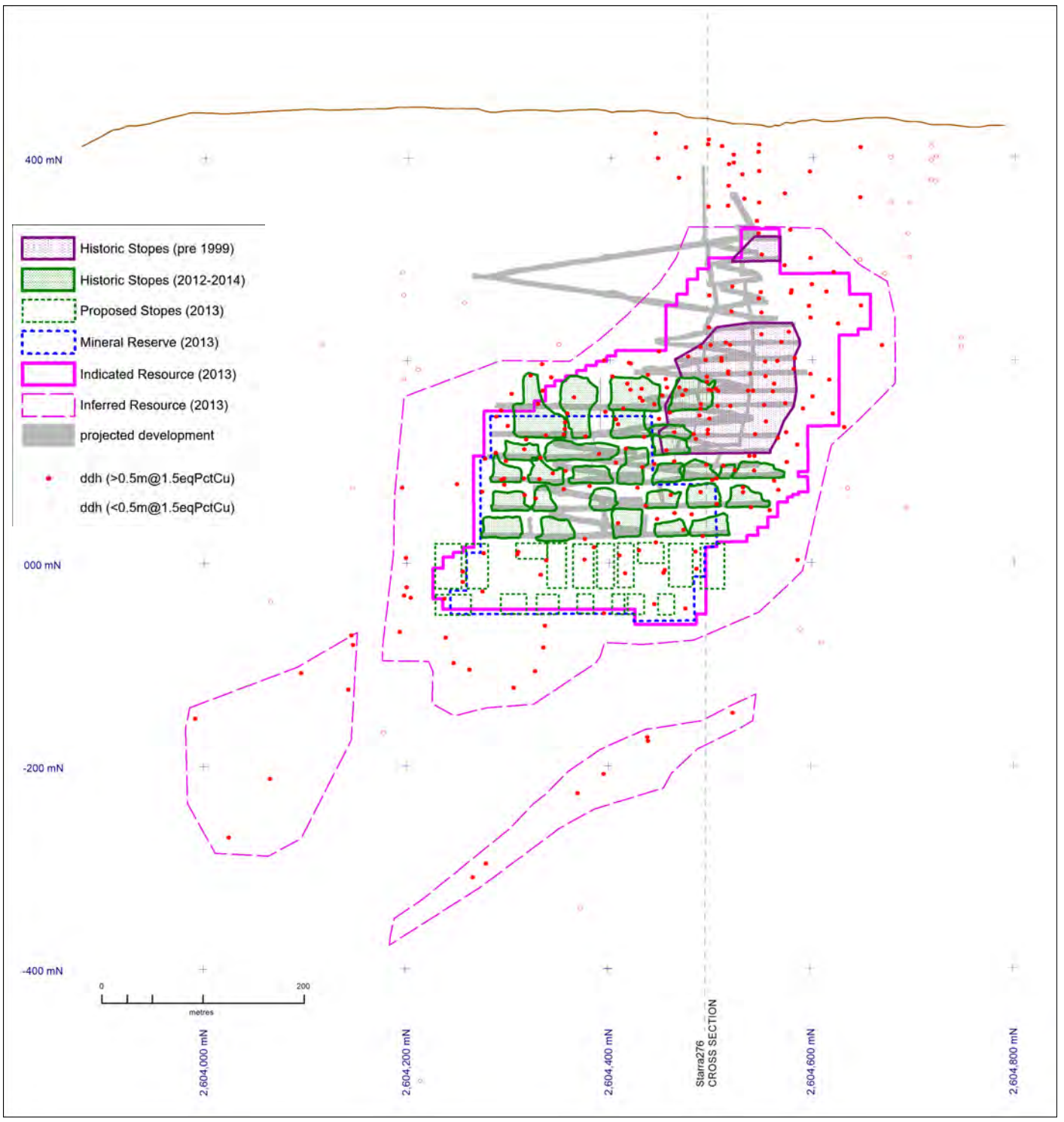

Figure 4.63 (top) Starra 276 Cross Section N27600 (local grid) highlighting (1) Starra Shear zone focussed along and above Double Crossing Metamorphics-Staveley Formation multiply-re-activated D1 contact, and (2) historic iron formation-hosted stopes and recent resources within a broader quartz-chlorite-magnetite schist volume. All sections same scale.

Figure 4.64 (botom) Starra 276 Long Section showing drilling pierce points, projected underground development, historic stoping, and recent 2013 indicated and inferred resources. Location of Cross Section N27600 shown. All sections same scale.

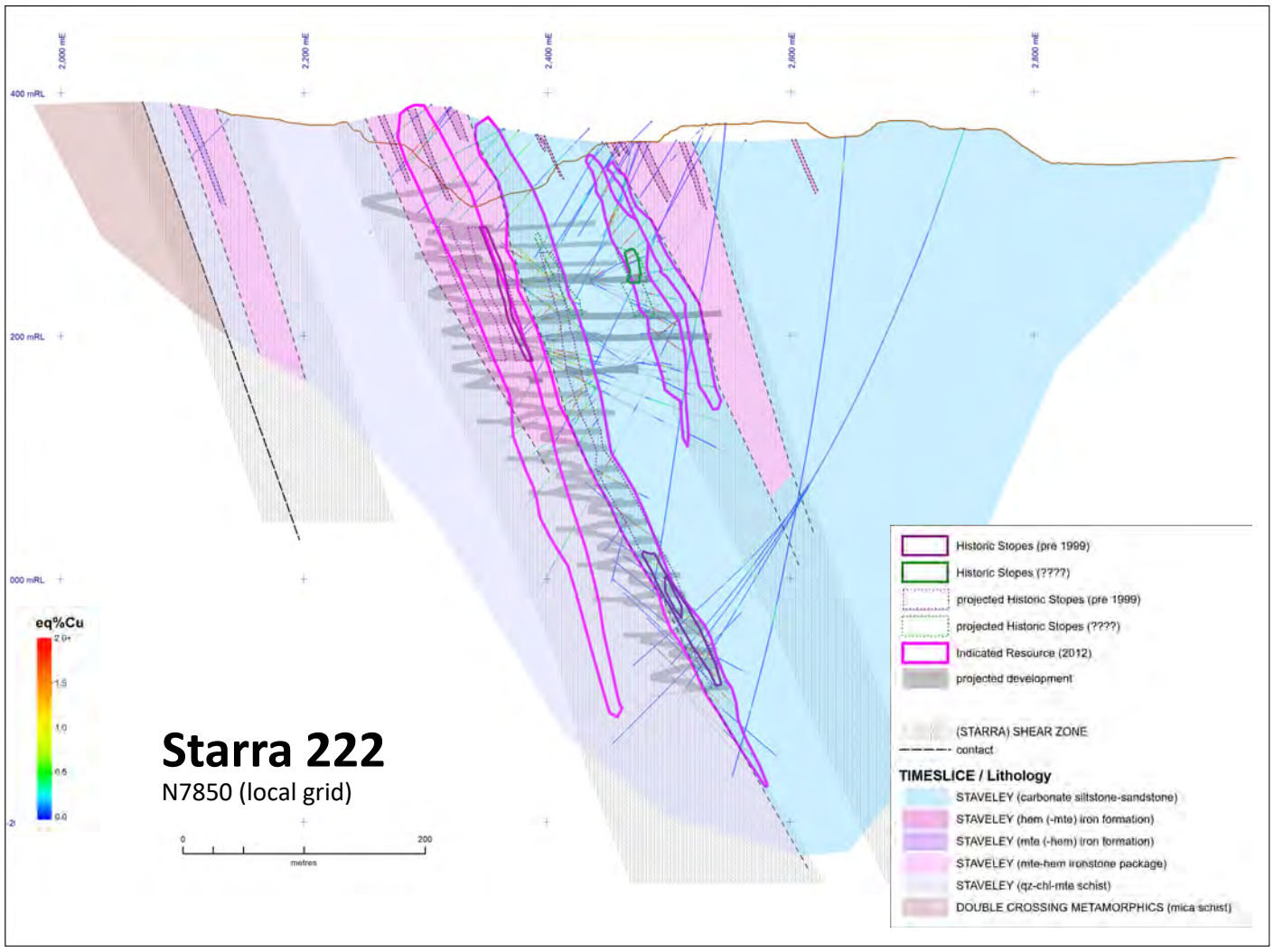

Figure 4.65 (top) Starra 222 Cross Section N7850 (local grid) highlighting (1) multi-stranded Starra Shear zone focussed along and above Double Crossing Metamorphic-Staveley Formation multiply re-activated D1 contact and within the Staveley Formation, and (2) historic iron formation-hosted stopes and recent resources within a broader quartz-chlorite-magnetite schist volume and within deformed Stavely Formation sandstones-siltstones. All sections same scale.

Figure 4.66 (botom) Starra 222 Long Section showing drilling pierce points, projected underground development, historic stoping, and recent 2013 stacked lense resource outlines. Location of Cross Section N7850 shown. All sections same scale.

rootless folds (Leishman, 1983) of metamorphically-recrystallized iron formation (Sleigh, 2002) along the Starra line are interpreted as originally east-west, structurally-attenuated remnants within an intense D1, layer-parallel, top-to-north to north-northwest-directed shear zone juxtaposing hanging wall Staveley Formation with footwall Double Crossing Metamorphics and Gin Creek Granite. The major D1 structure is folded during D2 (around the regional north-south Gin Creek antiform; Figure 4.4), and the Starra line segment rotated to steep easterly orientations resulting in the steeply-plunging ironstone remnants within a broader, strongly magnetic (Figure 4.60) magnetite-hematite-chlorite rich schist dominated by D2 fabrics but perhaps D1 geometries. Significant D2 reactivation and syn-D2 metamorphic re-crystallization of steeply-oriented S1 fabrics and geometries is suggested. No D2 folds along the Starra Shear have been identified apart from drill section-interpreted folds of metadolerite sills (Davidson, 1988). The D2-rotated, steeply-plunging D1 folds and ribbons of iron formation along the Starra Line are in stark geometric contrast with the sub-horizontal north-south D2 folds in the Staveley and Kuridala Formation packages to the south of the Mount Dore Granite (Figure 4.59).

A consensus of D3 crenulation with little to no macroscopic effect appears to be agreed by all workers. D2 and D3 reverse and transpressive reactivation along the Starra Shear resulted in complex fold, attenuation and faulted relationships along the Starra line. Murphy et al. (2017) support a late Isan, shallower crustal, northwest-directed, D4 sinistral transpressive reactivation of the Starra Shear (broadly synchronous with William-Naraku-aged intrusion) controlling extensional, brittle fracture and breccia deformation of amenable post-peak metamorphic lithologies controlling the focusing of Cu-Au mineralising fluids. They emphasise the lack of permeability generation in post-peak metamorphic assemblages with strong D2 fabrics due to their inherent ability to accommodate D4 re-activation by slip on pre-existing fabrics (also Kary & Harley, 1990). These process observations are in excellent accord with the ore geometry descriptions of Sleigh (2002) who highlighted lensoidal-shaped, high grade ore within more massive magnetite ironstones with lower grade halos in immediately adjacent chlorite/biotite-magnetite schists.

- Restating earlier worker's (Sleigh, 2002; Duncan et al., 2014) suggestions, Murphy et al. (2017) highlight a significant correlation between the spatial location of Starra line Au-Cu deposits with the projection of basement (Starra Shear footwall) northeast-trending, post-Wonga but pre-D1, Double Crossing Metamorphic-Gin Creek Granite structures (Figures 4.59 & 4.60, and allowing for some D2-D4 shortening rotation of

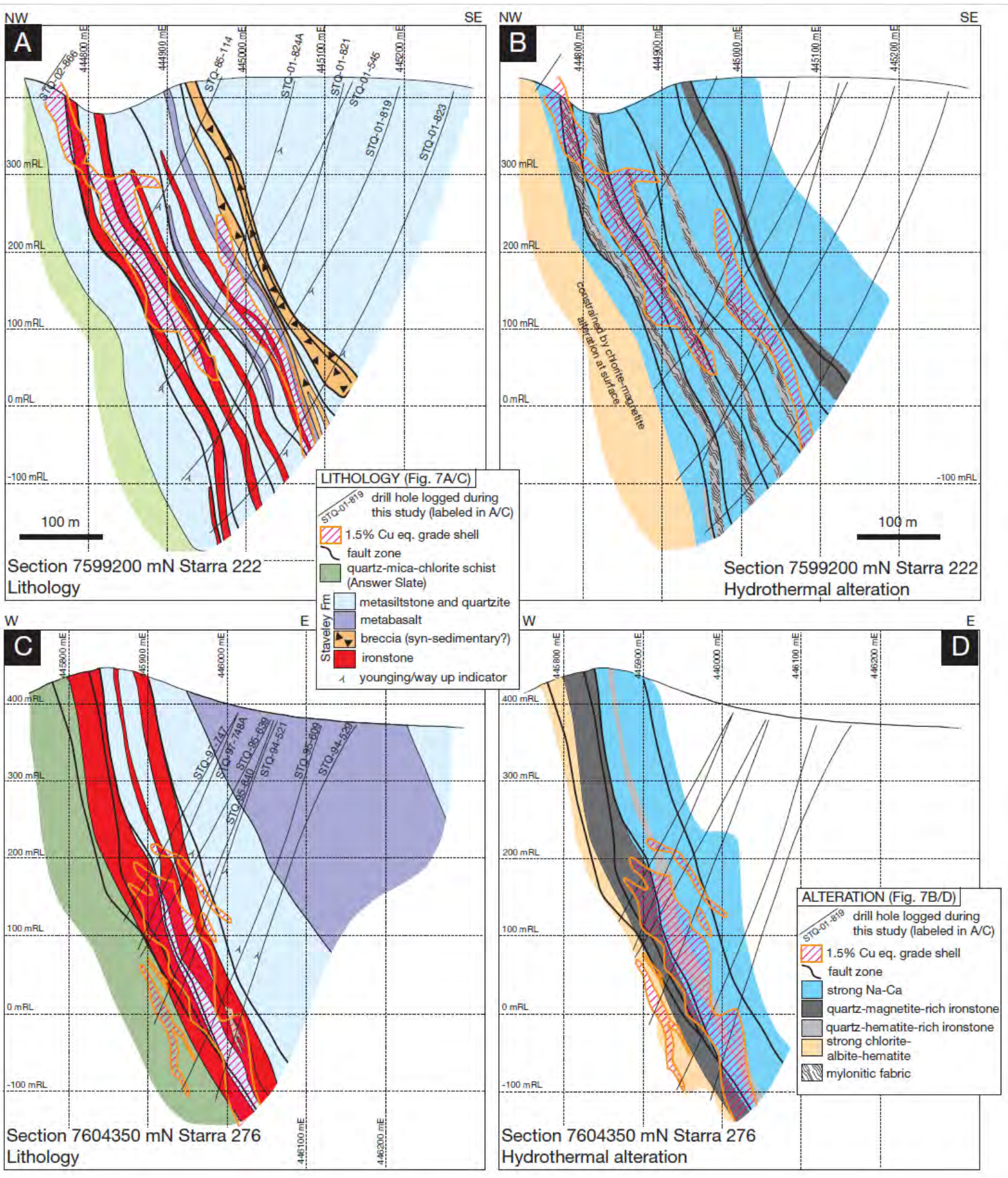

Figure 4.66 Starra 222 Cross Section 7599200N (A-Lithology; B-Alteration) and Starra 276 Cross Section 7604350N (A-Lithology; B-Alteration) from Duncan et al. (2014) highlighting Na-Ca alteration 'halo' and loose association of >1.5eq%Cu grade shells with ironstones. Answer Slate quartz-mica-chlorite schist footwall to Staveley Formation now considered to be Double Crossing Metamorphics.

them within the Double Crossing Metamorphics and the broader Starra Shear zone). Murphy et al. (2017) emphasise the Cu-Au targeting necessary and sufficient condition of the spatial coincidence of (1) a remnant lense of massive iron formation within the D4 re-activated, D1 Starra Shear with (2) a projected, northeast-trending footwall Double Crossing Metamorphic-Gin Creek Granite pre-D1 structure.

WALLROCK ALTERATION

General Characteristics

Rotherham (1997) in a drillcore-based study has identified three dominant post-peak metamorphic paragentic stages of alteration and mineralisation outline below and presented in Table 4.4. Peak metamorphism is marked by biotite (Figure 4.67B) in the Staveley Formation metasediments. No pre-D2, pre-metamorphic assemblages and geometries are considered by Rotherham (1997).

(Stage 1) Early widespread Na-Ca metasomatism consisted of albite-quartz-actinolite-scapolite-titanite assemblages that Rotherham (1997) times as syn-metamorphic to post-D2.

(Stage 2) More localised K-Fe metasomatism consisting of magnetite-hematitie-biotite-quartz-pyrite assemblages which Rotherham (1997) times as post-metamorphic. An Ar-Ar date on biotite associated with this pre-mineralisation stage returned ca1503Ma (Perkins & Wyborn, 1998) suggesting a late-Isan, post-metamorphic timing. Rotherham (1997) times all iron oxide formation to this paragenetic stage and does not recognise pre-metamorphic, D1 lensoidal ironstone body geometries as does Leishman (1983, Davidson et al. (1988), Laing et al. (1989), Kary & Harley (1990), Duncan et al, (2014), and Murphy et al. (2017).

(Stage 3) Copper-gold mineralisation stage (Figures 4.67 D, E, F) characterised by an oxidative assemblage comprised of quartz-anhydrite-calcite-hematite alteration of Stage 2 magnetite, and intense chlorite ±muscovite

Figure 4.67 (opposite) **A**- Staveley Formation interbedded calcareous sandstone and siltstone showing eastward younging. STQ-97-748A 177.9m West drilled hole with downhole to left (Duncan et al., 2014). **B**- quartz-albite-biotite-chlorite-magnetite schist micrograph showing intense chlorite replacement of metamorphic biotite. STQ-94-555 ~150m (Rotherham, 1997). **C**- Deformed breccia from Starra 257 footwall. Albite clasts in hematite-magnetite-quartz-chlorite matrix. NQ Core. STQ-93-427 ~200m (Rotherham, 1997). **D**– Multi-generations of magnetite 1. as inclusions in albite-hem clasts pre-dating fabric; 2. in pressure shadows of albite clasts and in fabric; 3. with chalcopyrite (Duncan et al., 2014). **E**- Potential relic bedding with shear- and extensional-crack controlled chalcopyrite mineralisation. (Duncan et al., 2014). **F**- Strongly sodic-calcic-potassic altered breccia with large magnetitie 'clasts' and interstitial chalcopyrite. (Duncan et al., 2014)

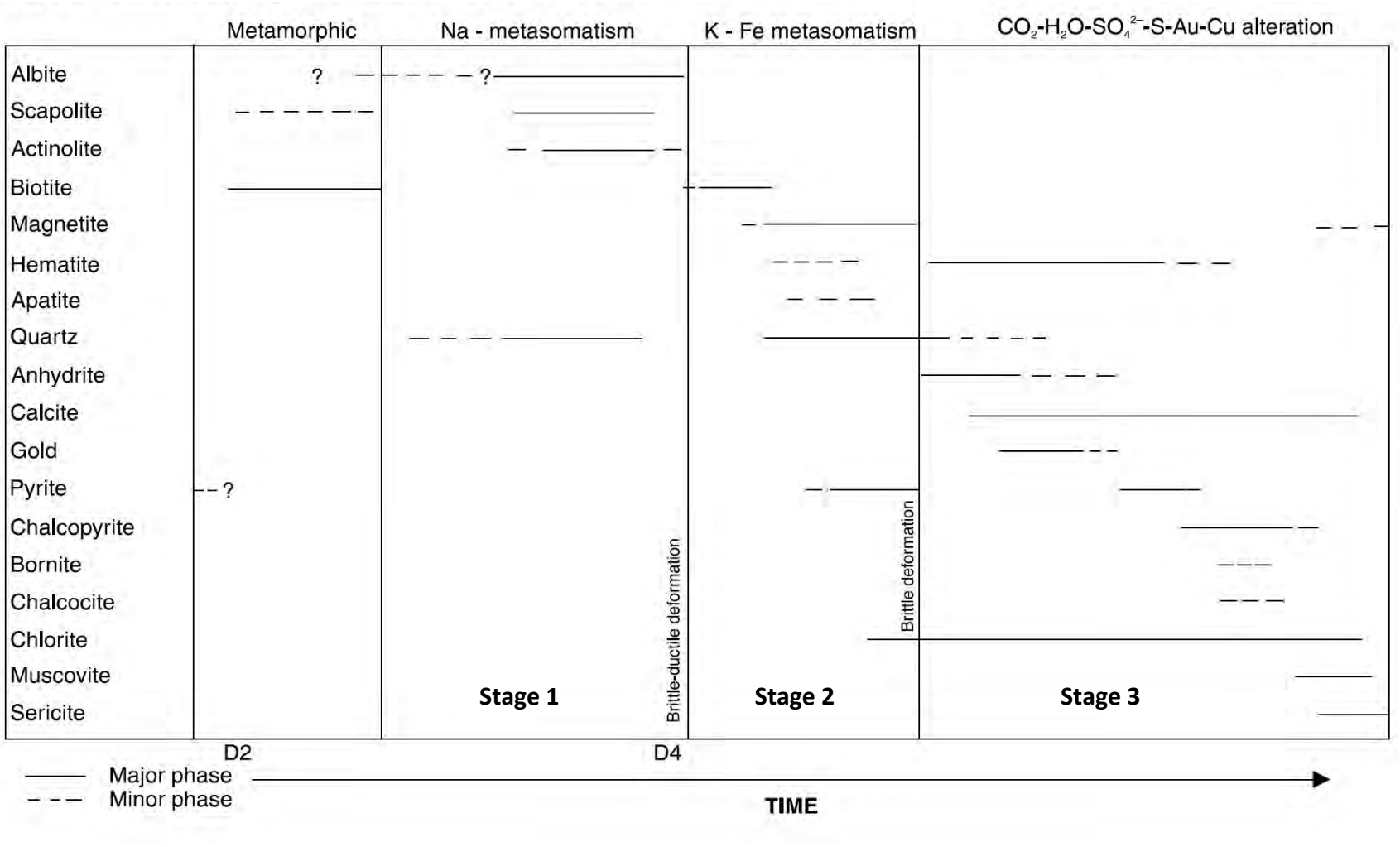

Table 4.4: Starra post-D2 paragentic stages after Rotherham (1997). Note Rotherham does not acknowledge pre-D2 and/or pre-D1 iron oxides as is the consensus view among other workers (Davidson et al., 1988; Laing et al., 1989; Kary & Harley, 1990; Duncan et al, 2014; Murphy et al., 2017)

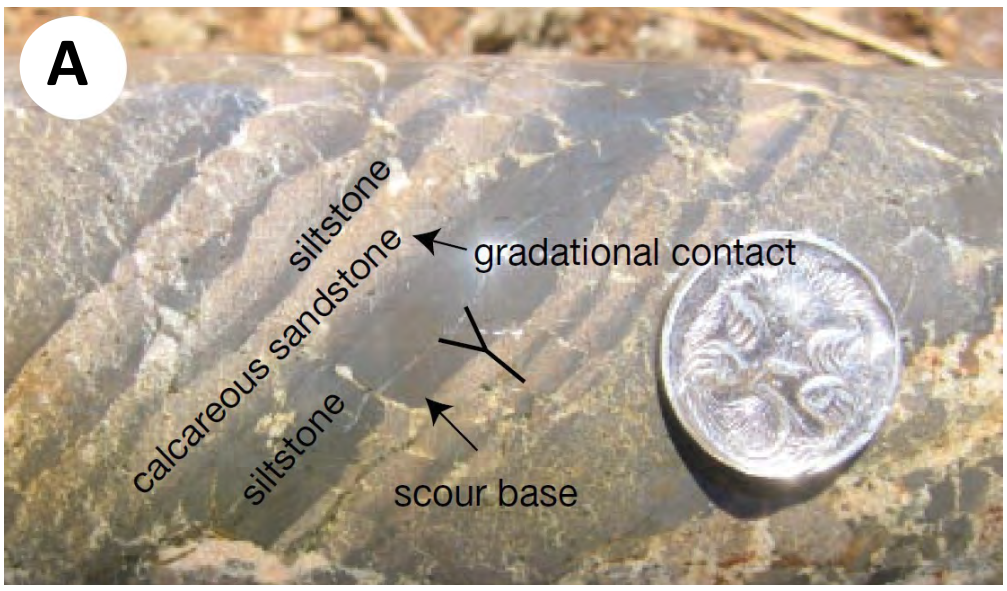

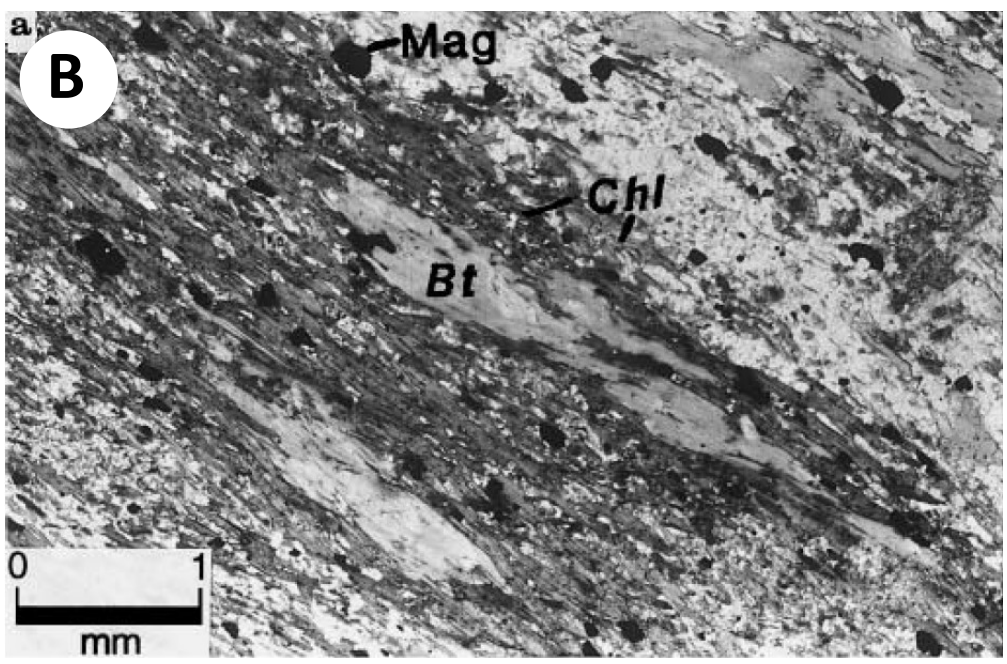

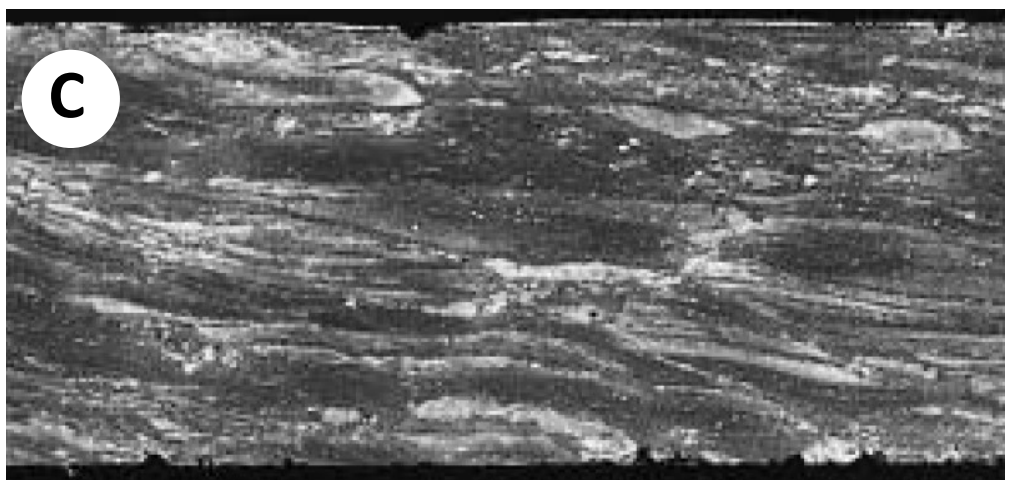

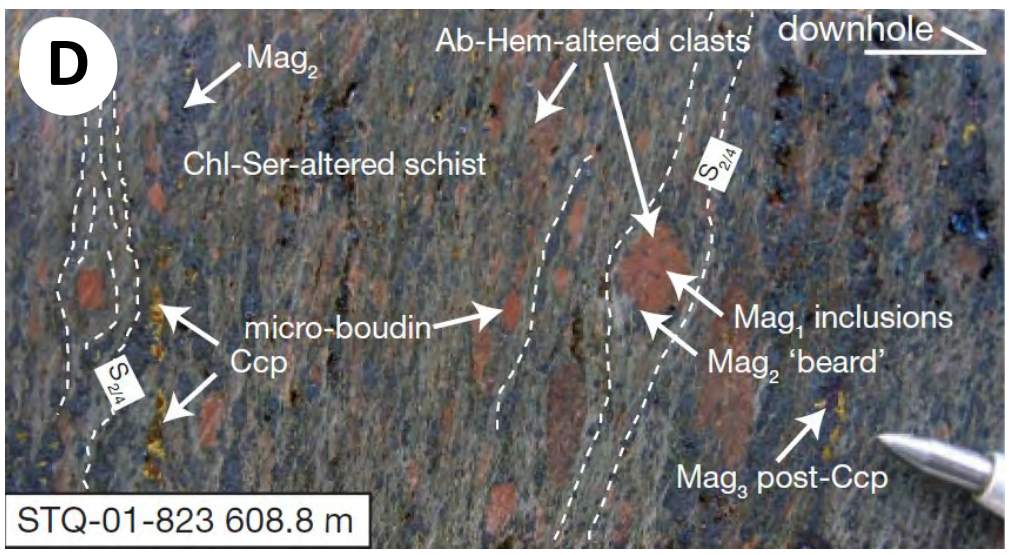

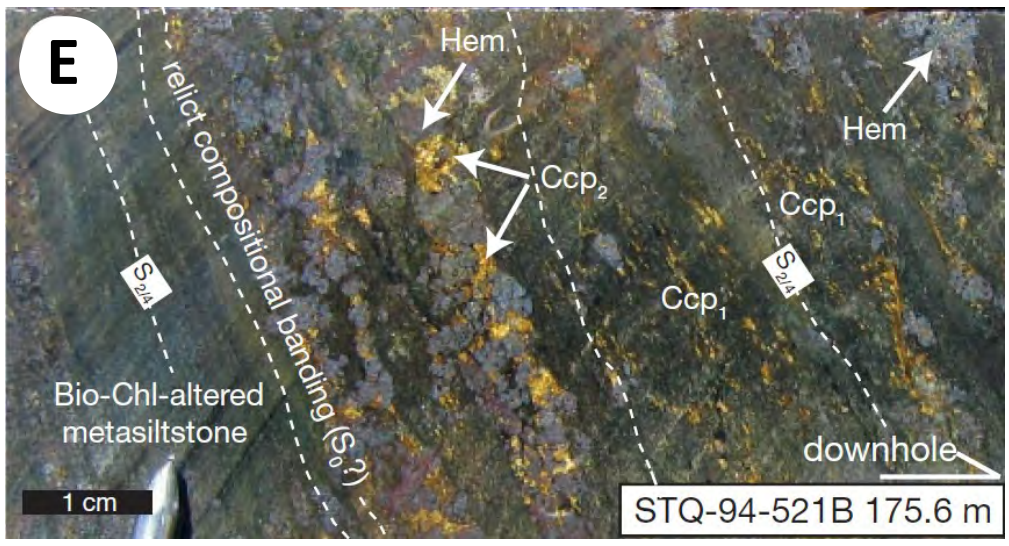

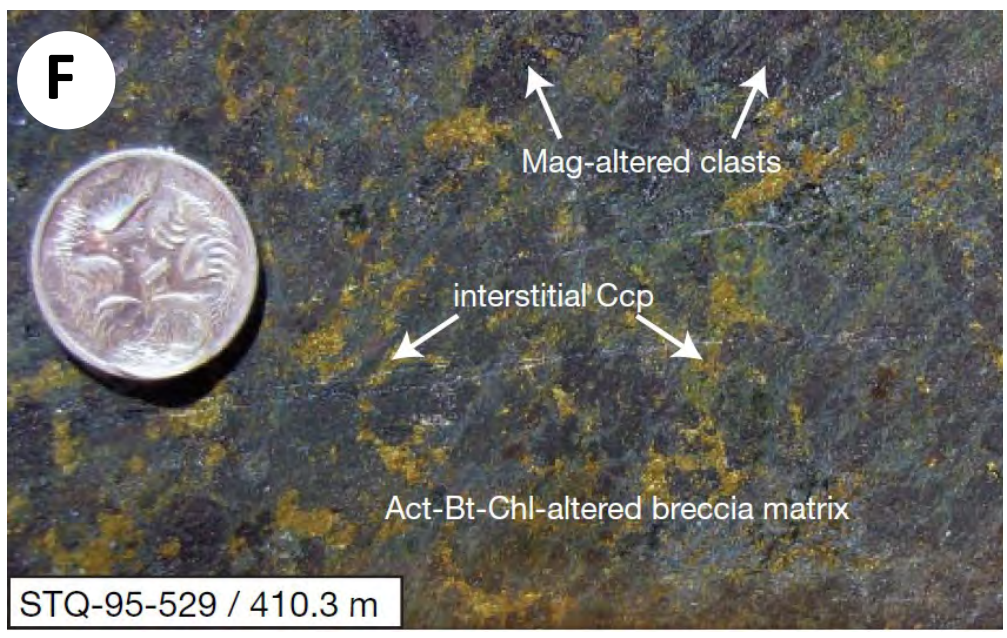

±sericite alteration of Stage 2 biotite (Figure 4.67B) and associated with ore minerals pyrite, bornite, chalcocite, chalcopyrite and native gold. Calcite is abundant and occurs as crackle breccias and extensional veins. Anhydrite was observed at depth (>700m) in Starra 251. Hematisation of magnetite is an important ore-forming process. Chlorite forms an extensive alteration halo with intense chlorite domains around ironstone remnants along the Starra Shear.

Some consensus regarding the late-D4 timing and brittle-ductlie re-activation control of copper-gold mineralisation along the Starra line does exist (Adshead-Bell, 1998; Kary & Harley, 1990; Sleigh, 2002; Duncan et al., 2014; Murphy et al., 2017).

Zonation

No focused deposit-scale mineral and/or alteration zonation studies have been completed on the Starra deposits. However, implicit in the paragentic studies of Rotherham (1997) and the structural-lithological controls described by Duncan et al. (2014) are a number of generalised relationships that unfortunately have limited zonation usefulness.

- Pre-mineralisation, sodic-calcic, quartz-albite-scapolite-actinolite alteration is strongly developed within the hangingwall Staveley Formation metasediments (Figure 4.66; Table 4.4) and is likely regional in extent (Sleigh, 2002; Duncan et al., 2014)
- Strongly developed, highly magnetic, chlorite-magnetite-hematite schists enveloping remnant ironstones along the Starra line (Figures 4.59, 4.60) reflect intense, ore-stage, chlorite (±muscovite ±sericite) alteration of metamorphic biotite and syn-ore precipitation (Rotherham, 1997; Figure 4.67B). Unfortunately no conclusive compositional variations and/or morphologies around ore have been identified.

HALOS

Extent

All of the Starra deposits were discovered using surface geochemistry. Rockchip anomalies including 70m@4g/tAu have been reported (Kary & Harley, 1990). No studies specifically focused on the aerial extent of lithogeochemical alteration have been completed along the Starra line.

Geophysical Expression

Figures 4.59 to 4.62 highlight the absence of any specific magnetic, gravity or EM response and Figures 4.14 to 4.17 any specific radiometric anomalism directly associated with the Starra ore bodies. Semi-regional magnetic and EM responses are associated with the overall Starra Shear and its internal alteration outline above but no specific geophysical anomalism is directly related to ore.

Geochemical Expression

Due to the outcropping nature of much of the Starra line limited soil geochemistry has been done between Starra 222 and 276. Figures 4.68 to 4.70 present the soil copper and gold geochemistry over the Starra line and to its north. The following geochemical responses are highlighted:

- Gold and/or copper soil anomalism (Au>50ppb; Cu>500ppm) is present at prospects (Starra 236, 286, 296, 302 & 306) where significant ore has not been located by drilling. Extensive low grade envelopes within chlorite-magnetite schist around ore bodies (and other focussing brittle hosts) identified by Sleigh (2002) significantly complicate geochemical targeting of ore.
- Strong copper and gold soil anomalism is associated with the Double Crossing Metamorphics-Gin Creek Granite-hosted Amethyst Castle prospect where drilling has identified a small oxide resource (pers comm Chinova Resources).

TIMING OF MINERALISATION

Relative Timing

Most workers (Laing et al. 1989; Adshead-Bell, 1998; Rotherham, 1997; Kary & Harley, 1990; Sleigh, 2002; Duncan et al., 2014; Murphy et al., 2017) agree on a late-Isan (syn to post D4) brittle-ductile timing of ore formation. As outlined above significantly different interpretations of the tectono-stratigraphic development of the complexly deformed and metasomatised host packages exist. Only Davidson et al. (1988) proposed a syngenetic origin for copper-gold in early iron formations subsequently modified by deformation.

Absolute Ages

Perhaps the age date most consistent with structural, metasomatic and geological relationships at Starra is the ca1503Ma Ar-Ar date (Perkins & Wyborn, 1998) on metasomatic biotite associated with Rotherham's (1997) pre-mineralisation potassic alteration (Stage 2, K-Fe metasomatism; Table 4.4). This date would time Starra mineralisation as late Isan D4 and syn to post Williams-Naraku magmatism.

Duncan et al. (2011, 2014) report a titanate U-Pb age of 1594±8Ma for sodic-calcic alteration in the footwall of Starra 251 mineralisation. This times a phase of sodic-calcic alteration to be synchronous with Isan D2 deformation and pre-peak-metamorphism.

A 1586±8Ma Re-Os model age for molybdenite intergrown with iron oxides, bornite, quartz and calcite from Starra 276 reported by Duncan et al. (2011) is argued by Duncan et al. (2014) to suggest a late- to post-D2, syn-metamorphic timing of alteration and mineralisation at Starra. This seems to be at odds with his own and other's structural and textural observations of post-peak-metamorphic, brittle deformation-controlled mineralisation.

The complexity of structural, metasomatic and mineralisation interplays along the Starra line leave plenty of scope for further detailed studies and well-constrained geochronology (if resources and prospectivity support further study).

GENETIC MODELS

While significant controversy and complexity has surrounded the detailed timing and origin of alteration and mineralisation at Starra, some consensus on a late Isan (syn to post D4), brittle re-activation timing has emerged (Laing et al. 1989; Adshead-Bell, 1998; Rotherham, 1997; Kary & Harley, 1990; Sleigh, 2002; Duncan et al., 2014; Murphy et al., 2017). Davidson et al. (1988) proposed an early syngenetic exhalative origin of copper and gold modified by later deformation.

While Duncan et al. (2011) proposed a metamorphic fluid origin of mineralisation and a syn-metamorphic timing (on the basis of a Re-Os date; see above), in his later paper (Duncan et al., 2014) he outlines the substantial evidence of late Isan, syn- to post-D4 mineralisation. The vagaries of Re-Os dating of deformed molybdenite have been outlined in the Merlin Absolute Ages section. Further studies are warranted.

Rotherham et al. (1998), on the basis of stable isotope and fluid inclusion studies, suggest Starra fluid compositions fall with magmatic or metamorphic fields but that based on thermodynamic constraints, a magmatic-metasomatic origin was favoured for the highly oxidised mineral assemblage associated with high grade Starra gold-copper mineralisation.

Murphy et al. (2017) after Barton & Johnson's (2004) IOCG schemes highlight the potential involvement of surficially-sourced oxidised fluids in the post Na-Ca-K, later H^+ (hydrolytic) stages of IOCG formation at Starra.

EXPLORATION

Discovery Method

Outcropping gold-copper mineralisation was discovered along the Starra line by prospecting in the late 1960s by Anaconda Australia Inc. All Starra deposits were discovered by rockchip sampling and follow-up drilling.

Confident conceptual targeting of blind mineralisation at Starra remains an elusive goal.

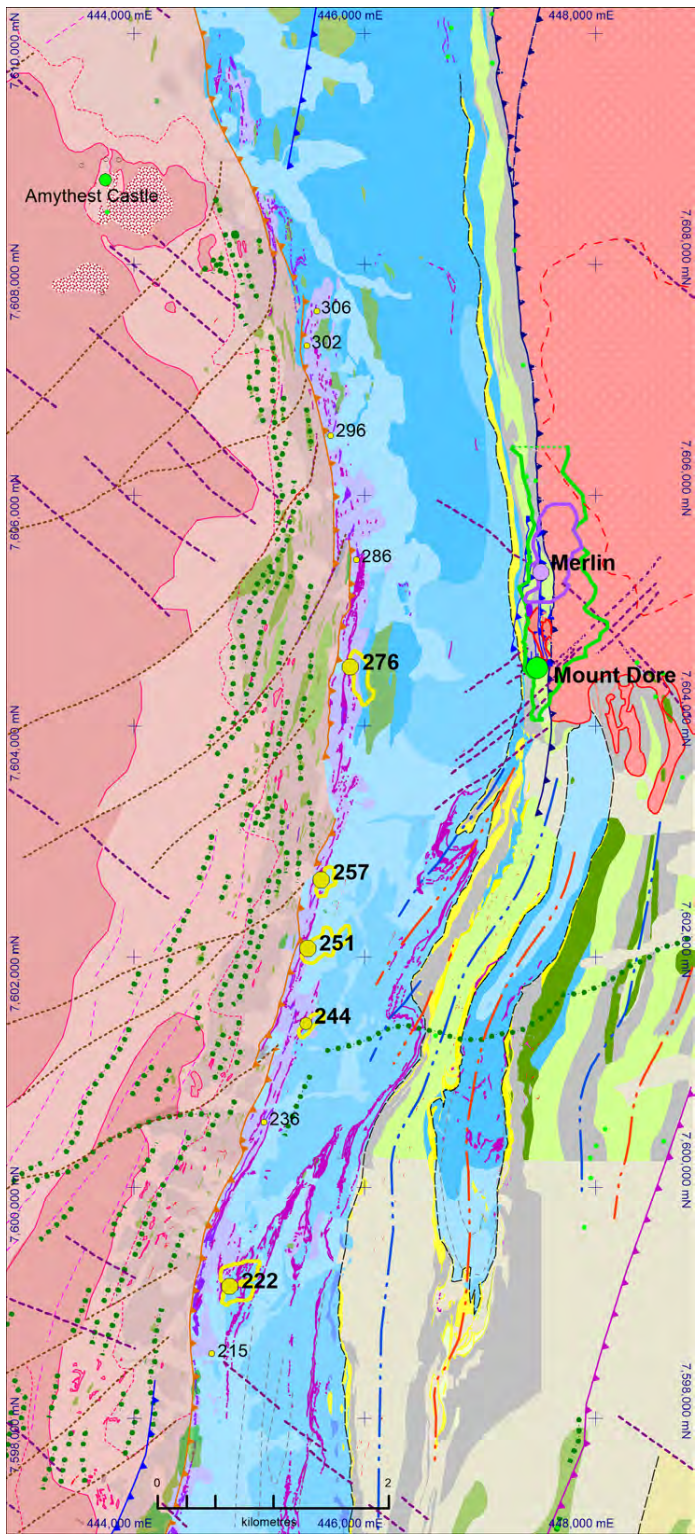

Figure 4.68 Solid geology compilation-interpretation of the Starra line of deposits and environs from Deep Mining Queensland (Murphy et al. 2017) Legend as for Figure 4.59. Map Projection GDA94 (MGA54)

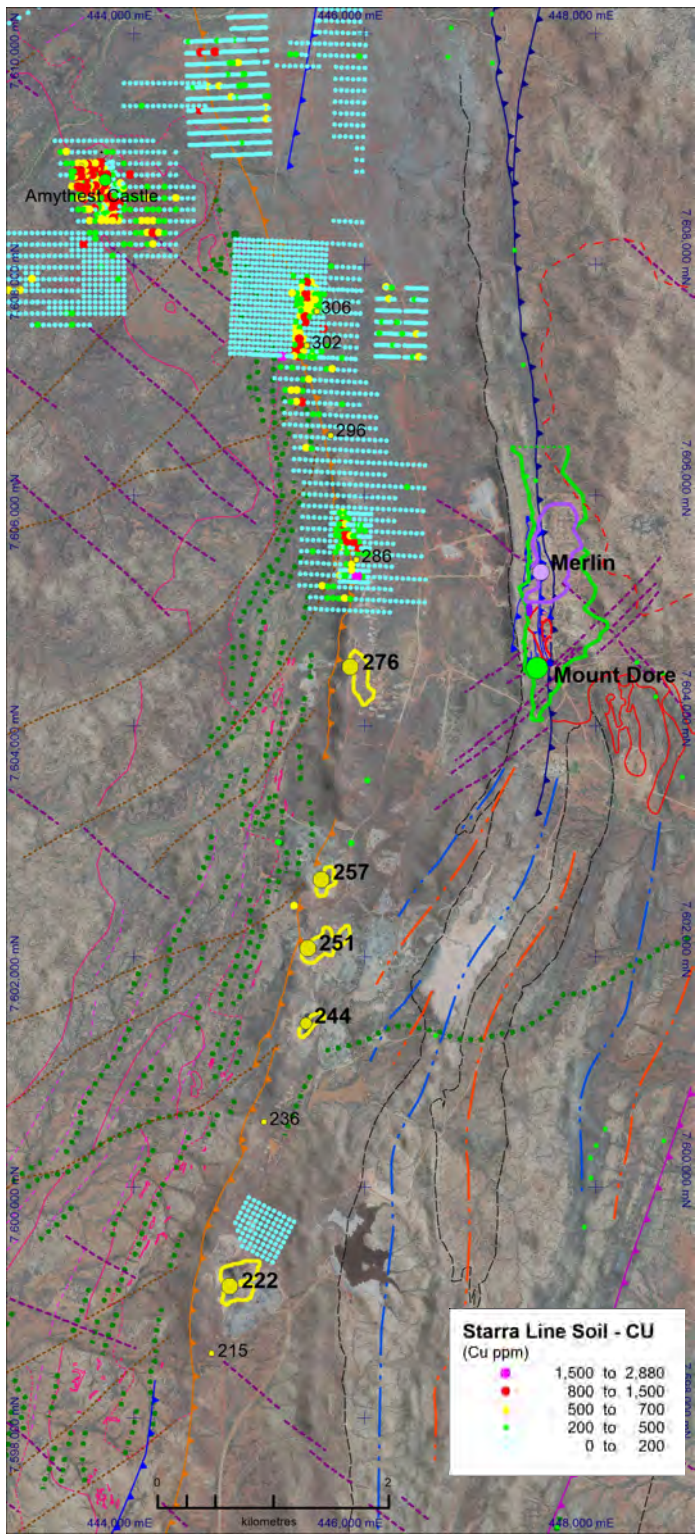

Figure 4.69 Starra line -80# soil Copper on Worldview image draped over DEM. Map Projection GDA94 (MGA54)

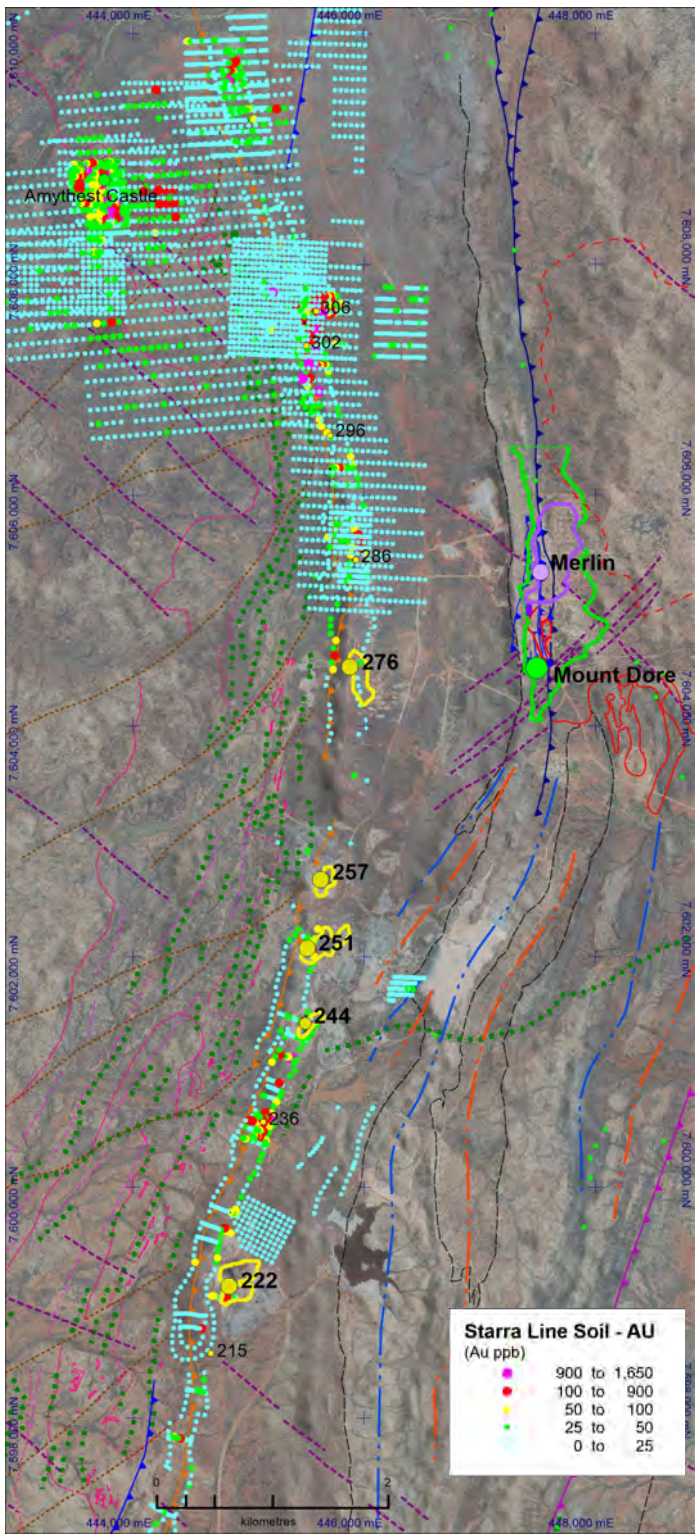

Figure 4.670 Starra line -80# soil Gold on Worldview image draped over DEM. Map Projection GDA94 (MGA54)

REFERENCES

Adshead-Bell, N.S., 1998, Evolution of the Starra and Selwyn high strain zones, Eastern fold belt, Mount Isa inlier: Implications for Au-Cu mineralization: Economic Geology, v. 93, p. 1450–1462.

Adshead-Bell, N.S., 2000, Structural constraints of the ironstone hosted Au-Cu Starra deposit and Selwyn Range region, Eastern fold belt, Mount Isa inlier: Unpublished Ph.D. thesis, Townsville, Queensland, James Cook University.

AMC, 2012. Preliminary Economic assessment of the Mount Elliott Project, Queensland, Australia. Unpublished Report for Ivanhoe Australia Ltd.

Austin, J.R., and Blenkinsop, T.G., 2008, The Cloncurry lineament: Geophysical and geological evidence for a deep crustal structure in the Eastern succession of the Mount Isa inlier: Precambrian Research, v. 16, p. 50–68.

Babo, J., Spandler, C., Oliver, N. H. S., Brown, M., Rubenach, M. J. and Creaser, R. A. 2017. The High-Grade Mo-Re Merlin Deposit, Cloncurry District, Australia: Paragenesis and Geochronology of Hydrothermal Alteration and Ore Formation. Economic Geology, 112, pp. 397-422.

Beardsmore, T.J., 1992, Petrogenesis of Mount Dore-style breccia-hosted copper ± gold mineralization in the Kuridala-Selwyn region of northwestern Queensland: Unpublished Ph.D. thesis, Townsville, Australia, James Cook University, 282 p.

Bell, T. H. and Hickey, K. A. 1998. Multiple Deformations with Successive Subvertical and Subhorizontal Axial Planes in the Mount Isa Region: Their Impact on Geometric Development and Significance for Mineralisation and Exploration. Economic Geology, 93, pp. 1369-1389.

Betts, P.G., Giles, D., Mark, G., Lister, G.S., Goleby, B.R., and Aillères, L., 2006, Synthesis of the Proterozoic evolution of the Mt Isa inlier: Australian Journal of Earth Sciences, v. 53, p. 187–211.

Brown, M. and Kirwin, D.J., 2009. The discovery and geology of the Mount Elliott-SWAN deposits - Eastern Fold Belt, Mount Isa Inlier, Northwest Queensland; Proceeding, NewGenGold 2009 Conference, 23-24 November, 2009, Perth, WA, Paydirt Media Pty Ltd, Perth, 14p.

Brown, M. and Porter, T.M., 2010 - The Mount Elliott IOCG System, Eastern Fold Belt, Mount Isa Inlier, Northwest Queensland; in Porter, T.M., (ed.), Hydrothermal Iron Oxide Copper-Gold & Related Deposits: A Global Perspective, v. 3 - Advances in the Understanding of IOCG Deposits; PGC Publishing, Adelaide, pp. 219-232.

Brown, M., Lazo, F., Kirwin, D.J. and Corlett, G., 2009. The SWAN and Mount Elliott IOCG deposits; in Williams, P.J. et al., (eds.), Smart Science for Exploration and Mining, Proceedings of the 10th Biennial SGA Conference, 17-20 August, 2009, Townsville, Australia, Extended abstracts, v. 1 pp. 47-49.

Chinova, 2015. SWAN Open Pit Resource as at 30th April, 2015. Unpublished Chinova Resources report.

Chinova, 2017. Current Resources and Historic Production provided by Chinova Resources.

Davidson, G., 1989, Starra and Trough Tank: iron formation hosted copper-gold deposits of northwest Queensland, Australia. Unpublished PhD Thesis, University of Tasmania, Hobart, Australia.

Davidson, G., Large, R., Kary, G., and Osborne, R., 1989, The BIF-hosted Starra and Trough Tank Au-Cu mineralization: A new stratiform association from the Proterozoic eastern succession of Mount Isa, Australia: Economic Geology Monograph 6, p. 135–150.

Dredge, C. P., 1992. EPM 3370-Selwyn Report for the twelve months ended 24th November, 1991. Cyprus Gold Australia Corporation Report No 770 to QDME

Duncan, R. J., Hitzman, M. W., Nelson, E. P., and Togtokhbayar, O. 2014. Structural and Lithological Controls on Iron Oxide Copper-Gold Deposits of the Southern Selwyn-Mount Dore Corridor, Eastern Fold Belt, Queensland, Australia Economic Geology v. 109, pp. 419-45

Duncan, R.J., Stein, H.J., Evans, K.A., Hitzman, M.W., Nelson, E.P., and Kirwin, D.J., 2011, A new geochronological framework for mineralization and alteration in the southern Cloncurry district, Eastern fold belt, Mount Isa inlier, Australia: Genetic implications for iron oxide-copper-gold deposits: Economic Geology, v. 106, p. 169–192.

Faulkner, I. L., and Phillips, K. G., 2017, Merlin molybdenum-rhenium deposit in Phillips, G. N. (ed) Australian Ore Deposits (The Australasian Institute of Mining and Metallurgy: Melbourne) p. 864

Fortowski, D.B. and McCracken. S., 1998. Mount Elliott copper-gold deposit; in Berkman D.A. and Mackenzie D.H., (eds.), Geology of Australia and Papua New Guinean Mineral Deposits, The Australasian Institute of Mining and Metallurgy, Melbourne, Monograph 22,

Garrett, S.J.M., 1992. The geology and geochemistry of the Mount Elliott copper±gold deposit, Northwest Queensland; Unpublished MSc thesis, University of Tasmania, Hobart.

Greene, J., 2011, Fluid and formational constraints of the Merlin Mo-Re deposit, Cloncurry. Unpublished Honours thesis, UTAS-CODES, School of Earth Sciences, Hobart, Tasmania.

Gunter, J., 2015. Mount Elliott-SWAN 3D modelling and target generation. Unpublished Report to Chinova Resources.

Hinman, M. C. 2012a. Merlin-Mt Dore Structure: Unpublished ppt Report to Ivanhoe Australia, Mar 2012

Hinman, M. C. 2012b. Regional mineralisation controls at Starra: Unpublished ppt Report to Ivanhoe Australia, Mar 2012

Hinman, M. C., Huisman, D., Little, G., and Porter, M., 2018. Solid Geology interpretation of the southern Eastern Fold Belt, Mount Isa, Northwest Queensland: An Industry-University-Governement Collaboration: DNRM-GSQ SREP Funded Industry Study.

Hinman, M.C., 2017, Proterozoic Time-Space Chart. Northwest Queensland Strategic Resources Exploration Program publication

Holcombe, R.J., Pearson, P.J., Oliver, N.H.S., 1991. Geometry of a middle Proterozoic extensional detachment surface. Tectonophysics 191, 255–274.

Jaques, A. L., Blake, D. H., and Donchak, P. J. T., 1982, Regional metamorphism in the Selwyn Range area, northwest Queensland. BMR Journal of Australian Geology and Geophysics, v.7; p. 181-196

Kary, G. L., and Harley, R. A., 1990 Selwyn gold-copper deposits in, Hughes, F. E., (ed) Geology of the mineral deposits of Australia and Papua New Guinea: The Australian Institute of Mining and Metallurgy: Melbourne. P. 955-960

Kirkby, P. G., 2009, Characteristics and origin of IOCG - Associated Mo-Re mineralisation in the Merlin deposit, Mt Isa Inlier: Unpubl. Honours Thesis, University of Tasmania.

Kirwin, D., 2009, Merlin-a new Mo-Re discovery in the Cloncurry District. Unpublished SMEDG presentation for Ivanhoe Australia Ltd.

Laing, W.P., Rubenach, M.J., and Switzer, C.K., 1989, The Starra gold-copper deposits: Syndeformational metamorphic mineralization in an early regional zone of decollement: Geological Society of Australia Abstracts, v. 21, p. 229.

Lazo, F., and Pal, T., 2009, The Merlin Mo-Re zone, a new discovery in the Cloncurry district, Australia: Biennial SGA Meeting, 10th, Townsville, Australia, 17−20 August 2009, Proceedings, p. 56–58.

Leishman, J., 1983, Report on 1:25,000, 1:5,000 and 1:1000 geological mapping, Starra / Selwyn Area, Northwest Queensland; Company Report to Amoco Minerals Australia

Little, G. A., 1997. Structural evolution and paragenesis of alteration and mineralisation at Mount Elliott Cu-Au Mine, Northwest Queensland. Unpublished Honours thesis, School of Earth Sciences, James Cook University of North Queensland, Townsville, Queensland

Lycopodium., 2012, NI 43-101 Technical Report Merlin Molybdenum Rhenium Project

Feasibility Study. Unpublished Consulting Report for Ivanhoe Australia Ltd

Mark, G., Foster, D.R.W., Pollard, P.J., Williams, P.J., Tolman, J., Darvall, M., Blake, K.L., 2004. Stable isotope evidence for magmatic fluid input during large-scale Na–Ca alteration in the Cloncurry Fe oxide Cu–Au district, NW Queensland, Australia. Terra Nova 16, 54–61.

Marshall, L.J., 2003. Brecciation within the Mary Kathleen Group of the Eastern Succession, Mt Isa Block. Australia: implications of district-scale structural and metasomatic processes for Fe-oxide-Cu-Au mineralisation. School of Earth Sciences. James Cook University, Townsville, 323pp.

McGeough, M. A., and Faulkner, I. L., 2017, Selwyn mineral field in Phillips, G. N. (ed) Australian Ore Deposits (The Australasian Institute of Mining and Metallurgy: Melbourne) p. 864

McLean, G. and Benjamin, P., 1993. The geology and development of the Mount Elliott copper-gold deposit; in Williams, K., (ed.), Symposium on Recent Advances in the Mount Isa Block, Australian Institute of Geoscientists, Bulletin 13, pp. 47-54.

Morrison, R. J., 2012 Starra-Mount Dore-Merlin 2012 Resource Geology Report and Strategic Proposals: Unpublished Ivanhoe Australia Ltd Report

Murphy, T. E., 2004. Structural and stratigraphic controls on mineralisation at the George Fisher Zn-Pb-Ag deposit, northwest Queensland, Australia. Unpublished PhD thesis, Department of Earth Sciences, James Cook University of North Queensland, Townsville.

Murphy, T., Hinman, M., Donohue, J., Pirlo, M., Valenta, R., Jones, M. & Pratt, A., 2017, Deep Mining Queensland: Prospectivity Analysis in the Southern Cloncurry Belt, Queensland, Australia: DNRM-GSQ Commissioned Industry Study.

Nisbet, B. W., 1980, Progress report for the period August 30, 1978 to February 28, 1979. Cloncurry River and Selwyn Hematites projects. Combined A to P 1530M, 1550M, 1822M and 1824M, Queensland, Australia. Unpublished Amoco Minerals Australia Company Report 136

Nunn, D., Alasfar, Z, and Williams, E., 2012, Mount Dore and Merlin FTIR Spectroscopy Results. Unpublished ppt report to Ivanhoe Australia Ltd

O'Dea, M. G., Betts, P. G., MacCready, T., and Ailleres, L. 2006. Sequential development of a mid-crustal fold-thrust complex: evidence from the Mitakoodi Culmination in the eastern Mt Isa Inlier, Australia: Australian Journal of Earth Sciences, v53, pp69-90.

Page, R.W., and Sun, S.-S., 1998, Aspects of geochronology and crustal evolution in the Eastern fold belt, Mt Isa inlier: Australian Journal of Earth Sciences, v. 45, p. 343–361.

Perkins, C., and Wyborn, L.A.I., 1998, Age and Cu-Au mineralization, Cloncurry district, eastern Mt. Isa inlier, Queensland, as determined by 40Ar/39Ar dating: Australian Journal of Earth Sciences, v. 45, p. 233–246.

Pollard, P., and McNaughton, N.J, 1997, U/Pb geochronology and Sm/Nd isotope characterization of Proterozoic intrusive rocks in the Cloncurry district, Mount Isa inlier, Australia: AMIRA P438 Cloncurry Base Metals and Gold Final Report, Section 4, 19 p.

Rotherham, J.F, 1997, A metasomatic origin for the iron-oxide Au-Cu Starra orebodies, Eastern Fold Belt, Mount Isa Inlier: Mineralium Deposita, v.32, p. 205-218

Rotherham, J.F, Blake, K.L., Cartwright, I., and Williams, P.J., 1998, Stable isotope evidence for the origin of the Mesoproterozoic Starra Au-Cu deposit, Cloncurry district, northwest Queensland: Economic Geology, v. 93, p. 1435–1449.

Rubenach, M.J., Foster, D.R.W., Evins, P.M., Blake, K.L. and Fanning, C.M., 2008. Age constraints on the tectonothermal evolution of the Selwyn Zone, Eastern Fold Belt, Mount Isa Inlier; Precambrian Research, v. 163, pp. 81-107.

Searle, R. A., 1952. Geology of the Mount Elliott Copper Mine, Selwyn, Queensland. BMR Geology and Geophysics Record 1952/27

Sharma, S., 2016. Microtextural molybdenite ore relations at Merlin, Cloncurry. pers comm. ppt slides.

Sleigh, D.W., 2002a. The Selwyn Line tabular iron-copper-gold system, Mount Isa Inlier, NW Queensland, Australia; in Porter, T.M. (ed.), Hydrothermal Iron Oxide Copper-Gold & Related Deposits: A Global Perspective, PGC Publishing, Adelaide, v. 2, pp 77-93.

Sleigh, D.W., 2002b. Digesting data to put on weight; in Exploration in the Shadow of the Headframe: Getting a New Life on Lease, SMEDG-AIG-ASEG Symposium, North Sydney, 11 October, 2002, The Australian Institute of Geologists, Perth, Bulletin 35, 9p.

SRK., 2010, Independent Technical Report on the Merlin Project, Queensland. Unpublished SRK Consulting Report for Ivanhoe Australia Ltd

Switzer, C., 1987, Implications of high strain for regional structural geometry and control on gold mineralization in the Selwyn region, northwestern Queensland: Unpublished B.Sc. (Hons.) thesis, James Cook University, Townsville

Valk, N., 2014, Merlin Molybdenum-Rhenium Project, Unpublished Chinova Resources ppt presentation.

Wang, S. and Williams P., 1996. The alteration and mineralisation styles of a skarn hosted Mount Elliott Cu-Au deposit and adjacent SWAN Prospect, Cloncurry District; in MIC'96; New Developments in Metallogenic Research; The McArthur-Mt Isa-Cloncurry Minerals Province; Extended Abstracts, Contributions of the Economic Geology Research Unit, James Cook University, Townsville, v. 55, pp. 139-142.

Wang, S. and Williams P., 2001. Geochemistry and origin of Proterozoic skarns at the Mount Elliott Cu-Au(-Co-Ni) deposit, Cloncurry District, NW Queensland, Australia; Mineralium Deposita, v. 36, pp. 109-124.

White, S., 1989, Structural controls on, and the origin and timing of ironstone and mineralization at Starra, northwest Queensland: Unpublished B.Sc. (Hons.) thesis, James Cook University, Townsville, 165 p